Leveraging Deep Learning and Advanced Statistical Methods for Investigating the Fate and Transport of Microplastics in a Waste Water Treatment Plant

by

Frank Zhu

A thesis

presented to the University of Waterloo

in fulfillment of the

thesis requirement for the degree of

Doctor of Philosophy

in

Civil Engineering - Water

Waterloo, Ontario, Canada, 2023

Examining Committee Membership

The following served on the Examining Committee for this thesis. The decision of the Examining Committee is by majority vote.

External Examiner	Edward McBean Professor School of Engineering University of Guelph
Supervisor	Wayne Parker Professor Department of Civil and Environmental Engineering University of Waterloo
Internal Member	Peter Huck Professor Department of Civil and Environmental Engineering University of Waterloo
Internal Member	Sigrid Peldszus Research Professor Department of Civil and Environmental Engineering University of Waterloo
Internal-external Member	Alexander Wong Professor Department of Systems Design Engineering University of Waterloo

Author's Declaration

This thesis consists of material all of which I authored or co-authored, see Statement of Contributions included in the thesis. This is a true copy of the thesis, including any required final revisions, as accepted by my examiners. I understand that my thesis may be made electronically available to the public.

Statement of Contributions

Chapter 3 of this thesis consists of a paper that was co-authored by myself, my committee member Dr. Alexander Wong, and my supervisor, Dr. Wayne Parker. The idea of leveraging deep learning for MP detection originated from myself, and Dr. Parker provided valuable input by suggesting testing the performance on spectra with variation. Dr. Wong guided the development of the deep learning model and provided insights to refine the model and improve its performance. This section has been submitted to a top environmental journal, *Environmental Pollution*, and received positive feedback from reviewers in May 2023.

Chapter 4 of this thesis was co-authored by myself, a research assistant professor, Dr. Philip Schmidt, and my supervisor, Dr. Wayne Parker. The initial idea for statistical modeling emerged from collaborative brainstorming sessions. I took the lead in developing and implementing the model, while Dr. Schmidt provided valuable guidance in model development. Dr. Parker offered valuable suggestions for implementing the model to study various operational factors. This chapter is planned for submission to a top-tier journal such as *Environmental Science and Technology*.

Chapter 5 of this thesis was co-authored by myself and my supervisor, Dr. Wayne J. Parker. The idea for this chapter originated from both myself and Dr. Parker. I conducted field sampling, experimental work, and data analysis. Dr. Parker provided valuable insights in the data analysis process. We intend to submit this chapter to a top environmental engineering journal, such as *Water Research or Environmental Science and Technology*.

Throughout the thesis, I have contributed significantly to the research design, data collection, model development, data analysis, and the overall writing of the manuscript. I am grateful for the guidance and support provided by my committee members and supervisor, as their expertise and valuable suggestions have played a crucial role in shaping the content and quality of this thesis.

Acknowledgements

I would like to express my deepest gratitude to my supervisor, Dr. Wayne Parker, for his unwavering patience, guidance, and support throughout the completion of this thesis and my entire graduate studies. His expertise, encouragement, and valuable insights have been instrumental in shaping the outcome of this research.

I extend my heartfelt thanks to Dr. Alexander Wong for his invaluable guidance in the development of the deep learning model, which significantly contributed to the success of this work. Additionally, I would like to thank Dr. Philip Schmidt for his expertise in advanced statistics, such as Bayesian analysis and MCMC, and his guidance in incorporating these methodologies into my research.

I am grateful to the members of my committee, Dr. Edward McBean, Dr. Peter Huck, Dr. Sigrid Peldszus, and Dr. Alexander Wong, for their time and effort in reviewing my thesis and providing invaluable feedback. Their constructive criticism and suggestions have greatly enhanced the quality of this research.

I would like to extend my sincere appreciation to Dr. Leung Tong and Dr. Joseph Jessy for providing access to the valuable FPA micro-FTIR resources, which were crucial for my experimental work. I am also grateful to Dr. Rodney Smith for his suggestion in spectral data analysis. My gratitude also extends to lab technician Mark Sobon for his assistance in fieldwork and lab experiments. I am indebted to my colleague Narasimman Meanakshi for his insightful contributions in analyzing the field data from the treatment plant.

Finally, I would like to express my deepest appreciation to my parents for their unwavering support and love. Their encouragement and belief in me have been the driving force behind my successful completion of this challenging PhD journey.

Abstract

Microplastics (MPs), defined as plastic particulates smaller than 5mm, pose significant environmental concerns due to their widespread distribution, adverse ecological impacts, and potential human health implications. The understanding of MP fate and transport in wastewater treatment plants (WWTPs) is crucial for effective management and mitigation strategies. This PhD thesis addresses key challenges associated with MP characterization in WWTPs and aims to enhance the understanding of MP fate and transport through improved MP identification, reduced data uncertainty, and the development of reliable count and mass balance models.

The accurate identification of MPs in samples using spectroscopic methods presents a significant hurdle. The first study introduces PlasticNet, a deep learning convolutional neural network developed to overcome the challenges in identifying MPs in environmental samples through spectral classification. PlasticNet was trained, validated, and tested using complex spectra and proved to be capable of accurately classifying multiple types of common plastics. Its capability extends to recognizing spectra affected by factors such as the presence of additives and weathering, and variations in MP thickness. Compared with conventional library search routines, PlasticNet exhibits significant improvements, thus highlighting its potential as a standard automatic recognition tool for MPs in environmental samples analyzed by FPA FT-IR imaging.

Uncertainty quantification in MP enumeration data is another challenge in MP research. The second study investigates and models the sources of error intrinsic to each step of MP analysis, including concentration heterogeneity, random errors during sample collection, and the loss of MPs during extraction. The impact of operational factors such as the number of replicates, MP size and shape variations, and differential recovery on data uncertainty is comprehensively examined. Bayesian uncertainty analysis, implemented through Markov Chain Monte Carlo (MCMC) methods, is utilized to quantify uncertainties and develop guidelines for reducing data uncertainty in MP enumeration. These findings provide valuable insights towards the development of standardized guidelines for analytical procedures quantifying MPs in wastewater and sludge samples.

Furthermore, the third study addresses the establishment of mass balance models for MPs in WWTPs. Mass balance models offer valuable insights into fragmentation dynamics, weight-based ecological ramifications, and potential standardization across different studies and environmental contexts. However, accurate MP mass quantification remains challenging. The thesis explores innovative strategies for MP mass quantification and applies these techniques to develop reliable mass balance models in the primary treatment process at a selected WWTP.

The third study also reveals the significant influence of MP size and sample type on recovery, hence the need for considering these variations in concentration estimations. The application of differential recovery resulted in significant improvement in the mass balance model, which underscores the importance of incorporating differential recovery into balance models studies. In sum, the third study shows the complementary nature of count and mass balance approaches in understanding the fate and transport of MPs in WWTPs.

Overall, the enhanced MP identification, reduced data uncertainty, and reliable mass balance models developed in this thesis significantly contribute to a comprehensive understanding of MP fate and transport in wastewater treatment plants (WWTPs). These advancements offer multiple benefits, including accurate MP identification, precise MP enumeration, and deeper insights into MP removal processes. The optimization of processes and methodologies driven by this research aids in mitigating MP pollution, reducing ecological risks, and fostering standardization and comparative analyses across diverse studies and environments. Overall, this research enhances the robustness of MP research in WWTP contexts and supports the development of effective strategies for managing MP pollution and promoting sustainable practices.

Table of Contents

List of Figures xi
List of Tables xii
Nomenclature xiii
Chapter 1. Introduction 1
1.1 Problem statement 1
1.2 Objectives and Scopes 4
1.3 Significance 5
1.4 Thesis structure 5
Chapter 2. Literature review 7
2.1 Leveraging deep learning Variation of MP spectra 7
2.1.1 Identifying MPs using FT-IR technology 7
2.1.2 Variation of MP spectra 8
2.1.3 Leveraging deep learning in addressing variation in MP spectra 10
2.1.4 Section Summary 12
2.2 Modelling uncertainties in MP enumeration 13
2.2.1 Existing uncertainty model and comparability with errors in MP enumeration 13
2.2.2 Uncertainties in MP concentration estimates caused by operating factors 14
2.2.3 Bayesian uncertainty inference coupled with MCMC 16
2.2.4 Section Summary 16
2.3 Count and Mass balance models of MPs in considering differential recovery 18
2.3.1 Mass balance models of MPs in WWTPs 18
2.3.2 Improve data reliability by considering differential recovery 20
2.3.3 Count and mass balance models of MPs in primary wastewater treatment 22
2.3.4 Section summary 23
2.4 Summary and recommendations 25
Chapter 3 Leveraging deep learning for automatic recognition of microplastics (MPs) via focal plane array (FPA) micro-FT-IR imaging 27
Abstract 27
3.1 Introduction 28
3.2. Methodology 33
3.2.1 Data acquisition 33

3.2.2 Overview of data processing 35
3.2.3 Data pre-processing 36
3.2.4 1-D to 2-D conversion 36
3.2.5 PlasticNet Architecture 36
3.2.6 Initial training, validation, and testing 39
3.2.7 Recognition of spectra with variation & re-training of model 41
3.2.8 Comparison of the performance of PlasticNet vs. Library search 41
3.2.9 Methodology summary 42
3.3. Results and discussion 43
3.3.1 1-D to 2-D conversion 43
3.3.2 Performance of training and testing 44
3.3.3 Errors indicated by the confusion matrix 47
3.3.4 Addressing variation of MP spectra due to additives and surface modifications 51
3.3.5 Impact of MP thickness 57
3.3.6 Comparison of the identification of MPs by PlasticNet and library search 59
3.4. Conclusion: 63
Chapter 4 Uncertainties in the enumeration of microplastics in wastewater samples: Model development, Bayesian analysis, and Markov chain Monte Carlo methods 64
Abstract 64
4.1. Introduction 65
4.2. Model development 68
4.2.1 Sources of error in MP enumeration 68
4.2.2 Adaptation of model to describe MP enumeration in wastewater 72
4.2.3. Probabilistic model specification 75
4.3. Investigation of uncertainties: Data simulation and Bayesian analysis via MCMC 77
4.3.1. Data simulation 77
4.3.2 Bayesian uncertainty inference using MCMC methods 78
4.3.3 Investigating uncertainties caused by operating factors using varied model structures 80
4.3.4 Data analysis 82
4.4. Results 83
4.4.1 Number of replicates 83
4.4.2 Categorization of MPs 86
4.4.3 Impact of recovery practices on enumeration and practical significance 88

4.5. Conclusion 93
Chapter 5 Mass and Count balances of MPs in Primary Treatment Considering Differential Recoveries during MP Analysis 94
Abstract: 94
5.1. Introduction 95
5.2. Material and methods 98
5.2.1 Field sampling 98
5.2.2 Extraction of MPs 99
5.2.3 Quantification of MP count 102
5.2.4 Quantification of MP mass 103
5.2.5 Recovery tests 105
5.2.6 Quality Assurance/Quality Control 106
5.2.7 Evaluation of count and mass balances 106
5.2.8 Removal efficiency 108
5.2.9 Statistical Analysis 108
5.3. Results and discussion 110
5.3.1 Procedure blank 110
5.3.2 Spiking tests results 110
5.3.3 TSS Mass balance 113
5.3.4 Concentration of MPs 113
5.3.5 Count balance of MPs in primary treatment 115
5.3.6 Mass balance of MPs in primary treatment 120
5.4. Conclusions 124
Chapter 6 Conclusions and recommendations 125
6.1 Conclusions 125
6.2 Recommendations 127
Appendices 140
Appendix A Supplementary information related to leverage deep learning for MP identification 140
Appendix B Supplementary information related to modelling uncertainties in MP enumeration 148
Appendix C Supplementary information related to count and mass balance models of MPs in Primary treatment plant 152
Appendix D WEAO Conference Paper: Quantification of the mass of Microplastics using FPA-based FT-IR Imaging 163

List of Figures

Figure 3- 1 (A) Overview of data processing (B) Schematic representation of PlasticNet. 37
Figure 3- 2 Convolution operation (A) and max pooling operation (B). 38
Figure 3- 3 (A) Sliding a Hamming window on a PP spectrum. (B) A spectrogram created from a PP spectra. 44
Figure 3- 4 Performance of PlasticNet as evaluated by a Normalized Confusion Matrix 46
Figure 3- 5 Analysis of spectra misclassified by PlasticNet (A) PE spectrum misclassified as PP. 49
Figure 3- 6 Spectra of PP with additives. (A) Glass fiber filler (B) fire retardant (C) $CaCO_3$ and virgin PP 52
Figure 3- 7 Spectra of PP with dyes (A) green (B) red (C) white and virgin PP. 53
Figure 3- 8 Spectra of PE with surface modification due to atmospheric weathering. 54
Figure 3- 9 Variation of transmission FTIR spectra due to variation of the thickness of pixels. 59
Figure 3- 10 Comparison of the recognition results of Dataset 3B by library search and PlasticNet approaches 62

Figure 4- 1 Steps of MPs analysis and sources of error associated with each step. 70
Figure 4- 2 Effect of replication on the uncertainties of MP enumeration (A) ECDF curves (B) 95% credible intervals obtained 86
Figure 4- 3 Effect of categorization on MP enumeration as illustrated by the ECDF curves. 88
Figure 4- 4 Impacts of recovery practices on the estimated total MP concentration (A) and the proportion of each category (B) 91

Figure 5- 1 Schematic of extraction procedure. 101
Figure 5- 2 Mass quantification of MP FPA micro-FTIR imaging. 104
Figure 5- 3 (A) Comparative Analysis of Microplastic Recovery: Eye-Based vs. Instrument-Based Techniques. (B) Influence of Microplastic Size and Sample Type on Recovery Efficiency 112
Figure 5- 4 TSS mass balance in primary treatment at Kitchener WWTP 113
Figure 5- 5 Concentrations of MPs in different streams on both count and mass basis corrected using different recovery practices. 115
Figure 5- 6 Count Balance of MPs within Primary Wastewater Treatment in Different Size Fractions. . 120
Figure 5- 7 Mass Balance of MPs within Primary Wastewater Treatment in Different Size Fractions ... 123

List of Tables

Table 2- 1 Current Studies Leveraging Machine Learning Models for MP Identification via Spectra Classification..... 12
Table 2- 2 Uncertainties in Microplastic (MP) Concentration Estimate Caused by Operating Factors Reflected in Recent MP Studies..... 15
Table 2- 3An Overview of Microplastic Studies in WWTPs: Emphasizing Quantitative Model Development, Recovery Practices, and Availability of Primary Treatment Microplastic Data 24

Table 3- 1 Meta-Statistics for the data employed in the study..... 35
Table 3- 2 Number of spectra used for initial training, validation, and testing 40
Table 3- 3 Errors of spectra classification as described in confusion matrix..... 47
Table 3- 4 Comparison of molecular structures of selected confused spectral pairs 48
Table 3- 5 Performance of the PlasticNet in recognizing spectra of varied PP 56

Table 4- 1 Description of errors in the analysis of discrete particles (Schmidt et al., 2010) and how they manifest in MP analysis. 71
Table 4- 2 Summary of assumptions in beta-Poisson model and compatibility with errors in the enumeration of MPs in wastewater..... 75
Table 4- 3 Parameter values employed for creating simulated MP data..... 78

Nomenclature

Acrylonitrile Butadiene Styrene (ABS);

Attenuated total reflectance (ATR);

Convolutional neural network (CNN);

Empirical Cumulative Distribution Function(ECDF);

Focal plane array (FPA);

Fourier transform infrared (FTIR);

K-Nearest Neighbor (KNN);

Markov chain Monte Carlo(MCMC);

Microplastics (MPs); One-dimensional(1-D);

Partial least squares discriminant analysis (PLS-DA);

Per- and polyfluoroalkyl substances (PFAS);

Polyamide (Nylon);

Polycarbonate (PC);

Polyethylene (PE);

Polyethylene Terephthalate (PET);

Polymethyl Methacrylate (PMMA);

Polyoxymethylene (POM);

Polypropylene (PP);

Polyurethane (PU);

Polyvinyl Chloride (PVC);

rectified linear unit (ReLU);

Silicone Rubber (Silicone);

Support vector machine (SVM);

Two-dimensional (2-D);

Total suspended solids(TSS);

Ultraviolet (UV);

Wastewater treatment plants (WWTPs

Chapter 1. Introduction

1.1 Problem statement

Microplastics (MPs), defined as plastic particulates smaller than 5mm, present a considerable environmental concern due to their pervasive presence, adverse environmental impact, and potential implications for human health. These debris pervade virtually all ecosystems, including oceans, freshwater systems, soil, and even the atmosphere (Andrady, 2011; Koelmans et al., 2019), asserting a persistent and ubiquitous environmental footprint. Understanding their impact is crucial due to their widespread distribution and enduring nature. From an ecological standpoint, MPs, capable of being ingested by a diverse range of organisms from minute plankton to large marine mammals and birds, can induce harmful physical effects such as blockages and internal injuries (Oehlmann et al., 2009). In addition, the discovery of MPs in various food and water supplies, including seafood, table salt, and bottled water, denotes their entry into the human system (Talsness et al., 2009; Mohamed Nor et al., 2021). Moreover, the fact that plastics may incorporate hazardous additives and adsorb toxic chemicals raises concerns about potential health effects following ingestion(Campanale et al., 2020).

The study of the fate and transport of MPs in WWTPs is of significant importance for several reasons. Firstly, WWTPs receive a substantial influx of MPs through both domestic and industrial wastewater, making them pivotal sites for assessing the concentration, diversity, and origins of MPs within a designated region (Sun et al., 2019). In addition, WWTPs play a crucial role in the removal of MPs from the wastewater before its discharge into the environment, hence understanding the efficiency and mechanisms of this process can inform better mitigation strategies and technological improvements in wastewater treatment (Hu et al., 2019). Moreover, despite the high removal efficiency, the residual MP release via effluent into the receiving water remains a matter of concern due to high flows (Sun et al., 2019). Hence, these studies can be used to assess potential ecological risks of MP pollution imposed by WWTPs. In conclusion, the study of MPs in WWTPs is not only integral to our understanding of the broader MP pollution problem but also crucial in developing effective strategies for its mitigation.

Though multiple studies regarding fate and transport of MPs in WWTPs have been conducted all over the world, there exist several challenges associated with characterizing MPs in WWTPs. One

significant hurdle is the accurate identification of MPs in samples using spectroscopic methods. Focal Plane Array (FPA)-based micro-FT-IR spectroscopy presents a promising method for fast and rapid identification of MPs in environmental samples. After the spectroscopic signals are obtained these techniques typically rely on library search strategies, where unknown spectra are matched with standard spectra in a library to determine the best similarity. However, this method is susceptible to error, largely due to the inherent disparities between the library spectra of virgin plastics and the spectra of environmentally sourced MPs. The complexity of these environmental MPs arises from factors such as the presence of additives (Hahladakis et al., 2018; Campanale et al., 2020), surface modifications (Chen et al., 2021; Miranda et al., 2021), adsorbed pollutants, and biofilm formation on the MP surfaces (Johansen et al., 2019; Shabbir et al., 2020) . Additionally, spectral variance associated with the thickness of MPs when spectra are collected via FPA imaging poses another obstacle to accurate library search outcomes (da Silva et al., 2020; Zhu et al., 2021). Consequently, this analysis could be improved through the development of more effective strategies to accommodate these spectral variances in MP identification.

A second challenge confronting MP research in WWTPs pertains to characterizing uncertainties intrinsic to enumeration data. A range of intrinsic errors associated with each step of MP analysis have been documented. Concentration heterogeneity may introduce considerable variability due to the non-uniform distribution of MPs in the source environment (Lam et al., 2020; Ovide et al., 2022). Further, the incidence of random errors during sample collection is acknowledged as a source of data variability (Morgado et al., 2022; De Frond et al., 2023), and the unavoidable loss of MPs during extraction (Halbach et al., 2021; Way et al., 2022) exacerbates uncertainty in concentration estimates. Furthermore, non-constant analytical recoveries between replicate samples during recovery tests have been observed (Simon et al., 2018; Konechnaya et al., 2020; Mari et al., 2021), thereby intensifying variability in enumeration outcomes. Errors from earlier steps of the analytical process propagate and accumulate throughout subsequent steps, thereby heightening overall variability in the MP enumeration. Consequently, it is important to comprehend the intrinsic errors associated with each analytical step, and to quantify the uncertainty in MP concentration estimates that originates from these errors.

Beyond the errors intrinsically embedded within the analytical procedure, several operational factors add to the variability in MP enumeration. First, differences in the number of replicates used

for sample analysis could introduce varying degrees of uncertainty in enumeration-based concentration estimates (Schmidt et al., 2010; Bruge et al., 2020). Second, early studies that grouped different types of MPs without considering variations in size and shape (Michielssen et al., 2016; Murphy et al., 2016) contrast with more recent research (Ziajahromi et al., 2017; Magni et al., 2019; Bruge et al., 2020; Mintenig et al., 2020), which have incorporated these distinctions into their enumeration methodologies. The level of uncertainties induced by collectively counting all MP types as compared to separate counting remains unclarified. Further, a significant number of studies disregard non-constant analytical recovery among replicate samples (Xu et al., 2019), as well as differential recovery tied to MP size, shape, and type (Long et al., 2019; Zhang et al., 2020). The degree of uncertainties that this neglect introduces into MP enumeration remains an unanswered question. Hence, a critical examination is required to understand how these operational factors contribute to uncertainties in MP enumeration and to develop methodologies for addressing such uncertainties, with the aim to enhance the accuracy and reliability of MP enumeration in environ mental samples.

A third challenge in conducting microplastic (MP) research within the context of WWTPs involves the establishment of mass balance models. Unlike traditional count balance models, mass balance models can offer deeper insights into fragmentation dynamics (Simon et al., 2018), elucidate the weight-based ecological ramifications of MPs (Poulain et al., 2018), and potentially enable standardization across a variety of studies and environmental contexts (Chen et al., 2022) . However, due to the current limitations in quantifying the mass of MPs accurately, there has only been one study (Rasmussen et al., 2021) successful in implementing a mass balance model in a WWTP. Consequently, there is a pressing need for innovative strategies for MP mass quantification, and for the subsequent application of these techniques in developing reliable mass balance models. The contrasting of these mass balance models with count balance ones could offer a richer perspective on the fate and transport dynamics of MPs within WWTPs.

The effects of differential recovery associated with MP size and sample type on the improvement of concentration estimates and the closure of count and mass balance models remains unclear. Recent reports indicate that MP recovery varies with size (Way et al., 2022) and sample type (Konechnaya et al., 2020). It is postulated that MP concentrations on both count and mass bases could be more accurately quantified when considering these differences. Yet, the variation of such

recoveries within the context of MP extraction from wastewater and sludge samples are still not clearly understood, and there are no studies incorporating these differences into balance model studies. Consequently, there is a necessity to systematically explore these differential recoveries as well as their potential impact on the completion of count and mass balance models in MP studies within the context of WWTPs. Further, recent studies (Mintenig et al., 2017; Simon et al., 2018; Chand et al., 2021) leverage automated instrument-based counting for expedited and accurate identification of MPs. However, these studies employed eye-based recovery for concentration calculations with no discussion regarding the consistency between recovery achieved in two ways. Hence, the discrepancy between eye-based recovery and instrument-based studies should be experimentally verified. If a significant disparity is found, it should also be integrated into quantitative MP models to enhance accuracy and reliability.

1.2 Objectives and Scopes

Motivated by the aforementioned problems in MP studies, the primary objective of this research is to achieve enhanced understanding of the fate and transport of MPs with a focus on 1) improved MP identification; 2) reduced data uncertainty; 3) establishment of reliable count and mass balances. This will be achieved through:

- Enhancing spectra recognition and hence MP identification: Given the spectral variance introduced by additives, surface modifications, and thickness variation, a robust strategy was developed to improve spectra recognition and identification. Deep learning techniques and specifically a Convolutional Neural Network (CNN) architecture, were introduced for this purpose.
- Investigating and modelling sources of error: An in-depth examination of random errors associated with each step of MP analysis was conducted. After that the errors were modelled mathematically using appropriate statistical assumptions.
- Evaluating the impact of operational factors on uncertainty: A mathematical model was implemented using Bayesian uncertainty analysis via Markov Chain Monte Carlo (MCMC) methods to study the contribution of various operational factors to uncertainties in MP

enumeration. Results from the modelling study were employed to develop guidelines for reducing MP data uncertainty.

- Developing mass balance models: The study aimed to devise methods for accurate quantification of MP mass, enabling the establishment of mass balance models in the primary treatment process at the Kitchener WWTP.
- Assessing recovery differences: The influence of MP size range and sample types (wastewater and sludge) on recovery rates was examined. Furthermore, the impact of differential recoveries on concentration estimates and subsequently the completion of count and mass balance models was investigated.

1.3 Significance

Enhanced MP identification, reduced data uncertainty, and reliable mass balance models provide multiple benefits. Each of these three separate, yet interconnected, dimensions significantly contribute towards a comprehensive understanding of the efficacy of varying stages within the wastewater treatment process in removing MPs. This understanding subsequently aids in deciphering the mechanisms underlying MP removal, thereby paving the way for the optimization of processes and the innovation of more efficient methodologies aimed at the mitigation of MPs. Further, these developments enhance the understanding of the ecological risks posed by WWTPs and foster comparative analyses and standardization across diverse studies and environments, thus improving the overall robustness of MP research in WWTP contexts.

1.4 Thesis structure

This dissertation is structured into six distinct chapters. Chapter 1 introduces the research problems and delineates the primary objectives of this study. Chapter 2 presents a literature review on MPs in WWTPs, emphasizing accurate MP identification, understanding data uncertainty, and the development of mass balance models. Chapter 3 presents a study that aims to enhance MP identification through leveraging of deep learning to address the challenges associated with spectral classification in conventional library search methods. In Chapter 4, the focus shifts to the

development of an uncertainty model that describes errors in MP enumeration. This chapter also includes the implementation of this model to explore the influence of various operational factors on the uncertainties in MP enumeration. Chapter 5 details the establishment of both count and mass balance models in the primary treatment phase at a local WWTP and explores how differential recovery considerations can enhance concentration estimates and the closure of balance models. Finally, Chapter 6 concludes the thesis by summing up the key findings and providing recommendations for future research.

Chapter 2. Literature review

2.1 Leveraging deep learning Variation of MP spectra

2.1.1 Identifying MPs using FT-IR technology

While early studies leveraged visual sorting for the recognition of MPs in environmental samples (Unice et al., 2013; Magnusson and Norén, 2014; Nor and Obbard, 2014), contemporary research predominantly utilizes spectroscopic methodologies for the accurate identification of MPs. Spectroscopic techniques, such as FT-IR spectroscopy, offer considerable advantages over visual sorting in the detection and analysis of MPs (Shim et al., 2017; Koelmans et al., 2019; Sun et al., 2019). The subjectivity and potential for misidentification inherent to visual sorting are mitigated by the unique FTIR spectral signatures identified by spectroscopy, enhancing accuracy in discerning MPs from natural materials. Furthermore, FTIR spectroscopic methods can detect MPs much smaller than the limit of the human eye, which generally struggles with particles less than 1 mm in size, thereby significantly improving sensitivity. These techniques facilitate not only the confirmation of MPs presence but also the identification of the specific polymer type via spectra fingerprint, providing valuable information for understanding MPs' sources and environmental impacts. The use of FPA micro-FT-IR imaging significantly improves the efficiency of detecting MPs in environmental samples because it simultaneously collects multiple spectra of MPs on a surface (Mintenig et al., 2017; Simon et al., 2018; Bergmann et al., 2019; Chand et al., 2021).

Correct FT-IR spectra classification is the key step to achieve accurate identification of MPs. The traditional methodology for this purpose involves the implementation of a library search strategy where the spectrum of interest is contrasted with individual spectrum within the library (Smith, 2011). This comparative process typically involves the computation of a similarity metric or a distance measure between the unknown spectrum and each spectrum of the library. Such similarity metrics can include correlation coefficients, Euclidean distances, or alternative statistical measures. These resultant matches are then systematically ranked in accordance with their respective similarity measures, whereby the library spectrum exhibiting the highest similarity to the unknown spectrum is accorded the premier rank, followed by others in decreasing order of similarity. Nonetheless, this matching methodology is susceptible to inaccuracies due to the fact that reference spectra within these libraries are collected from virgin plastic, while the spectra from

environmental MPs are more complex. The complexity is caused by the presence of additives (Hahladakis et al., 2018; Campanale et al., 2020), surface modifications encompassing chemical, physical, or biological factors that modify the chemical composition of MPs' surfaces (Andrade et al., 2019; Miranda et al., 2021), adsorbed pollutants, and the formation of biofilms on the MPs' surfaces (Harrison et al., 2018; Kinigopoulou et al., 2022). The variation inherent in the spectra of MPs poses a challenge for library search processes, resulting in a diminished similarity metric and subsequently leading to errors in identification. As such, there is a need for the establishment of robust search strategies that account for these spectral variations, which helps to achieve a more accurate identification of MPs within environmental samples.

2.1.2 Variation of MP spectra

The majority of MPs in environmental samples are not composed solely of virgin resins (Campanale et al., 2020). To alter their visual aspects such as color and transparency, and to improve their functional characteristics like electrical resistance or durability, additives are frequently employed in the creation of plastics. These additives can range from dyes and plasticizers to fillers, antioxidants, ultraviolet (UV) stabilizers, lubricants, and flame retardants (Hahladakis et al., 2018). Significant concentrations of additives have been identified in environmental MPs, as described by Zhang et al. (2018) who reported an organophosphorus ester concentration of 84,595.9 ng/g^{-1} within MPs collected from costal beaches. Consequently, the composition of MPs can be influenced by the type of base polymer and the type and concentration of additives utilized. Considering this, it is reasonable to anticipate that the inclusion of additives in MPs would alter their FT-IR spectra, and this modification could potentially introduce ambiguity when comparing these spectra with those found in spectral libraries. Hence, it is essential to rigorously explore the extent to which the presence of additives may cause variation in MP spectra, and to develop strategic methodologies to account for such variations if the matching between MP spectra and standard spectral libraries is influenced by the additives present within the MPs.

MPs present in environmental samples may undergo substantial surface alterations due to weathering that can stem from physical, chemical, and biological processes (Ter Halle et al., 2017; Waldman and Rillig, 2020). Biological weathering, for example, involves the action of organisms like bacteria and fungi, which can colonize the surface of MPs and contribute to their breakdown. The enzymes produced by these organisms can result in oxidation or break down of polymer chains

in the plastic, and such weathering can lead to changes in the molecular structure. Consequently, weathering causes the formation of carbonyl groups (Miranda et al., 2021) and halogen bonds (Kinigopoulou et al., 2022; Liu et al., 2021), which inevitably affect the FT-IR spectra of MPs due to formation of new bands at 3360–3240 cm^{-1} (hydroxyl bond), 1640 cm^{-1} (C = O groups), and 1100 cm^{-1} (C-O bonds) as observed by (Andrade et al., 2019). In light of these surface modifications that can potentially influence the correspondence between MP spectra and standard spectral libraries, the development of methods to appropriately address these variations is of significant importance for accurate MP identification.

The surfaces of MPs in environmental samples can be contaminated with pollutants or colonized by biofilms. Multiple studies have highlighted the role of MPs as carriers for a range of contaminants, including metals (Tunali et al., 2020; Selvam et al., 2021), PFAS (Scott et al., 2021; Enyoh et al., 2022), and pathogens (Kirstein et al., 2016; Wu et al., 2019). Moreover, biofilms supported by MPs can provide a habitat for pathogens (Harrison et al., 2018; Wu et al., 2019). While the pre-treatment of MPs from environmental samples conventionally involves various purification steps like Fenton oxidation, enzyme purification, and density separation (Loder et al., 2017; Hurley et al., 2018; Lavoy and Crossman, 2021), it is improbable that these substances adhering to the surfaces will be entirely eliminated. Thus, the substances adhering to the surfaces of MPs could significantly contribute to the spectral response, leading to deviations in the spectra when compared to the corresponding ones in a library. This scenario necessitates the development of strategies to accommodate spectral variations arising from these impurities on the surface.

The variation in thickness across the planar regions of particles can also contribute to spectral variation. This form of variance is pertinent to using FPA micro-FT-IR imaging in transmission mode for imaging MPs within the size range of 20-500 μm (Primpke et al., 2017; da Silva et al., 2020). When imaging MPs in transmission mode, the thickness of MPs corresponding to each pixel on the FPA detector influences the path of the IR beam (Zhu et al., 2021). Consequently, this alters the intensity of IR absorbance at the respective pixel. In regions of low thickness, such as the edges of particles where the thickness measures only a few microns, peak absorbance can be faint, thereby complicating the identification of these peripheral pixels (da Silva et al., 2020). In the case of thicker microplastic cross-sections, for instance, 200 μm or greater, the peak correlating with C-H bond can become broadened, causing a deviation in the spectral shape from that of

reference spectra in library (Zhu et al., 2021). Consequently, there is a need to develop strategies that effectively address the spectral variance related to the thickness of MPs. Such measures are essential for enhancing the utility of FPA-based FTIR imaging for accurate identification of MPs.

In summary, the variations observed in MPs can stem from multiple sources, including additives, surface modifications, adhered impurities, and variations in thickness across the region traversed by the IR beam. When employing library search methods for matching MPs spectra, all these variations can lead to a reduction in the correlation coefficients between MP spectra and the corresponding virgin plastic spectra in conventional libraries. A robust spectral classification strategy ought to not only identify MPs based on spectra derived from virgin plastics, but also effectively classify these MP spectra amidst their inherent complexities. To the best of our knowledge, no studies have systematically addressed the challenge of MP identification considering these spectral variations.

2.1.3 Leveraging deep learning in addressing variation in MP spectra

Deep learning models exhibit great potential in addressing intra-class variation owing to their proficiency in acquiring intricate and non-linear patterns through extensive data analysis (Goodfellow et al., 2017). Intra-class variation pertains to the distinctions that manifest within a singular class or category. To illustrate, within the class denoted as "dog," substantial variances emerge in aspects such as breeds, sizes, colors, and poses amongst diverse dog images.

Deep learning models offer notable efficacy in addressing intra-class variation due to several reasons (LeCun et al., 2015a; Goodfellow et al., 2017). Firstly, these models possess the ability to automatically learn hierarchical representations or features from raw data. Constructed with multiple layers of interconnected neurons, deep learning models progressively acquire abstract and informative features at each layer, thereby capturing intricate patterns and variations within a class. Moreover, deep learning models excel in capturing non-linear relationships between input features and output labels, making them adept at modeling and capturing the complex relationships and non-linear mappings often associated with intra-class variation. Additionally, the large-scale training of deep learning models proves advantageous, as exposing them to extensive datasets enables enhanced generalization and improved handling of intra-class variations. By training on a diverse range of data instances within a class, deep learning models become proficient in identifying common patterns while simultaneously recognizing and accommodating the variations

that exist within the class. Throughout this thesis, the terms "recognizing" and "identifying" of MPs are utilized interchangeably, with both denoting the process of detecting MPs through the correct classification of their associated spectra. The efficacy of deep learning in addressing intra-class variation has been substantiated through numerous studies focusing on image classification (Andrei et al., 2015; Makantasis et al., 2015; Poria et al., 2015). However, no study has leveraged deep learning techniques to tackle the aforementioned spectral variation that is required to achieve enhanced MP identification. As a consequence, there is considerable potential to employ deep learning approaches to address the inherent complexity of MP spectra.

There is a burgeoning interest in harnessing the potential of machine learning models to advance spectral classification and MP detection. As is reviewed in Table 2-1, different machine learning models have been explored for this purpose, encompassing K-Nearest Neighbour (KNN), support vector machine (SVM), random forest decision, Partial least squares discriminant analysis (PLS-LA), Long short-term memory networks (LSTMs). These investigations reveal that the utilization of machine learning models can enhance the accuracy of spectral classification, surpassing the efficacy of traditional library search approaches. Deep learning models are a type of superior machine learning models(Goodfellow et al., 2017), while the utilization of deep learning models for spectral classification remains relatively unexplored. Moreover, there has been little effort regarding the capacity of these machine learning models to effectively address spectra that have undergone modifications due to additives, weathering, the presence of pollutants, and variations in the thickness of MPs. Consequently, there exists a compelling need to delve into the potential of deep learning models in handling these complex spectral variations and improve MP identification.

Table 2- 1 Current Studies Leveraging Machine Learning Models for MP Identification via Spectra Classification

	Machine learning models	Deep learning model?	Performance on varied MP spectra?
Kedzierski et al. (2019)	K-Nearest Neighbour	No	No
Bianco et al. (2020)	support vector machine	No	No
Zhao et al. (2018)	Support Vector Machine	No	No
Hufnagl et al. (2021)	Random forest	No	No
da Silva et al. (2020)	Partial least squares discriminant analysis	No	No
Back et al. (2022)	Random Forests, Support Vector Machine Logistic Regression, K-Nearest Neighbors Decision Trees, Gaussian Naive Bayes,	No	No
Michel et al. (2020)	Support Vector Machine K-Nearest Neighbors Linear Discriminant Analysis	No	No
Massarelli et al. (2021)	K-Nearest Neighbour	No	No
Qiu et al. (2023)	Support Vector Machine Long short-term memory networks	No	No

2.1.4 Section Summary

To sum up, the usage of FPA-based micro-FT-IR spectroscopy for the identification of MPs in environmental samples faces challenges due to spectral variance. This variance arises from factors such as additives, weathering, biofilm or pollutant attachment, and variation in the thickness of the MPs. While deep learning exhibits promising potential in managing spectral variances, its application for addressing these variances remains unexplored. Consequently, there is a pressing need to investigate the application of deep learning for improving MP identification by effectively managing these spectral variances.

2.2 Modelling uncertainties in MP enumeration

2.2.1 Existing uncertainty model and comparability with errors in MP enumeration

The existing literature includes a probabilistic model that accounts for uncertainties in discrete particle enumeration. Emelko et al. (2010) conducted a comprehensive study regarding uncertainties in enumeration of discrete particles, where they categorized the errors associated with enumeration as concentration heterogeneity, random sampling error, random analytical error, non-constant recovery, and counting error. They established a Beta-Poisson model to describe these errors with assumptions that random sampling error is Poisson-distributed, analytical error is binomially distributed, and non-constant analytical recovery is beta-distributed. This model assumes absence of concentration heterogeneity, and treats counting errors as a constituent of the analytical error, which is implicitly incorporated within the analytical recovery data. Given that MPs are also discrete particles, this model serves as a valuable starting point for constructing an MP uncertainty model. Building upon the foundation established by Emelko et al. (2010), a refined a probabilistic model specifically tailored to address uncertainties in MP enumeration can be developed.

Nevertheless, a critical examination of the assumptions is necessary before extending the existing model to describe the errors associated with MP enumeration. Though concentration heterogeneity (Cowger et al., 2020), random sampling error (Morgado et al., 2022; De Frond et al., 2023), random analytical error (Halbach et al., 2021; Way et al., 2022), non-constant recovery (Konechnaya et al., 2020; Mari et al., 2021), and counting error(Brandt et al., 2021) have also been reported to influence MP analysis, the compatibility of these errors in MP enumeration with the assumptions of the existing model remains largely unexamined. For instance, an assumption in the existing model is that all particles in the sample have an equal probability of being observed or lost. This assumption is in conflict with recent MP studies that indicate the recovery of MPs is significantly influenced by factors such as size (Simon et al., 2018; Konechnaya et al., 2020), shape (Halbach et al., 2021; Way et al., 2022), and polymer type (Mari et al., 2021). Consequently, it is important to rigorously examine the sources of error associated with each step of MP analysis and critically evaluate their compatibility with the existing model. If incompatibilities exist, modifications should be made to the existing model.

2.2.2 Uncertainties in MP concentration estimates caused by operating factors

The number of replicates utilized during the sample collection process in MP studies is inconsistent amongst multiple studies, which primarily stems from the lack of standardized protocols for MP sampling. For instance, in some studies, sample collection has relied on a single sample (Carr et al., 2016; Mintenig et al., 2017; Ziajahromi et al., 2017), whereas other investigations have utilized a much larger number, ranging from 7 to 10 replicates (Bruge et al., 2020; Bauerlein et al., 2023). This large variation in number of replicates will lead to differing degrees of uncertainty in enumeration-based concentration estimates (Schmidt et al., 2010). A review of current literature showed that there is absence of focused research aiming to quantify the uncertainties in MP data associated with the number of replicates, and there are no established guidelines suggesting an optimal number of replicates to reduce uncertainty in MP analysis. This gap underpins the need for more investigation regarding the impact of replicates of MP sampling on uncertainties.

Early microplastic research often categorized all MPs collectively (Nor and Obbard, 2014; Michielssen et al., 2016), without taking into account their variations in terms of size and shape. This generalized approach significantly contrasts with more recent studies (Ziajahromi et al., 2017; Magni et al., 2019; Bruge et al., 2020; Mintenig et al., 2020) which have recognized and incorporated not only various size groups but also distinguishing between microplastic fibers and particles in their enumeration procedures. However, despite these advancements, the extent to which the cumulative vs separate counting of MPs introduces uncertainties into the enumeration process remains an unresolved issue. Hence, the uncertainties caused by ignoring of MP distinctions warrants further study.

Non-constant recovery and differential recovery of MPs have often been overlooked in prior studies investigating MPs in WWTPs . A few recent studies (Xu et al., 2019) have recognized the importance of distinguishing MPs based on their size and shape. However, these studies typically conducted a single recovery test using one category of MPs and then applied the resulting recovery universally to all MPs in all samples. This approach overlooks the potential variability in analytical recovery among replicate samples as well as the differential recovery that associated with the size and shape of the MPs. Some other studies which considered distinctions of MPs acknowledged the non-constant recovery by performing replicates of spiking tests (Long et al., 2019; Lv et al., 2019). However, these studies only spiked MPs in a specific category and use the non-constant

recovery from this category to correct for concentrations for all categories. There is, therefore, still an open question regarding the extent of uncertainties introduced by these oversights in the enumeration of MPs.

In summary, as is reviewed in Table 2-2, a variety of operational factors could introduce uncertainties in concentration estimates of MPs. These factors include number of replicates, ignorance of distinctions associated with size and shape, ignorance of non-constant recovery and differential recovery. There is an absence of studies examining how much uncertainties these approaches will introduce. Therefore, a clear need exists to quantitatively assess these uncertainties in order to accomplish a rigorous and accurate understanding of MP enumeration data.

Table 2- 2 Uncertainties in Microplastic (MP) Concentration Estimate Caused by Operating Factors Reflected in Recent MP Studies

Possible source of uncertainties	Studies	Approaches used for MP concentration estimates
Number of replicates	(Nor and Obbard, 2014)	Single replicate
	(Mintenig et al., 2017)	Single replicate
	(Ziajahromi et al., 2017)	Single replicate
	(Bruge et al., 2020)	7 Replicate
	(Bauerlein et al., 2023)	10 Replicate
Counting collectively vs. Counting separately	(Nor and Obbard, 2014)	Counting MPs collectively
	(Michielssen et al., 2016)	Counting MPs collectively
	(Ziajahromi et al., 2017)	Count MPs by categories
	(Magni et al., 2019)	Count MPs by categories
	(Bruge et al., 2020)	Count MPs by categories
Ignoring non-constant recovery and differential recovery	(Xu et al., 2019)	Ignoring both non-constant recovery and differential recovery
	(Long et al., 2019)	Acknowledge non-constant recovery and but ignore differential recovery
	(Lv et al., 2019)	Acknowledge non-constant recovery and but ignore differential recovery

2.2.3 Bayesian uncertainty inference coupled with MCMC

The robust and efficient approach of Bayesian analysis, coupled with MCMC methods, has led to its widespread adoption in the field of uncertainty quantification, offering advantages beyond the capabilities of conventional models (Nunes et al., 2021; Takeshita et al., 2022). Unlike conventional methods, Bayesian analysis provides a complete characterization of uncertainty through the full posterior distribution, offering a comprehensive understanding of the range of plausible parameter values. This allows for more reliable uncertainty quantification compared to conventional methods that often provide only point estimates. MCMC methods play a crucial role in the implementation of Bayesian analysis due to their ability to efficiently explore and sample from complex posterior distributions (Andrieu et al., 2003; Andrieu and Thoms, 2008). Therefore, it has proven effective to employ Bayesian analysis with MCMC methods to implement the model to quantify uncertainties associated with MP enumeration, once the probabilistic model that describes the random error in MP analysis has been developed.

The application of Bayesian analysis coupled with MCMC methods has demonstrated its effectiveness in recent studies on MPs. Vermeiren et al. (2021) employed Bayesian regression and observed an exponential decrease in MP abundance with increasing grain size in beach samples. de Souza Machado et al. (2019) utilized Bayesian inference to quantify credible intervals of parameters representing the impact of MPs on soil environment and root traits. Additionally, Covernton et al. (2021) employed Bayesian linear mixed models to investigate the influence of geographic, methodological, and ecological factors on reported MP concentrations. Despite these advancements, the specific application of Bayesian inference to quantify the extent of uncertainties in MP enumeration resulting from various operational factors remains unexplored. Consequently, there exists a critical need to conduct a study focusing on this aspect.

2.2.4 Section Summary

Overall, in order to enhance our understanding of and mitigate uncertainties associated with MP enumeration data, there is a need to develop a probabilistic model that accounts for the inherent variability in MP enumeration. This can be accomplished by conducting a critical examination of the assumptions made by (Emelko et al., 2010) in an existing model, evaluating their compatibility with the errors in MP enumeration. As necessary, the model can be refined through the modification or addition of assumptions. Once the model has been developed, Bayesian analysis

coupled with MCMC methods can be employed to implement it and evaluate the contribution of various operational factors to the uncertainties in MP enumeration. This integrated approach would provide valuable insights into the sources and magnitude of uncertainties, facilitating the development of strategies for improving the accuracy and reliability of MP enumeration data.

2.3 Count and Mass balance models of MPs in considering differential recovery

2.3.1 Mass balance models of MPs in WWTPs

Count balance models are vital in investigating MPs in WWTPs. As reviewed in Table 2-3, numerous studies have assessed MPs count concentrations in WWTPs all over the world. All these studies have developed count balance models within the treatment process, with some studies focused on concentrations in influent and final effluent (e.g. Dris et al. (2015), Mason et al. (2016)) while others focused MP concentrations across various stages of the treatment process (e.g. Carr et al. (2016), Ziajahromi et al. (2017)). These count balance models significantly contribute to the understanding of the fate and transport of MPs within the plant. Observations from the studies in Table 2-3 indicate that the MP removal efficiency throughout the complete treatment process exceeds 90% in all cases, implying high efficiency in MP removal in WWTP. Despite the high removal efficiency, the residual MP release via effluent into the receiving water remains a matter of concern due to the high flows. Hence, the count-based MP concentrations can be used to assessing potential ecological risks of MP pollution imposed by WWTPs. In summary, count balance models of MPs facilitate an understanding of MP dynamics, understanding of MP discharge into receiving waters, evaluation of the potential ecological risks, and provide a foundation for comparing outcomes across diverse studies.

However, it has been suggested that count balance models should be complemented by mass balance models to achieve more insights regarding MPs in WWTPs. Owing to the brittle nature of MPs (Andrady, 2011; Enfrin et al., 2019), the fragmentation of MPs could cause overestimation of MP concentrations to varying degrees (Simon et al., 2018; Lv et al., 2019). Mass, opposed to particle number, is a conserved unit which is independent of the physical and chemical processes to which the MP is exposed. Hence, there is a need to establish mass balance models for MPs in WWTPs, as these models offer insights into MP fragmentation (Poulain et al., 2018). Also, mass balance models estimate the total mass of MPs entering, exiting, and transforming within WWTPs (Chen et al., 2022), revealing the overall microplastic load on mass basis (Chen et al., 2022) and help assess weight-based ecological impacts (Redondo-Hasselerharm et al., 2018; Zhu et al., 2019). Upon reviewing the data presented in Table 2-3, it is apparent that only a limited number of studies

(Simon et al., 2018; Chand et al., 2021; Rasmussen et al., 2021) have supplemented count-based assessments with mass concentration measurements. Notably, there exists merely a single study (Rasmussen et al., 2021) applying a mass balance model within the context of WWTPs. This paucity of studies using mass balance models underscores the necessity to develop and utilize it within WWTPs, a step which would facilitate further insights into MP behaviour and contamination caused by MPs.

The establishment of mass balance models hinges on the precise estimation of the mass of MPs within samples. Pyrolysis coupled with gas chromatography and mass spectrometry (Py-GC-MS) has been harnessed for this analytical endeavor (Fries et al., 2013; Kirstein et al., 2021). In this procedure, the sample undergoes decomposition via heating, thereby yielding smaller molecules that are amenable to mass spectrometric evaluation and, consequently, permit the estimation of the MPs' mass. Nonetheless, this technique necessitates an intricate process of sample preparation and is predicated upon advanced technical expertise and sophisticated instrumentation, which may not be suitable for routine analyses owing to its inherent complexity and associated costs. Moreover, pyrolysis is inherently destructive, which imposes constraints on further analysis of the same sample particularly with respect to size and shape - two crucial parameters in MPs studies. Consequently, application of Py-GC-MS for mass quantification of MPs demands mindful consideration considering its limitations.

An alternative methodology for estimating the mass of MPs involves volumetric quantification based on images, subsequently multiplied by the appropriate polymer density (Simon et al., 2018). In this prior study this approach assumeds all MP particles to be ellipsoidal with a ratio of the longest axis: minor axis: thickness as 1: 0.66: 0.44, and fibers to be cylindrical with a 40% void fraction, with longest axis and diameters manually measured from images. Nevertheless, this technique is potentially error-prone due to the varied shapes of MPs such as fragments, films, foams, spheres, and pellets (Sun et al., 2019), rendering the assumptions of ellipsoidal and cylindrical shapes oversimplified. Despite its non-destructive nature and the initial direction it provides, this image-based volumetric quantification method requires the incorporation of more sophisticated algorithms for enhanced accuracy. Therefore, the development of improved methods for quantifying the volume of MPs based on sample images is a pressing need, necessitating further

research to devise refined approach which accurately represents the diverse morphologies of MPs in environmental samples.

In summary, there is a need for advancing traditional wastewater treatment plant (WWTP) studies on MPs, which are predominantly conducted on a count basis, by instituting mass balance models. These mass balance models proffer indispensable insights into the mass of MPs, fragmentation processes, and ecological impacts—elements that cannot be exclusively elucidated through count-based studies. Given the absence of an accurate method for precise mass estimation of MPs, prioritizing the development of mass quantification techniques becomes paramount. The image-based method emerges as a promising solution, contingent upon the development of sophisticated algorithms capable of accurately estimating the volume of MPs.

2.3.2 Improve data reliability by considering differential recovery

Recent studies have indicated that the recovery of MPs was strongly affected by the size. Recovery of large MPs (e.g. MPs large than 300 μm) was reported to exceed 90% (Simon et al., 2018; Konechnaya et al., 2020; Way et al., 2022) while recovery of small MPs (e.g. MPs smaller than 100 μm) was sometimes lower than 60% (Halbach et al., 2021; Way et al., 2022). Researchers attributed the low recovery of small MPs to several reasons. Firstly, characterized by a larger surface-area-to-volume ratio compared to larger counterparts, small MPs can demonstrate increased adhesion to glass vessels, filters, or extraction devices, potentially leading to diminished recovery (Sun et al., 2021). In addition, small MPs, with varying buoyancy or settling velocities, may settle differently during density-based separation methods (Laursen et al., 2022). Moreover, small MPs are more prone to aggregate with each other or other materials (Li et al., 2022), which could potentially obstruct their recovery. Taking into account the size-dependent variability in recovery rates, it can be postulated that concentrations derived utilizing such differential recovery methods would significantly diverge from those obtained using a constant recovery approach. However, as illustrated in Table 2-3, all published MP studies in WWTPs have not accounted for this differential recovery to enhance the accuracy of concentrations, potentially introducing substantial errors. Therefore, there is an evident need to incorporate these size-related differences in recovery to achieve more accurate results in quantitative studies of MPs, and this necessity becomes more pronounced when the objective is to establish mass balance models in WWTPs.

Studies regarding how sample types from WWTP impact the recovery of MPs are absent. The composition of the matrix exhibits substantial variability among influent, sludge, and effluent streams. The influent is typically rich in particulate matter and organic material, while sludge is densely concentrated with organic and inorganic matter (Li et al., 2018). These compositional distinctions could potentially introduce complexities into the separation and recovery of MPs during analysis due to factors such as aggregation or adsorption (Konechnaya et al., 2020). It has been noted that the concentrations of MPs fluctuate across raw influent, sludge, and effluent samples, with the former two generally presenting higher concentrations (Li et al., 2018; Corradini et al., 2019). This could escalate the aggregation and adhesion of MPs to surfaces or other materials, subsequently influencing their recovery. Addressing the knowledge deficit pertaining to the influence of WWTP sample type on the recovery of MPs necessitates a systematic conduction of spiking tests. If the impact is as substantial as presumed, the integration of differential recovery is imperative to ensure the accuracy of MP concentrations in WWTP samples and to enhance the development of mass balance models.

There may exist a potential divergence between eye-based and instrument-based recovery of MPs. A variety of studies (Mintenig et al., 2017; Simon et al., 2018; Chand et al., 2021) investigating MPs in WWTPs have implemented automatic instrument-based quantification while employing eye-based recovery techniques for concentration corrections. Herein instrument-based counting denotes the usage of spectroscopy instruments for sample mapping, along with image analysis algorithms for automated MP enumeration, while visual sorting and subsequent individual spectroscopic confirmation do not fall under this category. It is postulated that instrument-based recovery could be more susceptible to bias due to mistaken identification of native MPs with similar characteristics as the spiked ones, a conjecture that takes into consideration the underlying logic of the image analysis (Primpke et al., 2017) procedure. Also, image-based recovery will result in a potential underestimation when closely located spiked particles are perceived as a single unit (Mathworks, 2023). Despite this, current literature lacks comprehensive examination of the disparity between instrument-based and eye-based recovery. Given the prevailing trend towards instrument mapping for rapid and automated MP quantification, it is imperative to investigate the differences between eye and instrument-based recoveries. If such a difference exists and is significant, it needs to be accounted for to ensure accurate MP quantification particularly when samples are automatically analyzed by an instrument.

In summary, the differential recovery associated with size and sample type could potentially result in significant inaccuracies in the quantitative analyses of MPs in WWTPs, as well as in the establishment of mass balance models. Furthermore, the disparity between eye-based and instrument-based recovery should be acknowledged if MP quantification is conducted using an instrument. Addressing these variances is crucial to attaining a more accurate representation of MP concentrations, ultimately contributing to a more nuanced understanding of MPs in wastewater treatment systems.

2.3.3 Count and mass balance models of MPs in primary wastewater treatment

The establishment of count and mass balance models within WWTPs should start with the simplest scenario, which is the primary treatment stage. This choice is motivated by multiple reasons. The simple sedimentation physical process involved in primary treatment is comparatively more straightforward to model when contrasted with the intricate biological and chemical processes encountered in secondary and tertiary treatment stages (Henze et al., 2008; Grady Jr et al., 2011) . Furthermore, primary treatment exhibits well-defined inputs (e.g. influent, wasted activated sludge) and outputs (i.e. primary sludge and primary effluent), facilitating the establishment of balance models by quantifying the inflow and outflow of MPs within the system in a simplified way. Additionally, primary treatment often demonstrates significant removal of MPs (Murphy et al., 2016; Magni et al., 2019), thereby providing valuable insights into the effectiveness of this particular process. Lastly, comprehending the fate and transport of MPs in the primary treatment stage lays a foundation for assessing their behavior in subsequent treatment stages, thereby serving as a starting point for the development of more intricate models. In conclusion, the primary treatment stage offers a favorable opportunity for establishing count and mass balance models aimed at quantitative studies of MPs.

The literature reviewed in Table 2-3 highlights the need of count and mass balance models on the primary wastewater treatment stage. Although multiple studies have investigated the removal of MPs across the treatment plant, there is a noticeable scarcity of specific MP concentration data pertaining to the primary sludge and primary effluent. Consequently, the quantitative models developed for this process are currently deficient. Therefore, it becomes imperative to develop count balance and mass balance models tailored specifically to the primary treatment stage. Doing so will enable a more comprehensive understanding of the fate and transport of MPs within this

treatment stage, bridging the existing knowledge gap and enhancing our understanding of MP behavior in wastewater treatment processes.

2.3.4 Section summary

The comprehensive review of studies in WWTP indicates that while count balance investigations are relatively abundant, studies focusing on mass balance are limited due to the absence of effective mass quantification methods. Thus, it is imperative to develop robust mass quantification techniques and employ them in mass balance model studies. Additionally, the literature highlights the significance of considering the differential recovery associated with size and sample type, as this consideration can improve the estimation of MP concentrations. Consequently, incorporating these differences into the balance models becomes crucial. Given its straightforward processes and the absence of quantitative models specifically focused on this treatment stage, the primary wastewater treatment should be selected as the initial point for establishing such balance models.

Table 2- 3An Overview of Microplastic Studies in WWTPs: Emphasizing Quantitative Model Development, Recovery Practices, and Availability of Primary Treatment Microplastic Data

Study	Count balance model	MP Removal on count basis	Mass balance model	Recovery practice	Special focus on primary treatment?
Magnusson and Norén (2014)	Yes	Higher than 90%	No	Constant recovery	No data for primary sludge and primary effluent
Dris et al. (2015)	Yes		No	Constant recovery	No data for primary sludge and primary effluent
Carr et al. (2016)	Yes		No	Constant recovery	No data for primary sludge and primary effluent
Mason et al. (2016)	Yes		No	Constant recovery	No data for primary sludge and primary effluent
Michielssen et al. (2016)	Yes		No	Constant recovery	No data for primary sludge
Murphy et al. (2016)	Yes		No	Constant recovery	No data for primary sludge
Sutton et al. (2016)	Yes		No	Constant recovery	No data for primary sludge and primary effluent
Dyachenko et al. (2017)	Yes		No	Constant recovery	No data for primary sludge and primary effluent
Leslie et al. (2017)	Yes		No	Constant recovery	No data for primary sludge and primary effluent
Mintenig et al. (2017)	Yes		No	Constant recovery	No data for primary sludge
Talvitie et al. (2017a)	Yes		No	Constant recovery	No data for primary sludge
Talvitie et al. (2017b)	Yes		No	Constant recovery	No data for primary sludge and primary effluent
Ziajahromi et al. (2017)	Yes		No	Constant recovery	No data for primary sludge and primary effluent
Gies et al. (2018)	Yes		No	Constant recovery	No data for primary sludge and primary effluent
Lares et al. (2018)	Yes		No	Constant recovery	No data for primary sludge and primary effluent
Simon et al. (2018)	Yes		Supplemented count-based data with mass-based data but did not establish mass balance models	Reported differential recovery associated with size but applied constant recovery in concentration calculation	No data for primary sludge and primary effluent
Blair et al. (2019)	Yes		No	Constant recovery	No data for primary sludge
Conley et al. (2019)	Yes		No	Constant recovery	No data for primary sludge
Long et al. (2019)	Yes		No	Constant recovery	No data for primary sludge
Lv et al. (2019)	Yes		No	Constant recovery	No data for primary sludge
Magni et al. (2019)	Yes		No	Constant recovery	No data for primary sludge and primary effluent
Yang et al. (2019)	Yes		No	Constant recovery	No data for primary sludge and primary effluent
Zhang et al. (2020)	Yes		No	Constant recovery	No data for primary sludge
Ben-David et al. (2020)	Yes		No	Constant recovery	No data for primary sludge
(Rasmussen et al., 2021)	Yes		Yes	Constant recovery	No data for primary sludge and primary effluent

2.4 Summary and recommendations

This review provides an overview of MPs in WWTPs, focusing specifically on MP identification, data uncertainty, and the advancement of count and balance models. Drawing from the literature, the following knowledge gaps have been identified:

- The precise identification of MPs utilizing FPA micro-FT-IR spectroscopy presents challenges due to the spectral variance of environmentally-sourced MPs which is resulted from additives, weathering, and surface impurities, and thickness variation.
- The random errors intrinsic to each step of MP analysis have not been mathematically modeled.
- The contributions of various operational factors to uncertainties in MP enumeration remain largely unexplored. Consequently, the field lacks guidelines that would reduce uncertainties within wastewater and sludge samples.
- Methodologies for accurately quantifying the mass of MPs are largely absent, impeding the development of mass balance models within the context of WWTPs.
- The impact of MP size range and sample type on the recovery of MPs in the context of WWTPs remains ambiguous.
- The potential for differential recovery associated with size and sample type to enhance the estimation of MP concentrations, and consequently, to improve the closing of MP count and mass balance models, remains to be fully explored.

To enhance the understanding of fate and transport of MPs in WWTPs, future studies should focus on the following subjects;

- Leverage deep learning models for enhanced MP identification via FTIR spectra recognition, considering deep learning's great potential in addressing spectral variances
- Extend an existing uncertainty model to describe random errors in MP enumeration. This can be done by critically examining the compatibility of errors in MP analysis with the assumptions with the previous model, and refine the model by modifying or adding assumptions as necessary,

- Evaluate how various operational factors contribute to the uncertainties in MP enumeration by implementing the newly developed model. The results of these model evaluations could form the basis for guidelines that would promote a more accurate and rigorous understanding of MP data.
- Develop methods for accurate estimation of MP mass and subsequently apply these methods for establishing mass balances in WWTPs.
- Investigate the impact of MP size range and sample type on recovery by performing spiking tests, and apply this differential recovery for achieving more accurate concentration estimates as well as improved mass balance models in WWTPs.

Chapter 3 Leveraging deep learning for automatic recognition of microplastics (MPs) via focal plane array (FPA) micro-FT-IR imaging

Abstract

The fast and accurate identification of MPs in environmental samples is essential for the understanding of the fate and transport of MPs in ecosystems. The recognition of MPs in environmental samples by spectral classification using conventional library search routines can be challenging due to the presence of additives, surface modification, and adsorbed contaminants. Further, the thickness of MPs also impacts the shape of spectra when FTIR spectra are collected in transmission mode. To overcome these challenges, PlasticNet, a deep learning convolutional neural network architecture, was developed for enhanced MP recognition. PlasticNet was initially trained, validated and tested using 8,000+ spectra of virgin plastics, and was retrained by adding a limited number of more complex spectra to the training pool to test whether the model's performance in recognizing complex spectra from outside the training pool could be enhanced. Once trained with spectra of virgin plastic, PlasticNet successfully classified 11 types of common plastic with an accuracy higher than 95%. The errors in identification as indicated by a confusion matrix were found to be caused by edge effects, molecular similarity of plastics, and the contamination of standards. When PlasticNet was trained with spectra of virgin plastic it showed good performance (92%+) in recognizing spectra that had increased complexity due to the presence of additives and weathering. The re-training of PlasticNet with more complex spectra further enhanced the model's capability to recognize complex spectra. PlasticNet was also able to successfully identify MPs despite variations in spectra caused by variations in MP thickness. When compared with the performance of the library search in identifying MPs in the same complex dataset collected from an environmental sample, PlasticNet achieved comparable performance in identifying PP MPs, but a 16.9% improvement in identifying PE MPs. PlasticNet has the potential to become a standard approach for rapid and accurate automatic recognition of MPs in environmental samples analyzed by FPA FT-IR imaging.

3.1 **Introduction**

The ubiquitous presence of microplastics (MPs) and their potential threats to aquatic and human health have become a growing public concern (Ziccardi et al., 2016). WWTPs have been identified as one of the points of entry for MPs into the aquatic environment (Mintenig et al., 2017; Simon et al., 2018; Blair et al., 2019; Zhang et al., 2020). However, the methods for detecting MPs in WWTPs vary significantly and this presents challenges when comparing results from different studies. Of particular interest is the ability to accurately identify the composition of MPs as this is needed to differentiate MPs from other particles and can provide insight into MP sources (Sun et al., 2019; Elkhatib and Oyanedel-Craver, 2020; Habib et al., 2020).

Common methods for MP analysis include visual sorting, single-point Fourier transform infrared spectroscopy (FT-IR) analysis, and single point Raman spectroscopy analysis. Visual sorting with the naked eye or through dissecting microscopy is easy in operation but requires significant human labor and has been shown to have up to 70% error (Hidalgo-Ruz et al., 2012). Single-point FT-IR spectroscopy and single point Raman spectroscopy which analyze MPs one by one is time consuming especially when there are a large number of MPs in a sample (Primpke et al., 2017). The use of FPA micro-FT-IR imaging is a promising technology for rapid and accurate identification of MPs in environmental samples because it simultaneously collects multiple spectra of MPs on a surface (Löder et al., 2015; Bergmann et al., 2017; Mintenig et al., 2017; Primpke et al., 2017; Simon et al., 2018; da Silva et al., 2020). The output of an FPA micro-FT-IR measurement is a 3-D matrix, with each pixel represented by x-y coordinates and the associated FT-IR spectrum. A key question in data analysis is the composition of each pixel and, by extension, the MP particle.

A conventional approach for MP recognition is the use of a library search strategy, where a correlation coefficient between an unknown spectrum and one or few standard spectra (which are usually collected in Attenuated total reflectance (ATR) mode) in a reference library is calculated to determine which plastic type most closely matches the unknown spectrum (Smith, 2011). However, this matching approach is prone to error as the reference spectra in the libraries are typically collected from virgin plastics, while the spectra of environmentally sourced MPs can be more complex due to the presences of additives (Hahladakis et al., 2018; Campanale et al., 2020), surface modification caused by weathering (Chen et al., 2021; Miranda et al., 2021), adsorbed

pollutants and the formation of biofilms on the surface of MPs (Johansen et al., 2019; Shabbir et al., 2020).

Most MPs in environmental samples do not consist of only virgin resins. Additives are widely used in the production of plastics to modify their appearance through changing colors or transparency and to enhance their performance by modifying properties like electrical resistance or resistance to degradation (Campanale et al., 2020). Commonly used additives include dyes, plasticizers, fillers, antioxidants, ultraviolet (UV) stabilizers, lubricants, and flame-retardants (Hahladakis et al., 2018). Hence, the composition of microplastics can vary depending upon the type of base polymer and on the types and concentrations of additives. It can be anticipated that the presence of additives in MPs will modify their FT-IR spectra and hence comparisons with conventional spectral libraries may be confused.

MPs in environmental samples might have experienced significant surface modification that were caused by weathering (Miranda et al., 2021). The weathering of MPs can result from physical, chemical, and biotic mechanisms (Sun et al., 2020). Weathering can cause changes in molecular structure (Ter Halle et al., 2017; Waldman and Rillig, 2020) that can include the creation of carbonyl groups (Miranda et al., 2021) and halogen bonds (Liu et al., 2021; Kinigopoulou et al., 2022), which will modify the FT-IR spectra of MPs. The surface modification of MPs may cause the spectra of MPs to differ from their virgin correspondents that are typically present in spectral libraries.

The surfaces of MPs in environmental samples can be fouled with various pollutants or colonized with biofilms (Kinigopoulou et al., 2022). MPs have been reported to act as vectors of a variety of pollutants such as metals (Tunali et al., 2020; Selvam et al., 2021), PFAS (Scott et al., 2021; Enyoh et al., 2022), and pathogens (Kirstein et al., 2016; Wu et al., 2019). Microplastics have also been reported to support biofilms that can harbour pathogens (Harrison et al., 2018; Wu et al., 2019). While the analysis of MPs in environmental samples typically includes a series of purification steps such as Fenton oxidation, enzyme purification, and density separation prior to the spectral analysis (Loder et al., 2017; Hurley et al., 2018; Konechnaya et al., 2020; Lavoy and Crossman, 2021), it is unlikely that the attached substances will be completely removed. Therefore, the presence of these additional substances on the surface of MPs may cause the spectra of MPs to differ from library spectra.

In addition to changes in MP composition, the thickness of MPs can change across their planar areas and this can affect the spectra that are collected. This type of spectral variance is particularly important when FPA micro-FT-IR microscopy is used to image MPs in the size range 20-500 μm (Primpke et al., 2017; da Silva et al., 2020). At low thickness (e.g. near the edge of particles where the thickness is only several microns), the absorbance of peaks can be weak, making it challenging to recognize these edge pixels (da Silva et al., 2020). For thicker MP cross-sections (e.g. 200 μm or thicker), the peak associated with C-H stretching can become broad thereby causing the shape of the spectrum to deviate from that of typical reference spectra (Zhu et al., 2021). Therefore, differences in thickness may cause low matching scores and consequent misidentification when conventional library search routines are employed for MP recognition.

There is a growing interest in leveraging machine learning models for spectral classification and MP detection. Machine learning models include K-Nearest Neighbour (KNN) (Kedzierski et al., 2019), support vector machine (SVM) (Zhao et al., 2018; Bianco et al., 2020), random forest decision (Hufnagl et al., 2021) and Partial least squares discriminant analysis (PLS-LA) (da Silva et al., 2020). Viewed collectively, it is apparent that the use of machine learning models can improve accuracy in spectral classification compared with that achieved by the library search approach. However, studies regarding the leveraging of deep learning models for spectral classification are scarce. Also, there has been little discussion of the capability of these machine learning models to address spectra that have been modified by additives, weathering, the presence of pollutants and variations in the thickness of MPs.

The use of convolutional neural networks (CNN), a type of deep learning neural network, represents a breakthrough in image classification (Simonyan and Zisserman, 2014; He et al., 2016; Goodfellow et al., 2017). The earlier implementation of machine learning models for spectra classification has required laborious feature engineering, which refers to the use of domain-specific knowledge coupled with algorithms to extract effective features (e.g. the position and intensity of specific peaks) that describe properties of interest. There are several issues associated with feature engineering (Guyon et al., 2008; Zhao and Du, 2016). Feature engineering depends heavily on the domain knowledge of the modeler and even with this expertise some features that are important for classification might be inadvertently overlooked. In addition, the hand-crafted features are often at the discretion of the modeler and lacks a unified approach. Moreover, the creation of hand-

crafted features is a tedious process. Compared with the machine learning models, one of the most significant advantages of deep learning models is that they circumvent feature engineering steps since the deep learning models can extract features from the data automatically. Consequently, the pipeline for data processing should be greatly simplified when deep learning models for the classification of spectra are leveraged.

Deep learning has been found to be successful in challenging image classification tasks that have intra-class variation (Wei et al., 2015; Shi et al., 2016; Asif et al., 2017; He et al., 2018) of images due to changes in i) color; ii) illumination; iii) shapes. In image classification tasks, deep learning models are usually trained with large datasets for the same class that incorporate intra-class variation, that allows the model to extract invariant features that are robust to heterogeneous intra-class variations (Wei et al., 2015; Shi et al., 2016; He et al., 2018). It is hypothesized that the training of CNNs with numerous spectra from MPs that exhibit variations in spectra should allow a model to learn discriminative spectral features that characterize each class of MP in a way that accounts for intra-class spectral variances, which will solve low-matching problems associated with library search methods.

There is a growing trend in leveraging CNNs for spectral classification (Acquarelli et al., 2017; Berisha et al., 2019; Lee et al., 2019; Padarian et al., 2019a), but the use of CNNs for MP detection via the classification of FT-IR spectra is limited. A possible reason that hinders the wide application of deep learning models in spectral studies is the requirement of large-scale data (at least 1000 data for each class) to effectively train the model. Though the collection of thousands of spectra for each type of MP is not easy using single point data collection, it is possible with micro-FTIR imaging, because each particle can contribute dozens to thousands of spectra in the dataset. Hence, the analysis of MPs using FPA micro-FT-IR imaging provides a unique opportunity for the implementation of deep learning models for spectra classification and MP detection due to the large amount of data generated in data collection. However, the capability of deep learning to address the variance of spectra has not been reported. Hence, this study explores the feasibility of leveraging deep learning for improved spectra classification and automatic MP recognition via FPA micro-FT-IR imaging. This is accomplished through the introduction of PlasticNet, a CNN architecture designed specifically for these purposes. Specifically, this study focuses on the performance of deep learning for the recognition of the spectra of MPs that had a range of thickness,

additives, and surface modification. The knowledge generated from this study will contribute to the development of methods for fast and rapid automatic MP recognition in datasets acquired by FPA micro-FT-IR imaging.

3.2. Methodology

3.2.1 Data acquisition

The development and testing of PlasticNet was conducted through a series of activities. Each activity sought to address a specific aspect of development and hence employed a unique dataset. The type of spectra, details of data collection, and the number of spectra employed are summarized in Table 3-1 which is subsequently discussed.

Dataset 1 consisted of spectra from 11 types of virgin plastic particles and spheres which were collected using FPA micro-FT-IR imaging and was employed for the training and testing of PlasticNet. The size of particles and spheres range between 20-500 μm and hence were consistent with those commonly measured in wastewater and environmental samples (Enfrin et al., 2019; Sun et al., 2019). The virgin PE microspheres were purchased from Cospheric, U.S. The remaining plastics were purchased from Hongyu Modified Plastic, China., and were ground using a metal file. The generated particles were sequentially screened with 500 μm and 20 μm sieves to select for particles in the 20-500 μm range.

The various particles in dataset 1 were imaged using a Bruker Tensor 37 spectrometer connected to a Hyperion 3000 micro-FT-IR microscope equipped with a 64 × 64 FPA detector. The data were collected using a × 15 Cassegrain objective, in transmission mode using a BaF_2 window. All data were collected with 4 × 4 binning and a spectral resolution of 8 cm^{-1} with 32 co-added scans. Each imaging file contains multiple spectra depending on the area of imaging, and the Bruker OPUS© 7.5 software was used to extract multiple spectra from each file. Notably, the extracted spectra encompassed both the central and edge regions of each particle within the imaging file, aiming to address thickness variations within individual particles.

Dataset 2 consisted of spectra of PE that had experienced surface modification and spectra of PP that contained dyes and additives. Dataset 2 was employed to assess PlasticNet's capability to recognize spectra of MPs with added complexity. For this purpose, the spectra of PE reported by Miranda et al., 2021 that had experienced various simulated or real weathering conditions were employed. In addition, colored PP items that had a recycling PP code were collected from local recycling (e.g. pill bottle, coffee capsule, caps of container). PP plastics containing $CaCO_3$ flame retardant, and glass fiber fillers were purchased from Hongyu Modified Plastic, China. PP

containing these 3 types of additives were selected for testing purpose because these are commonly used additives to enhance the performance of PP in applications (Hahladakis et al., 2018). The spectra of colored and modified PP in Dataset 2 were imaged employing the same procedure described for dataset 1.

Dataset 3 consisted of spectra of PET films with various thickness (3A), and a mapping file from a real environmental sample (3B). Dataset 3A was employed to evaluate the how the thickness of MPs impact on the shape of spectra, as well as to evaluate the capability of PlasticNet in addressing this variation of spectra. The spectra of PET films in Dataset 3A were imaged employing the same procedure described for dataset 1. Dataset 3B was previously reported by Primpke et al. (2018) and was employed to conduct a critical comparison of the recognition results derived from a library search with that derived from PlasticNet. In brief the MPs in the dataset had been collected at a wastewater treatment plant, cleaned with an enzyme digestion protocol, and were imaged by a Bruker Tensor 27 spectrometer connected to a Bruker Hyperion 3000 FPA FT-IR microscope equipped with a 64 × 64 FPA detector. The imaging was performed with 4 × 4 binning, a spectral resolution of 8 cm^{-1}, and had 6 co-added scans.

Table 3- 1 Meta-Statistics for the data employed in the study.

Dataset	Data collection	Number of spectra and purpose
1	FPA micro-FTIR imaging 8 cm^{-1} spectral resolution, 32 co-added scans	60+ FPA micro-FTIR imaging files; Each imaging file contains 16 × 16 spectra or more depending on the area of imaging A total of 8848 spectra were extracted from the imaging files for the initial training, validation, and test of PlasticNet
2 (A)	ATR FTIR 4 cm^{-1} spectral resolution, 128 co-added scans.	10 ATR FTIR spectra of PE that experienced surface modification.
2 (B)	FPA micro-FTIR imaging 8 cm^{-1} spectral resolution, 32 co-added scans.	6 FPA micro-FTIR imaging files; Each file contained an image from one type of colored & modified PP. Approximately 100 spectra for each type of colored & modified PP were extracted for testing PlasticNet's capability to address spectra complexity. A total of 790 spectra were used for test purpose.
3 (A)	FPA micro-FTIR imaging 8 cm^{-1} spectral resolution, 32 co-added scans.	7 FPA micro-FTIR imaging files. Each file contained an image from one PET film. The thickness of film varied from 12.5 μm to 500 μm
3 (B)	FPA micro-FTIR imaging 8 cm^{-1} spectral resolution, 6 co-added scans.	1 FPA micro-FTIR imaging file that contained 1024 × 1024 spectra.

3.2.2 Overview of data processing

The spectra collected FPA-FTIR imaging experienced a series of steps of data processing to get the results. The spectra were firstly pre-processed to remove undesired trends that might confuse the classification of spectra. After pre-processing, the 1-D spectra were converted to 2-D images

and then classified through a deep learning architecture. The output of the deep learning classification includes information regarding whether a particle is MP or not as well as the type of MP this particle belongs to. An overview of data processing is summarized in Fig.3-1A.

3.2.3 Data pre-processing

Normalization and baseline correction were applied prior to converting spectra to spectrograms. Normalization preprocessing is needed for regularizing data with respect to variations in sample preparation, detector settings, and any other aspects of the measurement (Randolph, 2006). The normalization was achieved using the Matlab normalize function which returns the distance of a data point from the mean in terms of the standard deviation of the spectrum (Mathworks, 2022b). Baseline correction is needed to remove undesired trend in the baseline of the spectra (Randolph, 2006). The baseline correction was achieved using the Matlab detrend function which subtracts the trend from the spectrum (Mathworks, 2022a). The data preprocessing removed undesired features that would complicate the classification of spectra by the deep learning model.

3.2.4 1-D to 2-D conversion

PlasticNet was designed for the classification of 2-D images while the FT-IR spectra are 1-D signals, hence each 1-D FT-IR spectrum was transformed to a 2-D spectrogram representation prior to processing by the CNN. This was achieved by sliding a Hamming window across the 1-D spectrum and producing a 2-D stack of overlapping spectral segments. A Fast Fourier transform was then applied to the spectral segment stack to obtain the final 2-D spectrogram. The spectrum to spectrogram conversion was derived from that employed for recognition of 1-D voice signals (Kingsbury et al., 1998; Satt et al., 2017; Huang et al., 2019) and has been employed for spectra classification by CNNs in other applications (Ng et al., 2019; Padarian et al., 2019a; Ng et al., 2020).

3.2.5 PlasticNet Architecture

PlasticNet has a tailored CNN architecture that was constructed to explore the feasibility of leveraging deep learning for automatic MP recognition via FT-IR spectroscopy. The PlasticNet network architecture is based on a VGG deep convolutional neural network architecture (Simonyan and Zisserman, 2014), and is comprised of 8 convolution layers, 3 max pooling layers,

3 fully connected layers, and 1 softmax layer. The convolution layers and max pooling layers consisted of multiple 3×3 and 2×2 filters respectively. PlasticNet was constructed, trained, and tested in Mathwork Matlab© R2018a. PlasticNet was designed to initially learn features from the input spectrogram and this was achieved by the convolution +ReLU and pooling layers. The fully connected layers and softmax layers then classify the input based on the learned features. The subsequent discussion describes the role of each of the CNN components.

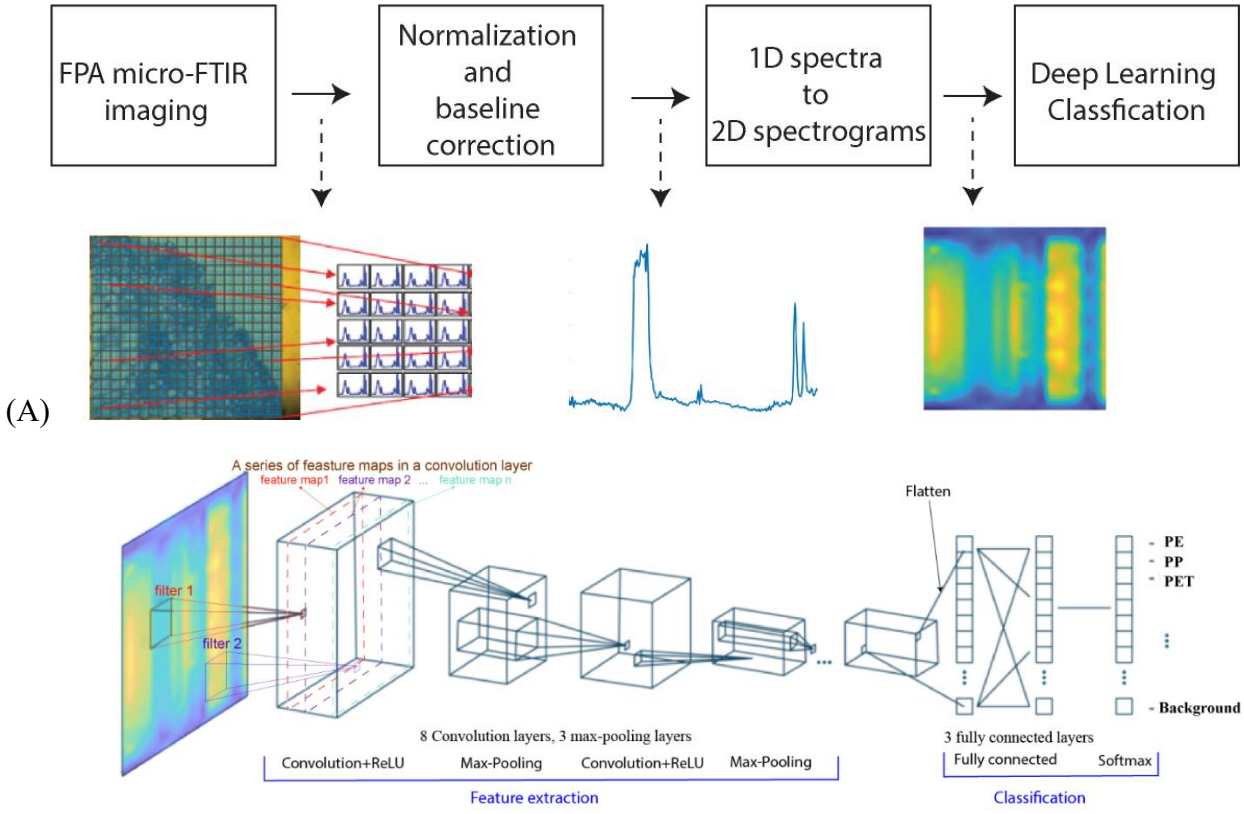

Figure 3- 1 (A) Overview of data processing (B) Schematic representation of PlasticNet.

3.2.5.1 Convolution layers +ReLU activation

The convolutional layers are used to extract features from the 2-D spectrograms that are prepared from spectra (Goodfellow et al., 2017). An effective extraction of the important features from the input facilitates the correct classification of the spectra at the later stages of the model. As shown in Fig.3-1, each convolution layer consists of multiple filters, the size of which is smaller than that

of the input. Each filter slides across the input, calculating the summed dot products between the input and filter at every spatial position (as shown Fig.3-2A) and resulting in an independent feature map. The use of multiple filters at one convolution layer results in a series of feature maps (as shown in Fig.3-1) that serves to extract various features from the input and possibly enhance the accuracy of the classification.

Activation functions are essential in deep learning models to prevent linearity (Goodfellow et al., 2017). Without them, the data would pass through the layers of the network only going through linear functions, making it difficult to train the model, because data usually is not modelled well by linear equations in complex problems such as the classification of spectra. In PlasticNet, the rectified linear unit (ReLU) activation function is used for the activation of the output from the convolution layer. The ReLU activation function adds nonlinearity to the model by outputting the input directly if it is positive, otherwise, outputting the input as zero. The ReLU was selected as the activation function because it is the default activation function for deep convolutional neural networks and models that utilize ReLU activation have been demonstrated to achieve better performance.

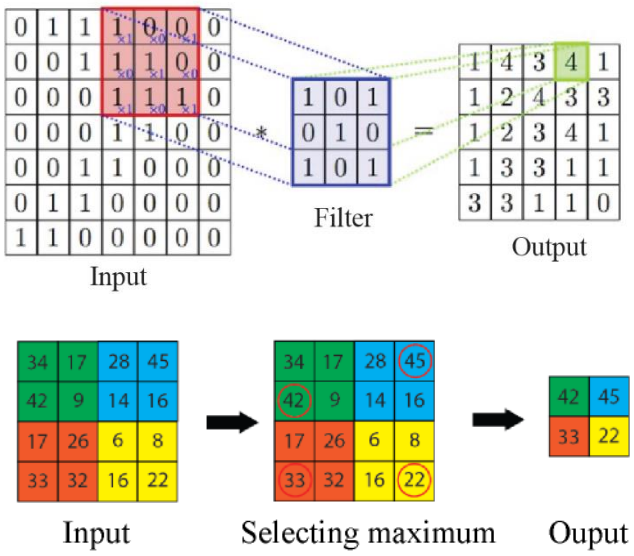

Figure 3- 2 Convolution operation (A) and max pooling operation (B).

(A) The summed dot production operation between the input and 3×3 filter. (B) Max pooling by a 2×2 filter. Only the maximum value in a filter was kept after max pooling.

3.2.5.2 Max pooling

Max pooling layers are used to i) extract predominant features by down-sampling the previous layer; 2) reduce computational complexity, and; iii) make the model invariant to small translations (Goodfellow et al., 2017). Though considerable features were extracted from the data by the convolution layers, a lot of them might be redundant for the purpose of spectra classification. Also, the computation cost of a model without down sampling is high and makes it difficult to train. Hence, there is a need to remove some features that are not important. As shown in Fig 2B, the max pooling operation keeps the maximum within each filter, with the goal of retaining the key features (i.e. maximum value) for the classification while ignoring features that are less-important (i.e. values smaller than the maximum). After max pooling, the model should become invariant to small translations, which means that the model outputs the same response regardless of small shift in input. For example, when the smaller values in a filter increase slightly, the output of the filter stays the same because only the maximum was retained due to max pooling. The invariance to the translation contributes to the model's capability to address the variance of spectra, because the model's output will be the same regardless of the small change in the intensity of spectral peaks.

3.2.5.3 Fully connected layer+ softmax layer

The fully connected layers are responsible for classification of the features that were extracted by the initial layers. As shown in Fig.3-1, the first fully connected layer serves to flatten the features extracted from the convolution layers and max pooling layers, while each neuron in the second and third fully connected layer is connected with all the neurons in the previous layer. A softmax layer is used as the last layer which outputs the likelihood of an input FT-IR spectrum belonging to each plastic type under consideration.

3.2.6 Initial training, validation, and testing

Spectra from dataset 1 that were generated from a variety of virgin plastics were employed to initially train, validate, and test the model. The dataset was split into a ratio of 50: 25: 25 for training, validation, and testing. This allocation resulted in 50% of each type of microplastic spectra being assigned to the training set, 25% to the validation set, and another 25% to the testing set, ensuring a balanced distribution for each plastic type across the three categories. Table 3-2 summarizes the number of spectra from each type of plastic that were employed for training, validation, and testing purposes respectively.

Table 3- 2 Number of spectra used for initial training, validation, and testing

	Number of spectra			
Type of plastic	Training	Validation	Test	Total
PE	596	298	298	1192
PP	748	374	374	1496
PET	158	79	79	316
Nylon	350	175	175	700
PMMA	312	156	156	624
ABS	300	150	150	600
Silicone	232	116	116	464
PVC	264	132	132	528
PC	68	34	34	136
POM	110	55	55	220
PU	92	46	46	184
Background	1014	507	507	2028
Total				8488

The training dataset was the used to fit the model, while the validation dataset was used to evaluate the performance of the model fit on the training dataset, and to determine the appropriate number of iterations at which point training was terminated. The model was initialized with random weights, and the default settings provided by Matlab were employed for the loss function, optimizer, and evaluation metric. Specifically, the categorical cross-entropy was chosen as the loss function for the multi-class classification task, stochastic gradient descent was utilized as the optimizer to update the model's weights based on gradients, and accuracy was adopted as the evaluation metric to assess the model's performance in correctly predicting the class labels. Training was stopped when the total accuracy of the validation exceeded 97.5%. The test dataset was used to independently evaluate the performance of the final model and evaluate its limitations. All training, validation, and testing were implemented using Matlab© R2018a on a desktop computer with a 11th Gen Intel i7-11700K processor, 32GB memory, and NVIDA GeForce RTX 2060 Super graphic card. The Matlab script for training, validation, and testing of PlasticNet can be found in appendix A.

3.2.7 Recognition of spectra with variation & re-training of model

It was hypothesized that the deep learning model that was trained with spectra from the virgin plastics in dataset 1 could extract robust features, such that the model could classify spectra from plastics that had additional complexity due to presence of additives or had been surface modified. To test this hypothesis, a version of PlasticNet that was trained with dataset 1 was employed for recognition of spectra from dataset 2 and the performance with respect to recognition was evaluated.

It was also hypothesized that the addition of a limited number of the more complex spectra from dataset 2 to the training pool would enhance the model's performance in recognizing complex spectra from outside the training pool. To test this hypothesis, the spectra from one of the PP types in dataset 2 were added into the training pool and the model was retrained. The retrained model was employed to evaluate the other 5 types of PP spectra in dataset 2 that were outside the updated training pool, and the success of recognition was assessed as previously described.

It was also hypothesized that the model could classify spectra that had complexity due to the variation of the thickness of particle. To test this hypothesis, spectra of PET films in dataset 3A were plotted to examine how the thickness of MPs impacted the shape of spectra, and the performance of PlasticNet in classifying these spectra was evaluated.

3.2.8 Comparison of the performance of PlasticNet vs. Library search

The MPs in dataset 3B were analysed using PlasticNet and the results were compared with that achieved by a library search method. The purpose of comparison was to evaluate if PlasticNet could achieve improved performance in identifying MPs that were missed by a library search. PE and PP MPs were the predominant MPs in dataset 3B and hence these were selected to compare and contrast the recognition results derived from the two methods. If a suspected PP MP was missed by the library search but was recognized by PlasticNet, a manual re-analysis was conducted to determine its composition based on the presence or absence of essential or additional peaks from PE and PP. The FTIR spectra of PE and PP have readily identifiable peaks that made the reanalysis exercise robust.

3.2.9 Methodology summary

In summary, the development of PlasticNet involved the adaptation of an existing deep learning architecture, followed by original contributions in data acquisition, model training and testing using the acquired data, and assessment of the model's efficacy in addressing spectral complexity. Notably, this research represents the pioneering endeavor in employing deep learning techniques for the MP identification, and in evaluating the model's proficiency in handling spectral variations associated with MP samples.

3.3. Results and discussion

The goal of this study was to critically assess the potential of deep learning for improved MP recognition via FT-IR spectroscopy with a focus on the performance of leveraging deep learning for the recognition of the spectra of MPs with variation. The following sections 1) evaluate whether the converted data structure was suitable for the classification by CNN by characterizing the conversion of the 1-D to 2-D spectrogram; 2) evaluate the performance of the training and testing of PlasticNet and critically evaluate the errors as indicated by a confusion matrix; 3) evaluate whether the PlasticNet trained based on a variety of MP thicknesses can extract robust features in spite of thickness variation; 4) Evaluate whether the PlasticNet trained based on virgin plastic can recognize varied spectra with additional peaks, distorted baseline and noise resulting from the presence of additives and surface modification; 5) Evaluate whether the adding of varied spectra into the training pool enhanced performance in recognizing varied spectra; 6) Compare the ability of PlasticNet in identifying MPs in a complex dataset with that of a library search approach.

3.3.1 1-D to 2-D conversion

The spectrogram that is generated from a spectrum, presents the frequency of occurrence of each wavelength of a signal in the x-y domain, while the intensity of the peaks at each wavelength is presented along the z-axis. The transformation from spectrum to spectrogram was carried out by sliding a Hamming window across the spectrum (Fig.3-3A) and then employing a fast Fourier transformation. Transforming the FT-IR spectra into 2-D spectrogram representations structures the spectral relationships between adjacent spectral frequencies (Padarian et al., 2019a; Padarian et al., 2019b) in a way that facilitates improved spectral feature learning by a CNN architecture such as PlasticNet.

A spectrogram that was generated from a spectrum obtained from a polypropylene MP is presented as an example of those developed in this work to illustrate the appropriateness of the translation to generate a data structure that was suitable for CNN analysis (Fig.3-3). From Fig.3-3B it can be seen that the signals in the spectrogram are highly locally correlated. The bright pixels tend to cluster instead of distributing in a scattered way, forming distinctive motifs then assembling into bright zones that might easily detected by the deep learning model (LeCun et al., 2015a). In addition, the signals are compositionally hierarchical. The individual bright pixels form larger

bright spots, and the bright spots have assembled into bright zones. These two characteristics are consistent with the characters in 2-D images where the local conjunction of features form edges, motifs, parts, objects, and patterns in a hierarchical way (LeCun et al., 2015b). The local correlation and compositional hierarchies in the spectrogram make it feasible for the spectra to be classified by the CNN model.

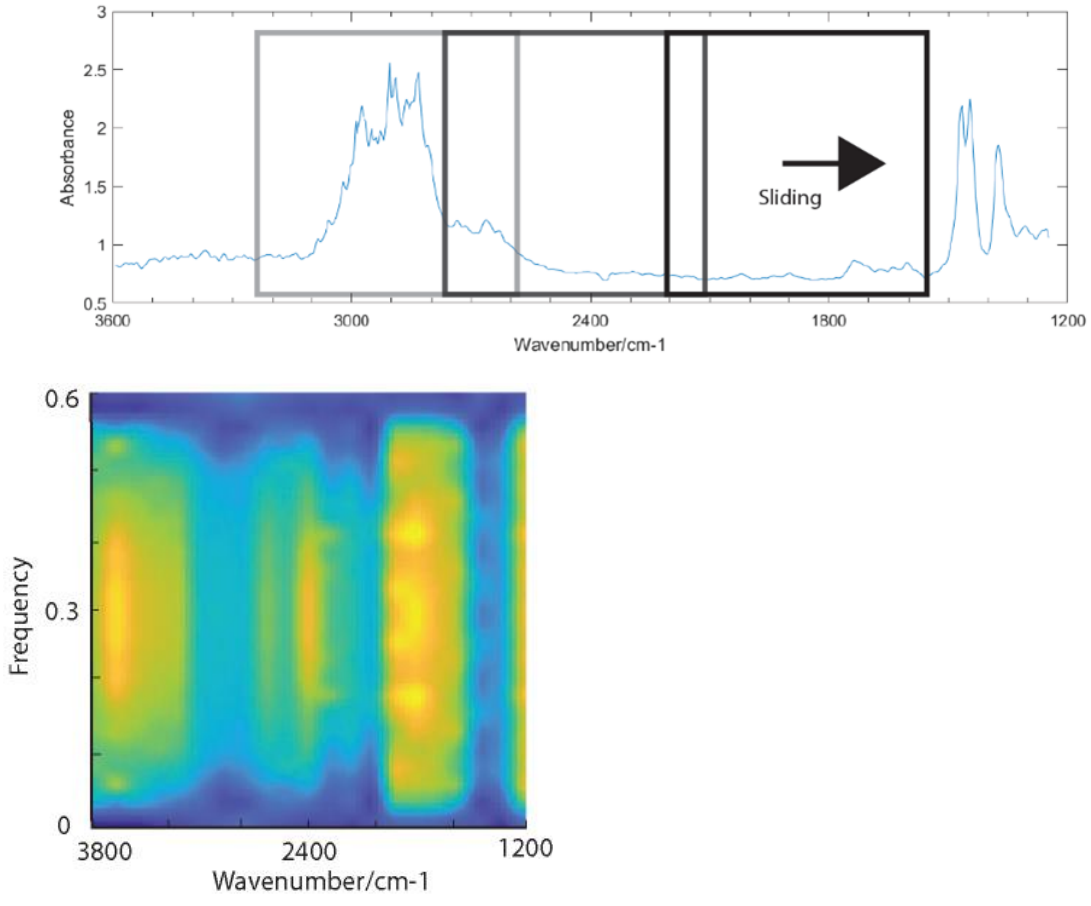

Figure 3- 3 (A) Sliding a Hamming window on a PP spectrum. (B) A spectrogram created from a PP spectra.

3.3.2 Performance of training and testing

The performance of the trained PlasticNet with respect to identifying MPs in test dataset 1 was visualized using a normalized confusion matrix (Goodfellow et al., 2017) that is shown in Fig.3-4. The accurate differentiation between microplastic types holds significant importance due to

several factors. Firstly, regarding the environmental impact, diverse polymers exhibit varying degrees of persistence and degradation rates in the environment (Koelmans et al., 2022). Certain polymers display higher resistance to degradation, leading to their prolonged presence in ecosystems and potential bioaccumulation within the food chain. Secondly, in terms of toxicity and chemical interactions, various polymers may encompass distinct additives, stabilizers, or impurities that can leach out and interact with the surrounding environment (Zimmermann et al., 2020). The differentiation between polymer types facilitates the identification of potential chemical interactions and allows for the overall toxicity assessment of microplastics. Thirdly, with respect to remediation strategies, effective removal and mitigation techniques for MPs may be influenced by the diverse surface charges that different polymer type of MPs may carry (Prajapati et al., 2022). For instance, specific methods like electrocoagulation or electrostatic separation might be more suitable for MPs with distinct surface charges, while other techniques like filtration or flocculation could be more effective for MPs with different surface properties. Therefore, the acquisition of correct understanding regarding the MP polymer type is indispensable in risk assessment the development of targeted mitigation within the environment.

The diagonal elements of the confusion matrix represent the percentage of spectra for which the prediction was correct, while off-diagonal elements represent the percentage of spectra that were mis-identified by PlasticNet. As shown in Fig.3-4, the true positive percentage was higher than 0.95 for all plastic types except PU. The results demonstrate an overall high performance of PlasticNet in recognizing MPs. However, to gain further insights into whether the model could be further improved, the situations where misprediction occurred were examined in detail.

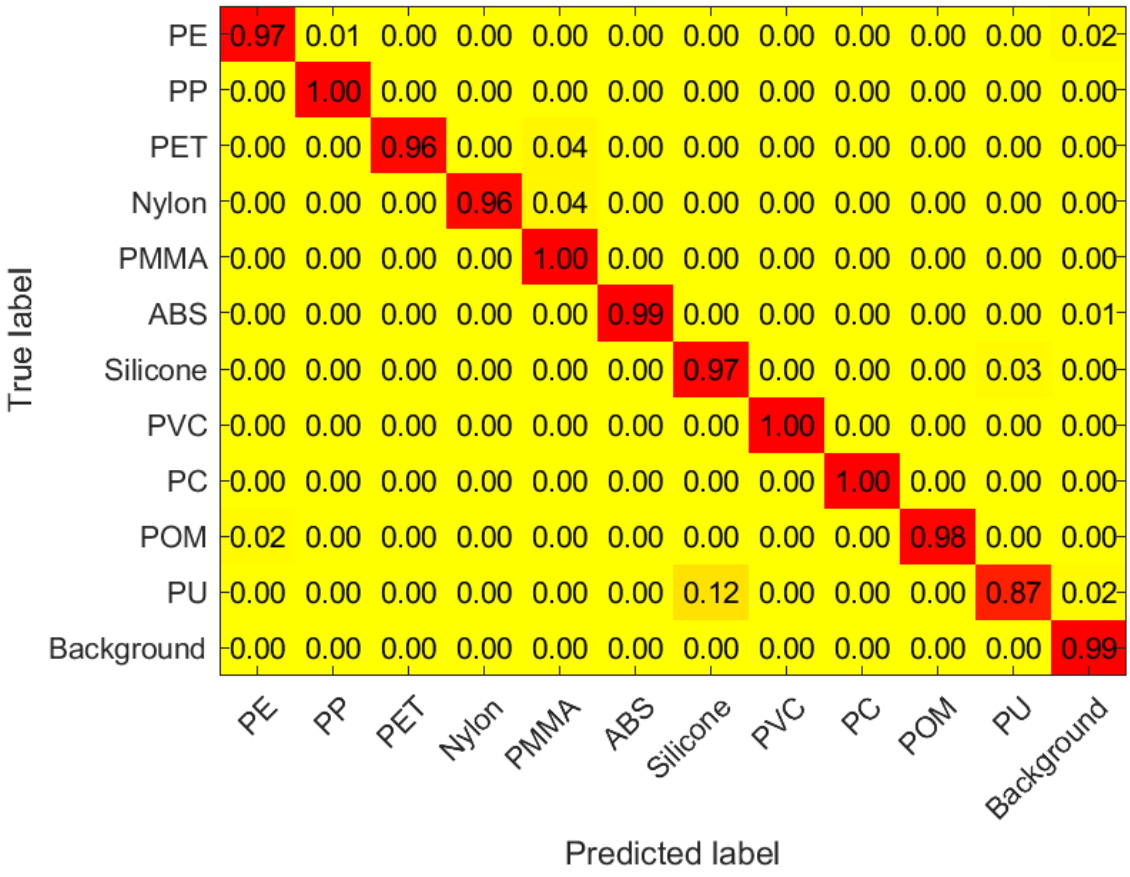

Figure 3- 4 Performance of PlasticNet as evaluated by a Normalized Confusion Matrix

3.3.3 Errors indicated by the confusion matrix

Though the accuracy of classification of spectra was considered very good for most types of plastic, a few errors were indicated in the confusion matrix. For example, 12% of PU MPs were reported as Silicone. In cases where mis-identification occurred the spectra were qualitatively assessed to gain insight into potential causes of errors and thereby identify any limitations of the model. The percentage and number of spectra that were misidentified are indicated by in Table 3-3 and are discussed subsequently.

Table 3- 3 Errors of spectra classification as described in confusion matrix.

Plastic type	1st mis classification		2nd mis classification	
	Mis-classified as	Percentage	Mis-classified as	Percentage
PE	PP	1%	Background	2%
PET	PMMA	4%		
Nylon	PMMA	4%		
ABS	Background	1%		
Silicone	PU	3%		
POM	PE	2%		
PU	Silicone	12%	Background	2%
Background	PE	0.5%	Nylon	0.5%

For each cell of the confusion matrix where misidentification was indicated, the molecular structures of the two types of MPs were initially compared to assess whether the confusion might have been caused by molecular structure similarity. Subsequently, the remaining erroneously classified spectra were reviewed to determine if the confusion resulted from spectral distortion that was associated with pixels that were located on the edges of MPs (edge effects). The percentage that each source of confusion contributed to the overall confusion was then calculated.

To illustrate how molecular structure, edge effects, and unidentifiable causes contributed to error in spectral classification, the confusion between PE and PP, Silicone and Nylon, PE and background were selected as representative examples respectively and are discussed subsequently. The discussion regarding the confusion between PET and PMMA, PMMA and Nylon are presented in the Appendix A as these misidentifications could be attributed to the above-mentioned errors.

Table 3- 4 Comparison of molecular structures of selected confused spectral pairs

Confusion pairs	Comparison of molecular structure	
PE and PP	PE	PP
	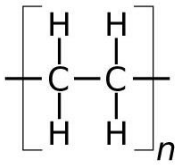	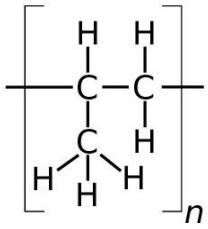
Silicone and PU	Silicone	PU
	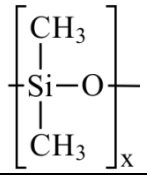	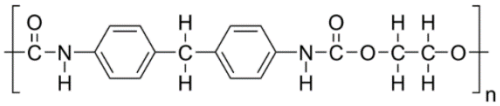

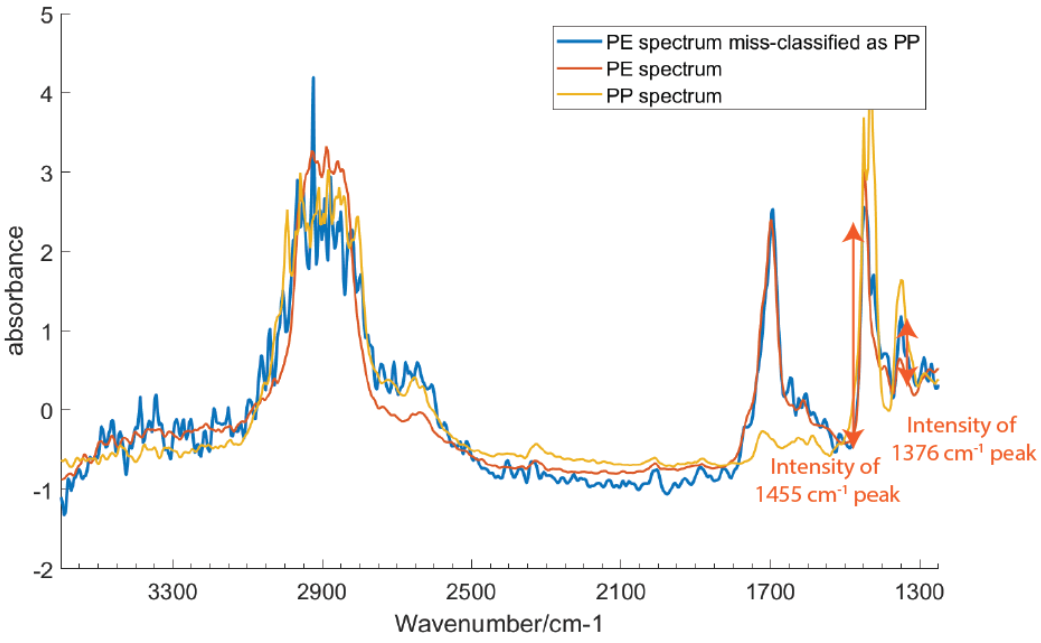

(A)

(B)

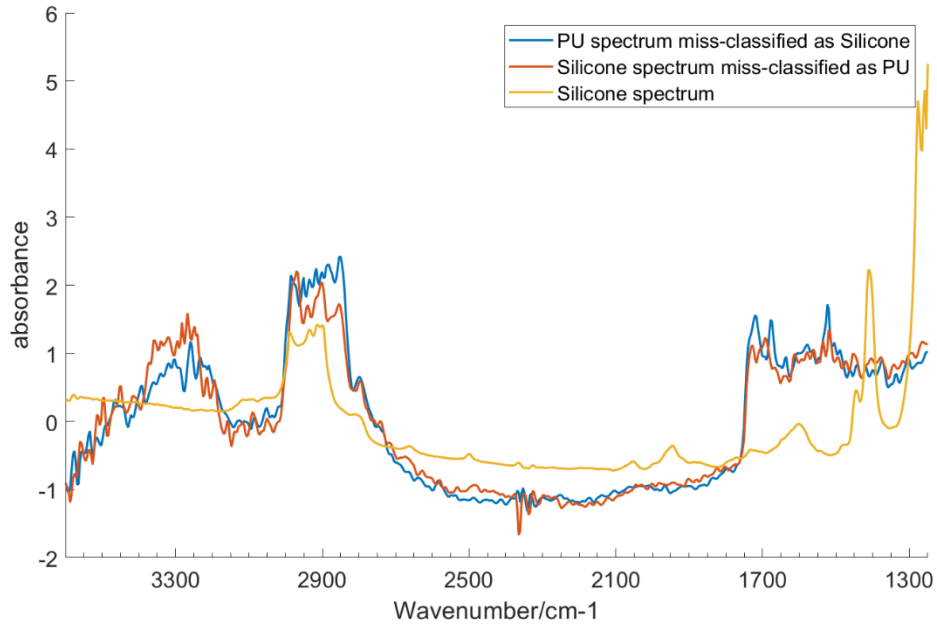

(C)

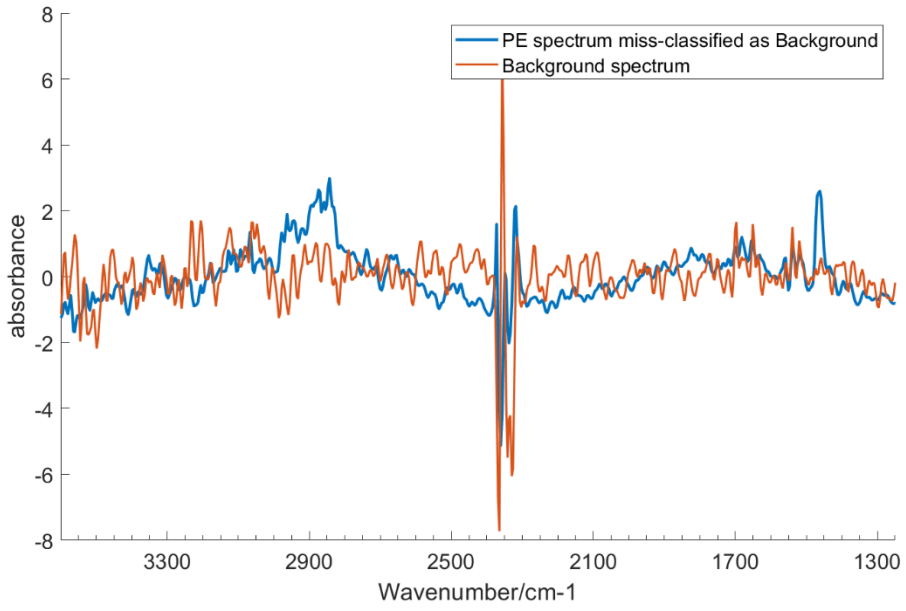

Figure 3- 5 Analysis of spectra misclassified by PlasticNet (A) PE spectrum misclassified as PP. Correctly classified PE and PP spectra are plotted in the same figure. The ratio between 1376 cm^{-1} and 1455 cm^{-1} peaks were used to distinguish between PE and PP. An additional peak at 1740 cm^{-1} on both PE spectra that was correctly classified and mis-classified, indicating the PE spectra experienced surface modification. (B) A PU spectrum that was misclassified as Silicone and a

Silicone spectrum that was misclassified as PU. (C) PE spectrum that was misclassified as background.

PP and PE have considerable molecular similarity as both plastics are comprised exclusively of C-H and C-C bonds (Table 3-4). The molecular structure similarity was expected to cause confusion between PE and PP spectra. An example of a PE spectra that was misclassified as PP was plotted and compared with a known spectra for PP (Fig.3-5A). The ratio of the intensity of the 1376 cm^{-1} and 1455 cm^{-1} peaks on the misidentified spectrum is higher than that of the ratio of the spectrum of a correctly classified PE, while this ratio is closer to the ratio of the PP spectrum. The results suggest that the trained PlasticNet distinguishes between PE and PP based on the ratio of 1376 cm^{-1} and 1455 cm^{-1} peak. If a PE spectrum has a higher ratio, the model may erroneously classify it as PP. In summary, the similar molecular structures and hence the corresponding IR spectra of PP and PE are similar and this appeared to be the main source of confusion between PP and PE. Since, the error in identification appears to be a function of the similar chemistry of the plastics it was concluded that additional training may not mitigate this issue and this type of error would need to be accepted as a limitation of the model.

The molecular structures of Silicone and PU were reviewed (Table 3-4) and found to differ considerably. Silicone is mainly comprised of Si-O and C-Si bonds, while PU is mainly comprised of C=O, C-N, benzene ring, and N-H bond. Hence, it was concluded that molecular structure was likely not the reason for confusion in identification. Hence, the spectra were further examined to determine whether other causes of confusion could be identified.

A misclassified PU spectrum and a misclassified Silicone spectrum were plotted along with a Silicone spectrum in Fig. 3-5B to explore other sources of error. From Figure 3-5 it can be seen that a peak indicating N-H bonding peak appeared on the misclassified Silicone spectrum, but the spectral response of N-H bonds should not appear in Silicone spectra, as shown on the correctly classified Silicone spectra. The presence of this peak on the mis-classified Silicone spectra indicates that some of the Silicone spectra that were used for training and testing were mislabelled. The results obtained for this pairing highlight the importance of critically evaluating situations where misidentification occurs in model training. MP standards can contain contamination and improved model training will be achieved when erroneous standard MPs are identified.

PE particles had the largest number of spectra that were erroneously classified as background and hence and an example of one of these spectra was reviewed (Fig. 3-5C). The spectra was collected near the edge of a particle, and the signature peaks of PE at 3200-2800 cm^{-1}, 1455 cm^{-1}, 1376 cm^{-1} were weak. Hence the spectra were similar to the background signal. This error indicates that the model tends to confuse signals at the edge of particles with the background. A solution to this is to ignore pixels that are identified to be near an edge of the particle.

3.3.4 Addressing variation of MP spectra due to additives and surface modifications

The trained PlasticNet was employed to evaluate spectra of PP and PE that had additives and surface modification. In this regard we sought to assess whether the deep learning algorithm could be leveraged to extend from simple to complex scenarios. In this section, the varied spectra were initially plotted to observe how the presence of additives and surface modifications contributed to the modification of spectra. Subsequently, the performance of PlasticNet was assessed.

3.3.4.1 Variation of spectra

The spectra of PP particles with glass fiber, flame retardant and $CaCO_3$ fillers (see Fig.A3 for pictures of samples) were plotted along with the spectra of virgin PP to assess how the presence of additives impact spectra. Fig. 3-6A illustrates a strong and broad additional peak at 1040-1050 cm^{-1} in the presence of the glass fiber filler. Additional peaks were observed at 1720 cm^{-1}, 1580 cm^{-1}, and 1500 cm^{-1}, 1435 cm^{-1}, 1400 cm^{-1} in the presence of the flame retardant (Fig.3-6B) while an additional peak at 1760 cm^{-1} was observed in the sample containing $CaCO_3$ (Fig.3-6C). In addition, the presence of additives contributed noise to the signals in the range 3850-3600 cm^{-1} in all 3 spectra, and resulted in a curved baseline in the range of 2500-1800 cm^{-1} for the PP containing flame retardant and $CaCO_3$. Viewed collectively, the presence of fillers and fire retardants contributed to additional peaks, increased noise, and a curved baseline. Hence these spectra were employed to assess the ability of PlasticNet to recognize the spectra of PP in the presence of these features.

The spectra of the colored PP particles (see Fig.A4 for pictures of samples) were plotted together with the spectra of virgin PP to examine how the presence of dyes impacted the spectra. From the spectra in Fig.3-7A it can be seen that there was little difference between the spectra of the light

green PP and that of virgin PP. Hence, the presence of green dye caused limited spectral variation. In contrast, in the presence of a red dye (Fig. 3-7B) the primary C-H peak in the range of 3100-2695 cm^{-1} was slightly distorted due to the increased intensity at 2695 cm^{-1} and was noisier in the range 3850-3600 cm^{-1}. Similarly, the spectra from the white PP (Fig. 3-7C) had no additional peaks but the spectra had increased noise in the same range (3850-3600 cm^{-1}) as the red PP. It was concluded that the presence of dyes can cause additional peaks in the PP spectra, and hence these spectra were also employed for assessing the ability of PlasticNet to recognize PP spectra that were modified by the presence of dyes.

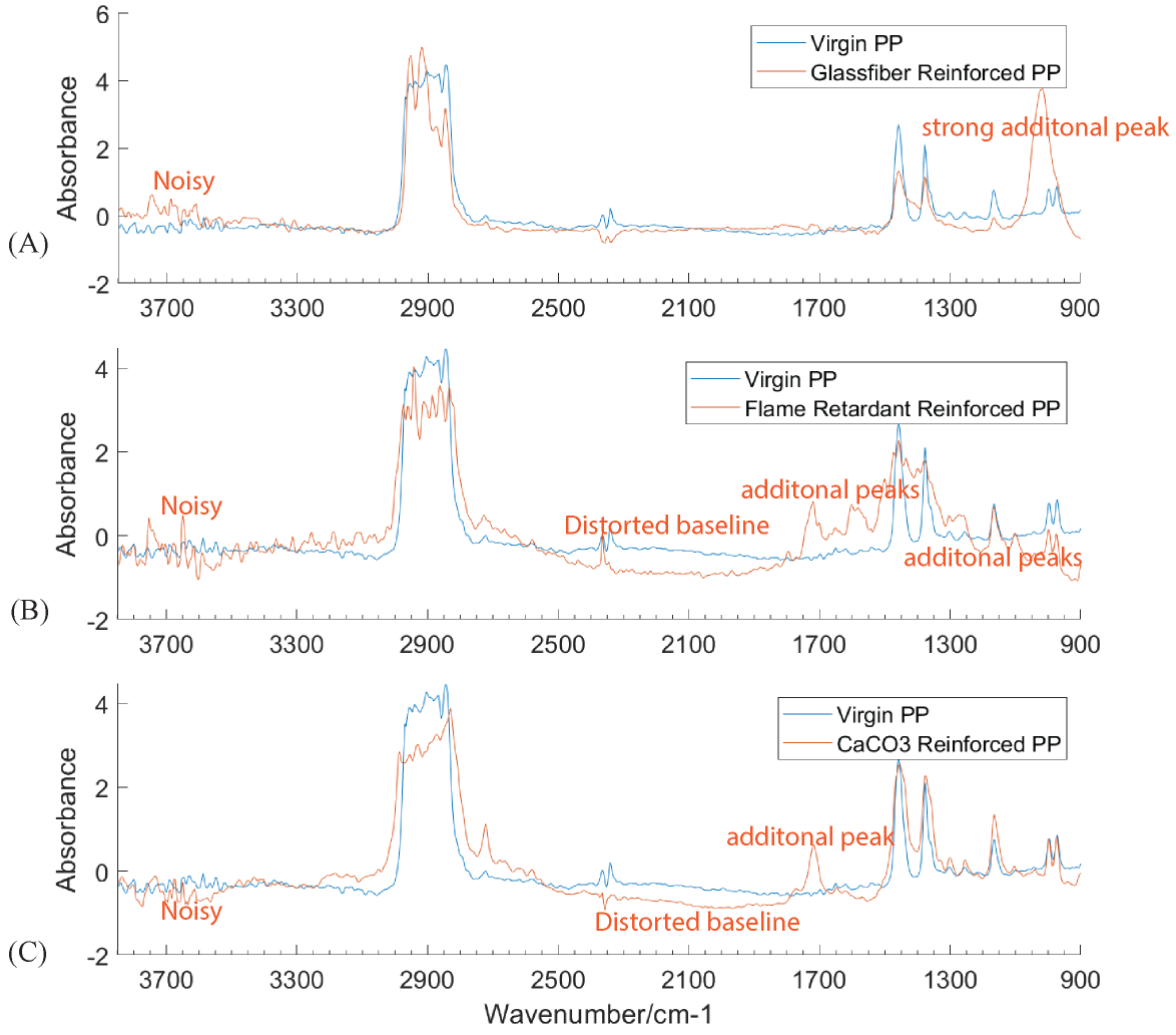

Figure 3- 6 Spectra of PP with additives. (A) Glass fiber filler (B) fire retardant (C) $CaCO_3$ and virgin PP

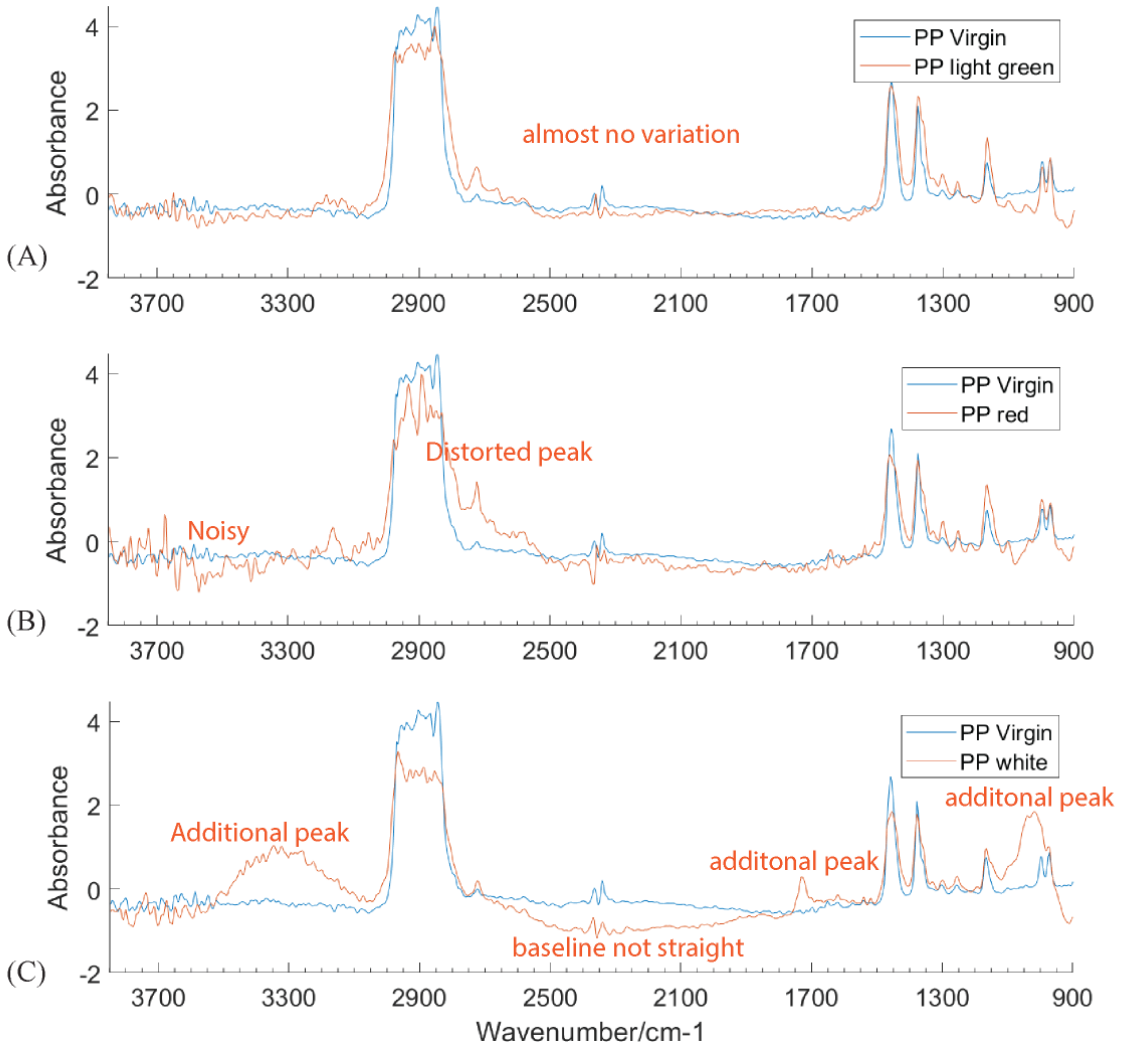

Figure 3- 7 Spectra of PP with dyes (A) green (B) red (C) white and virgin PP.

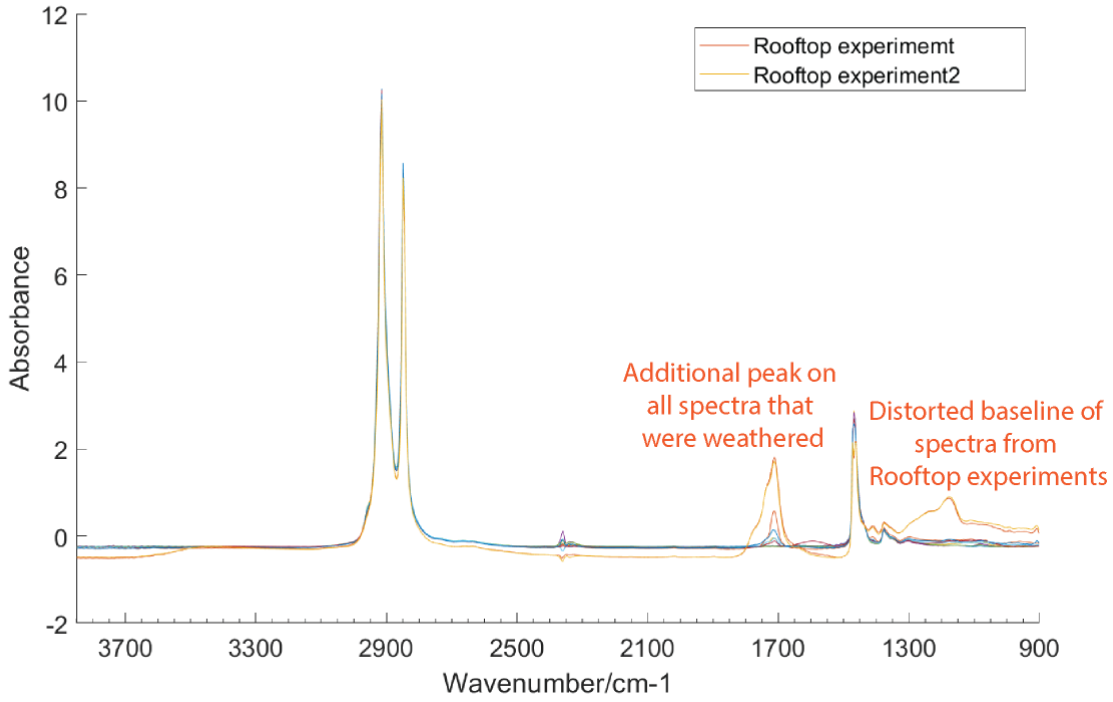

Figure 3- 8 Spectra of PE with surface modification due to atmospheric weathering. Created from data of (Miranda et al., 2021). All spectra were collected using ATR mode.

The spectra of PE that had experienced surface modification due to atmospheric weathering were plotted together with the spectra of virgin PE to examine how surface modification impacted upon spectra (Fig.3-8). The surface modified spectra (Miranda et al. (2021) were obtained from PE samples that had been exposed to various simulated or real weathering conditions. Though these spectra were collected via ATR (instead of transmission mode), it was deemed appropriate to classify them with PlasticNet as all spectra were pre-processed with normalization that made the magnitude of the values consistent. From Fig.3-8 it can be seen that weathering resulted in the presence of an additional peak on the spectra of all plastics at 1760 cm^{-1} indicating the introduction of a C=O bond (Liu et al., 2020; Sun et al., 2020; Miranda et al., 2021). The 1760 cm^{-1} peak created by the rooftop weathering was stronger when compared to those created in a simulated weathering experiment. The two rooftop experiments also contributed a peak at 1200 cm^{-1} that corresponds to C-O stretching and caused an uneven baseline in the ranges of 3850 cm^{-1} -3600 cm^{-1} and 2500cm^{-1} to 1700 cm^{-1}. In summary, the surface modification contributed to the intra-class variation of the spectra of PE by introducing additional peaks and a distorted baseline when compared to the

spectra of virgin PE. These spectra were employed to test the performance of PlasticNet with PE spectra that had undergone modification due to weathering.

3.3.4.2 Recognition performance

The ability of PlasticNet to recognize the spectra from the variously modified MPs was initially assessed using a version that was trained with the spectra of virgin PP and PE. In the second phase of testing PlasticNet was re-trained with a training pool that had the spectra from one varied PP added. In this regard the spectra from the white PP were added because the magnitude of variation in this spectra was larger compared to the other 5 types of PP with additives. The retrained version of PlasticNet was then employed to classify all of the varied MPs. In all cases the success of classification was defined as the fraction of the total number of spectra that were correctly identified. Table 3-5 presents the success in classifying the PP samples that had additives. From Table 3-5 it can be seen that when the version of PlasticNet which was trained with virgin PP was employed greater than 90% of the MPs were successfully classified. This indicates the deep learning model can recognize varied spectra due to the presence of dyes and additives. When the re-trained version of PlasticNet was employed for classification (Table 3-5) there was a modest increase in accuracy (i.e. range of increase -1.9~5.3, median of increase 3.7) after the spectra of white PP was added to the training pool. The results indicate that the addition of varied spectra into the training pool can enhance the model's performance in recognizing varied spectra and future versions of the model will benefit from more diverse training pools.

The version of PlasticNet trained with spectra from virgin plastic was also employed for the classification of spectra from PE with surface modification. In this exercise a 90% success in spectra recognition was attained indicating that the deep learning approach could resolve the issue of additional peaks caused by surface modifications. The only error amongst 10 recognitions was that of the spectrum of rooftop experiment 2 which was recognized as PP by PlasticNet. The extent of variation caused by rooftop experiment 2 was only slightly higher than that of experiment 1 (As shown Fig.3-8), but the spectrum from experiment 1 was successfully recognized as PE while the spectrum from experiment 2 was not. The cause of this error could not be identified and requires further exploration. The successful results indicate that PlasticNet performance was not negatively affected by the mode of data collection, as the training data was obtained by transmission mode

while the spectra of the weathered plastics were collected in ATR mode. This indicates the robustness of the model when classifying data from different sources.

Table 3- 5 Performance of the PlasticNet in recognizing spectra of varied PP

Plastic Type	Number of spectra tested	Trained with virgin PP		Re-trained with virgin PP+white PP		
		number of errors	Success (%)	number of errors	Success (%)	Change in success
White PP	196	9	95.4			
Red PP	154	12	92.2	15	90.3	**-1.9**
Green PP	131	13	90.1	6	95.4	**5.3**
Glassfiber reinforced PP	89	7	92.1	4	95.8	**3.7**
PP with flame retardant	130	10	92.3	5	96.5	**4.2**
PP with $CaCO_3$	91	8	91.2	6	93.2	**2.0**
PE experienced surface modification	10			1	90	

3.3.5 Impact of MP thickness

When the FPA FTIR microscope was employed to collect spectra of MPs in transmission mode, the shapes of spectra were observed to be significantly affected by the thickness of the MP at different pixel locations. The different beam path lengths resulted in different intensities of absorption (Zhu et al., 2021). To assess how the thickness of MPs impact the shape of spectra, PE spectra collected from different locations on a sphere were compared (Fig. 3-9A). The spectra from three selected pixels that had different beam travel lengths (i.e. center, middle, edge) are presented in Fig.3-9B. From the plots it can be seen that the intensities of the characteristic peaks of PE at 3100-2650 cm^{-1}, 1455 cm^{-1} and 1376 cm^{-1} obtained for the middle pixel were weak compared with those of the center pixel, causing the distortion of the shape of peaks. It was anticipated that this might result in confusion in the recognition of the spectra. Fig.3-9B also shows that the intensities of essential peaks of the edge pixel were very weak compared with those of the other two pixels, making it appear to be similar to the response from the background. This was consistent with the findings of da Silva et al. (2020) where spectra from pixels at the edge of irregular particles showed deteriorated qualities. In summary, it was anticipated that the variation of spectra due to differences in thickness of MPs might cause difficulty in the recognition of spectra.

A dataset of spectra that was collected in transmission mode from a range of thicknesses of PET films was analyzed to obtain an improved understanding of the impact of beam length on the characteristics of plastic spectra and the generated spectra are plotted in Fig.3-9B. As is shown in Fig.3-9B, the absorbance of the peak at 3100-2900 cm^{-1} increased as the thickness increased from 12 μm to 250 μm, but the absorbance of this peak saturated when the thickness exceeded 250 μm. In contrast, the absorbance of peaks at 3250 cm^{-1} and 2840 cm^{-1} increased as the thickness increased from 12 μm to 250 μm, and the absorbance of these two peaks continues to increase as the thickness exceeded 250 μm. Hence, the overall C-H stretching peak at 3250-2840 cm^{-1} appeared broader when thickness exceeded 250 μm, and this peak became concave at thickness 500 μm. This phenomenon is consistent with that reported by (Primpke et al., 2018) that total absorbance caused the loss of characteristic peaks for large particles. In summary, it was anticipated that the saturation of peaks and associated distortion of spectra at high thickness might cause difficulty in identifying thick particles.

A strategy to address the variation of spectra with MP thickness was evaluated. In the strategy multiple spectra from different locations (i.e. from both the edge and the center of particles) of the same particle were extracted and hence the training, validation, and test datasets included numerous spectra that were obtained over a range of thicknesses. This approach was intended to enable the model to learn discriminative spectral features in a way that accounts for this variation. The testing data for generating Fig.3-5 consisted of 25% of spectra from Dataset 1 that were randomly selected and which incorporated spectra from center, middle and edge of different particles. The high performance (95%+ accuracy) shown in Fig.3-5 indicates the PlasticNet's capability to classify spectra correctly despite the variation of spectra due to the change of the thickness.

(A)

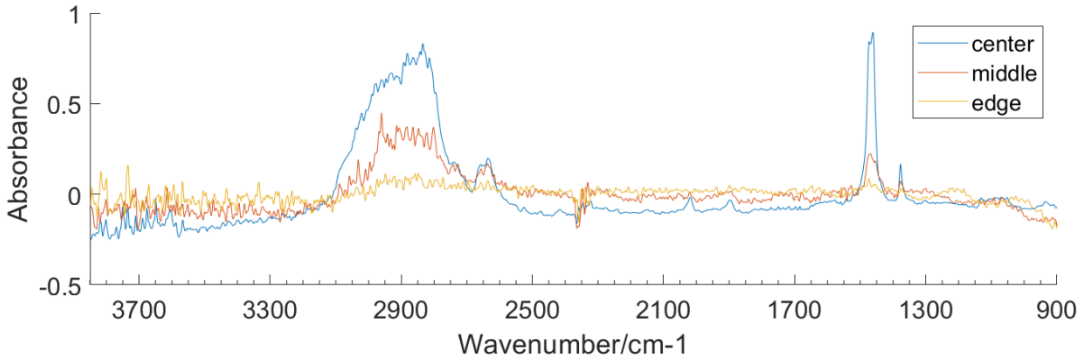

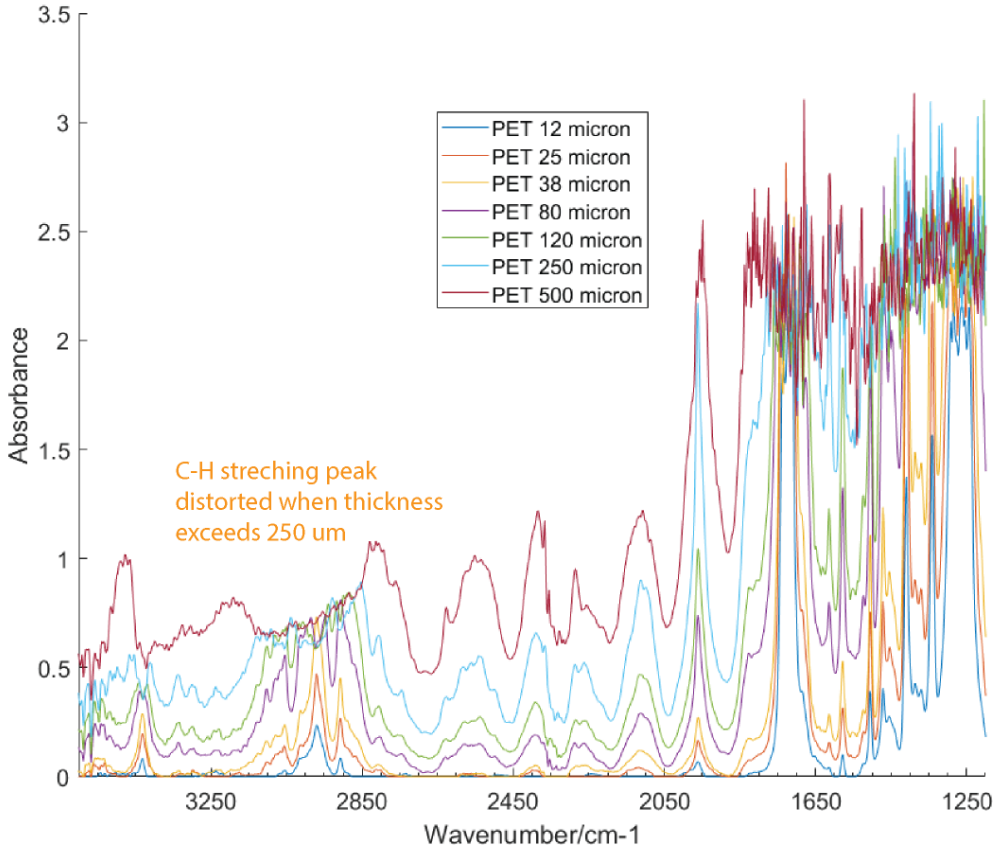

(B)

Figure 3- 9 Variation of transmission FTIR spectra due to variation of the thickness of pixels.

(A) PE spectra collected from different locations in a sphere (B) PET spectra collected from films of different thickness

3.3.6 Comparison of the identification of MPs by PlasticNet and library search

The ability of PlasticNet to identify MPs in a complex dataset was compared with that achieved by a library search approach (Primpke et al., 2018) for dataset 3B. The analysis focused on the

recognition of PE and PP as these two types of MPs were the predominant type of MP in the dataset and the spectra of PE and PP have relatively simple structures that made it possible to manually assess whether false-positive or false-negative detection was occurring. In this exercise, particular attention was paid to the analysis of PE and PP MPs that exceeded 50 μm in size. This size range was chosen due to its amenability to manual locating of the MPs for examination of associated spectra, and the circumvention of potential noise-related issues, such as the presence of single-pixel objects. Following isolation of the PE and PP MPs using a MATLAB-based image analysis, their respective polymer types were compared with those made by PlasticNet. The evaluation yielded 59 and 81 PE MPs identified by library search and PlasticNet, respectively, while 82 and 78 PP MPs were identified by the corresponding methods. While the majority of MPs were consistently identified by the two approaches, some MPs were identified by only one of them.

To address these differences, a manual assessment was carried out, with a focus on assessing potential false-positive or false-negative identifications made by the two methods. In the assessment, the characteristic peaks of PE and PP were used to ascertain whether the identified particles were MPs. Specifically, a particle was designated as PE if its spectra exhibited signature peaks at 3200-2800 cm^{-1}, 1455 cm^{-1}, and a weak 1376 cm^{-1} peak, which was consistent with the spectra structure of the PE particle depicted in Fig. S5. A particle was designated as PE despite the presence of a 1760 cm^{-1} peak, since such a peak can be indicative of weathering, as discussed in section 3.4. In contrast, a particle was designated as PP if its spectra exhibited signature peaks at 3200-2800 cm^{-1}, 1455 cm^{-1}, and a strong 1376 cm^{-1} peak, consistent with the spectra structure of the PP particle in Fig. S5. If the spectra of an identified particle exhibited other complex features in addition to the characteristic spectra of PP and PE, it was designated as 'other'.

As previously mentioned, a total of 59 particles were identified as PE by the library search, and 81 PE particles were detected by PlasticNet (Fig.3-10A). Among them, 55 particles were consistently identified by both methods, accounting for 77.5 % of the total PE MPs that were independently correctly identified by the two methods. Moreover, 4 additional particles were detected by the library search, while 26 additional particles were detected by PlasticNet. Two of the 4 additional particles detected by the library search were correctly identified as PE as verified by manual assessment, while the remaining 2 particles were mis-identified as PE and were identified as PP by manual assessment. Among the 26 additional particles detected by PlasticNet, manual

assessment revealed that 14 of them were correctly identified as PE, while the remaining 12 particles could not be manually verified as PE and were designated as ‘other’. Taken together, PlasticNet correctly identified 97.2 % of all PE MPs while library search correctly identified 80.3% of PE MPs, indicating a 16.9% improvement in the recognition performance.

A total of 82 particles were identified as PP by the library search while 77 PP particles were reported as such by PlasticNet (Fig.3-10B). Among them, 73 particles were consistently identified by both methods, accounting for 88.0 % of the PP MPs that were independently and correctly detected by the two methods. Moreover, 9 additional particles were detected by the library search, while 4 additional particles were detected by PlasticNet. Among the 9 additional particles detected by the library search, 5 of them were verified as PP by manual assessment while the remaining 4 particles were identified as PE. The 4 additional particles detected by PlasticNet were all verified as PP by manual assessment. Taken together, the analysis indicates that PlasticNet and the library search correctly identified approximately similar fractions of the PP MPs in a complex dataset.

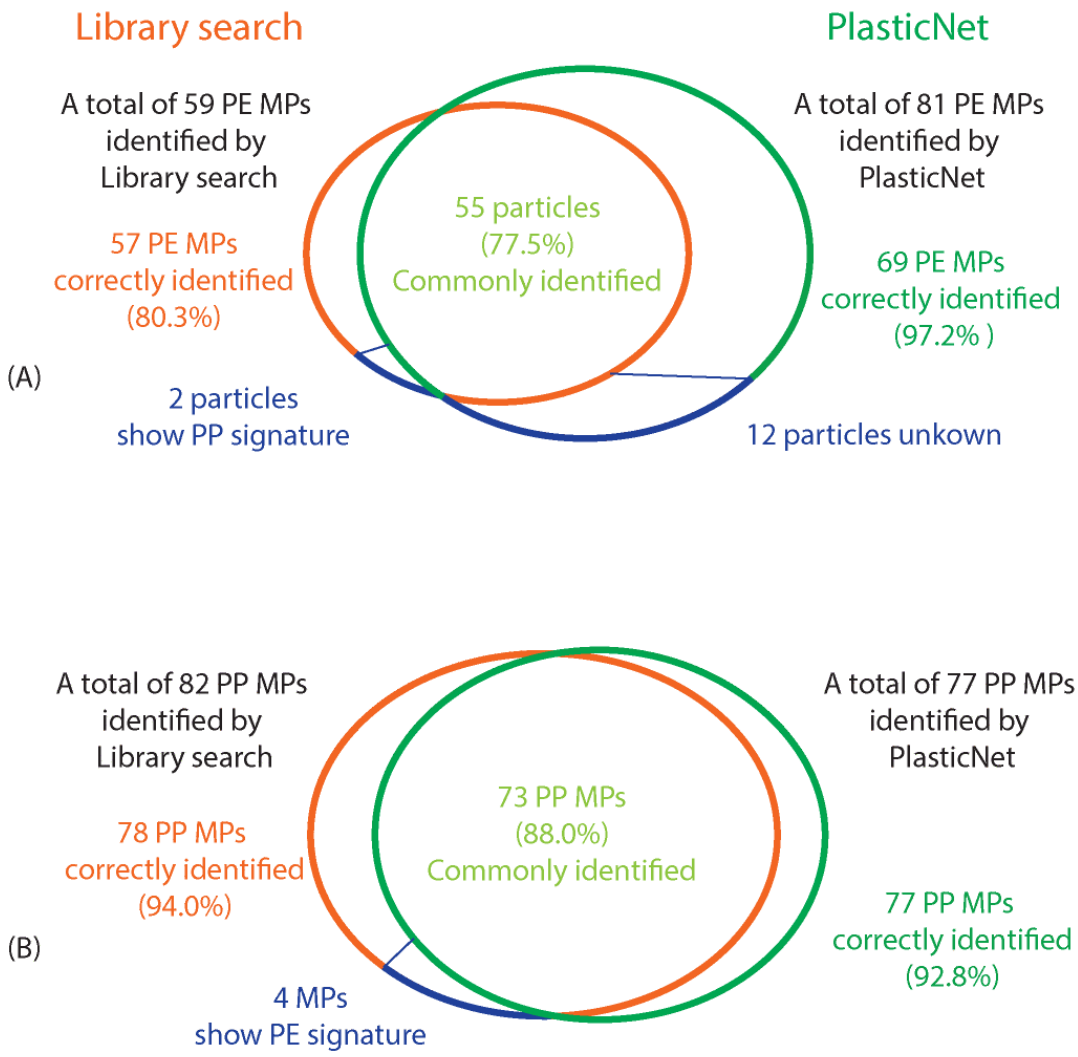

Figure 3- 10 Comparison of the recognition results of Dataset 3B by library search and PlasticNet approaches.

(A) Identification of PE by two approaches. Fraction is calculated using the number of MPs that were independently correctly identified as a denominator (57 by Library search+14 additional by PlasticNet=71 correctly identified PE MPs). (B) Identification of PP by two approaches.

3.4. Conclusion:

This study explored the feasibility of leveraging deep learning for automatic MP recognition of MP images generated by FPA-based micro-FT-IR microscopy. PlasticNet, a deep convolutional neural network architecture that was tailored for MP recognition was developed trained and tested and the following conclusions were arrived at:

- Once trained with virgin spectra, Plastic Net successfully classified 11 types of common plastic with accuracy higher than 95%.
- Critical analysis of the errors in identification, as indicated by a confusion matrix, showed that they could be attributed to 1) edge effects 2) molecular structure similarity 3) contamination of MP standards.
- The PlasticNet shows good performance (92%+) in recognizing spectra that had increased complexity due to the presence of additives and weathering. Re-training of PlasticNet with more complex spectra enhanced the model's capability to recognize complex spectra.
- PlasticNet was able to successfully identify MPs in spite of variations in spectra caused by variations in MP thickness, and showed a 16.9% improvement compared with that achieved by library search when identifying PE MPs in a complex dataset .

Chapter 4 Uncertainties in the enumeration of microplastics in wastewater samples: Model development, Bayesian analysis, and Markov chain Monte Carlo methods

Abstract

WWTPs accumulate and discharge MPs into the environment and hence an accurate understanding of the fate and transport of MPs in WWTPs is vital. However, achieving this accuracy is challenging due to multiple inherent uncertainties in the analytical procedure. This study rigorously investigated uncertainties in microplastics (MPs) enumeration in wastewater using a modelling approach. In this regard, we examined the sources of random errors in each step of MP analysis and refined an existing uncertainty model by modifying and adding assumptions as necessary. Specifically, we undertook a critical analysis of the factors causing variability in the recovery of MPs, which are influenced by differences in size, shape, and type, and integrated these considerations as assumptions in the updated model. The new model was then applied using simulated data and Markov chain Monte Carlo methods to quantify uncertainties. We found that increasing the number of replicates, categorizing and counting MPs separately, and accounting for differential recovery and non-constant recovery significantly improved the accuracy of MP enumeration. The study's findings contribute to developing standardized guidelines for analytical procedures quantifying MPs in wastewater and sludge samples, thereby facilitating more accurate and reliable MP data for environmental studies.

4.1. Introduction

Microplastics (MPs), defined as plastic particles smaller than 5 mm in size, have become a widespread contaminant in the global environment. The increasing production and improper disposal of plastic waste have resulted in the accumulation of microplastics in various ecosystems, including marine, freshwater, and terrestrial habitats (Andrady, 2011; Blair et al., 2017). Wastewater treatment plants (WWTPs) have been recognized as significant sites for MP accumulation, serving not only as collectors of MPs (Michielssen et al., 2016; Mintenig et al., 2017; Talvitie et al., 2017a) but also as a pivotal source of MP discharge into natural aquatic environments (Ziajahromi et al., 2017; Prata, 2018; Blair et al., 2019). Quantifying MPs in samples from various stages of wastewater treatment is essential for elucidating the fate and transport of MPs within WWTPs as well as evaluating the efficiency of treatment technologies for removing MPs (Carr et al., 2016; Chand et al., 2021). Furthermore, the accurate assessment of microplastic pollution in wastewater is crucial for understanding its potential impacts on aquatic ecosystems and developing appropriate mitigation measures (Gies et al., 2018; Ben-David et al., 2020). Nevertheless, achieving accurate enumeration of MPs in wastewater samples presents considerable challenges due to the wide-ranging uncertainties inherent to the analytical procedure.

Intrinsic errors associated with individual steps of the analysis of MPs collectively contribute to variation in the enumeration. The analysis of MPs in wastewater and sludge streams typically entails sample collection, extraction, and enumeration (Hu et al., 2019; Sun et al., 2019). As is summarized by Emelko et al. (2010) and Schmidt et al. (2010) for enumeration of microorganisms and other discrete particles including microplastics used as surrogates in pathogen removal studies, concentration heterogeneity and random sampling errors are linked to the collection step, while loss and non-constant analytical recovery correspond to the extraction step. Concentration heterogeneity may introduce significant variability due to the non-uniform distribution of MPs in the source environment (Lam et al., 2020; Ovide et al., 2022). Additionally, random errors in sample collection have been identified as a source of variability in data (Morgado et al., 2022; De Frond et al., 2023), and the loss of MPs during extraction is inevitable (Halbach et al., 2021; Way et al., 2022), further contributing to uncertainty in concentration estimates and potentially bias when the count per unit volume is used as the estimate. The recovery of labeled MPs in replicate samples has been found to be non-constant (Simon et al., 2018; Konechnaya et al., 2020; Mari et

al., 2021), further leading to variability in enumeration outcomes. Errors originating from earlier stages of the analytical procedure propagate to subsequent steps, resulting in the accumulation of variability throughout the analysis of MPs. Therefore, understanding the intrinsic errors associated with the analytical procedure and quantifying the uncertainty in microplastics concentration estimates arising from these errors is crucial for enhancing the accuracy and reliability of microplastic enumeration in wastewater and sludge samples.

Apart from the errors inherent to the analytical procedure, several operational factors contribute to variability in the enumeration of MPs. Firstly, variations in the number of replicates employed in sample collection, resulting from the absence of standardized protocols for microplastic sampling, may lead to differing degrees of uncertainty in enumeration-based concentration estimates (Schmidt et al., 2010; Bruge et al., 2020). The number of replicates employed in MP studies has ranged from single samples (Carr et al., 2016; Mintenig et al., 2017; Ziajahromi et al., 2017) to 7–10 replicates (Bruge et al., 2020; Bauerlein et al., 2023). There has, however, been limited research quantifying the associated uncertainties and a lack of guidance for a cost-effective number of replicates to reduce uncertainty. Secondly, early studies (Michielssen et al., 2016; Murphy et al., 2016) counted various types of MPs collectively without considering variations in size and shape, which differs from more recent investigations (Ziajahromi et al., 2017; Magni et al., 2019; Bruge et al., 2020; Mintenig et al., 2020) that have incorporated these distinctions (such as counting MPs in different size groups and distinguishing between MP fibers and MP particles) in their enumeration procedures. The extent of uncertainties introduced by counting all types of MPs together compared to separately remains unclear. Moreover, even the most recent studies considering these distinctions have employed the same recovery for all MPs in a given sample, neglecting non-constant analytical recovery among replicate samples (Yang et al., 2019; Wang et al., 2020), and differential recovery attributable to MP size, shape, and type (Long et al., 2019; Xu et al., 2020; Zhang et al., 2020). Recovery of MPs has been found to be strongly influenced by these characteristics (Simon et al., 2018; Konechnaya et al., 2020; Halbach et al., 2021; Mari et al., 2021; Way et al., 2022). The extent of uncertainties introduced in the enumeration of MPs when ignoring non-constant analytical recovery and differential recoveries remains an open question. In summary, there is a need to critically examine how these operational factors contribute to uncertainties in the enumeration of MPs and develop methodologies to account for such uncertainties to improve the accuracy and reliability of MP enumeration in environmental samples.

Bayesian analysis, in conjunction with Markov chain Monte Carlo (MCMC) methods, are widely employed in the field of uncertainty quantification due to its robust and efficient approach (Covernton et al., 2021; Nunes et al., 2021; Takeshita et al., 2022; Thiros et al., 2023). It offers a comprehensive and flexible approach to quantifying uncertainty in parameters of a probabilistic model that incorporates prior knowledge about possible values of the parameters and the available data in a coherent framework (Berger et al., 1994; Ghosh et al., 2006). The result is a posterior distribution characterizing how well alternative values of unknown parameters are supported by the data and prior. MCMC is a computational algorithm that generates a Markov chain of variables that collectively represent the posterior distribution (Andrieu et al., 2003; Andrieu and Thoms, 2008). MCMC methods play a crucial role in the implementation of Bayesian analysis and have proven to be a potent tool in MP research (Covernton et al., 2021; Kahane-Rapport et al., 2022). Emelko et al. (2010) applied a beta-Poisson model to describe random errors in the enumeration of microorganisms and implemented the model using Bayesian analysis coupled with MCMC for the quantification of uncertainties in concentration estimates. Given the similarities between enumerating MPs and microorganisms, it is plausible to extend this model to quantify the uncertainties in MP enumeration. Consequently, this study aimed to develop a probabilistic model that accounts for inherent variability in MP enumeration and investigates the contribution of various operational factors to uncertainties in enumeration-based MP concentration estimates. To achieve this, this study: 1) explores the sources of random errors associated with each step in MP analysis, 2) critically examines the assumptions made by Emelko et al. (2010) and Schmidt et al. (2010) to determine their compatibility with the errors in MP enumeration and further refine the model by modifying or adding assumptions as necessary, and 3) evaluates how various operational factors contribute to the uncertainties in MP enumeration by implementing the newly developed model using simulated data in conjunction with MCMC. This is achieved by contrasting the full model's output which incorporated all assumptions with outputs from simplified models that were implemented with altered inputs or fewer features. The outcomes of this model-based investigation will facilitate a more accurate and rigorous understanding of MP data and contribute to the development of guidelines for analytical procedures quantifying MPs in wastewater and sludge samples.

4.2. Model development

This section presents a probabilistic model for describing the sources of variability in MP enumeration, building upon a probabilistic model presented by Emelko et al. (2010) for enumeration of microorganisms and other particles. To achieve this goal, the sources of error associated with each step in a typical MP analytical procedure are identified and their compatibility with assumptions of the Emelko et al. (2010) model are discussed. Additional assumptions are introduced to extend and adapt the model to represent errors in MP enumeration.

4.2.1 Sources of error in MP enumeration

Gaining an understanding of the occurrence of the errors throughout the steps of MP analytical procedure serves as a foundation for the establishment of statistical methods to reflect these errors in the interpretation of MP enumeration data. A summary of these errors is presented in Figure 4-1 and Table 4-1 for a more systematic understanding. These errors may also apply to analysis of MPs in other media such as freshwater and sediments.

Concentration heterogeneity, associated with sample collection, refers to the spatial variability in concentration of discrete particles throughout a source from which samples are taken (Schmidt et al., 2010). The concentration heterogeneity of MPs mainly arises due to the vertical stratification within the source, as denser MPs settle while lighter MPs tend to float (Lam et al., 2020; Cowger et al., 2021).

Random sampling error, associated with sample collection, pertains to the inherent variability in the quantity of MPs contained within a sample originating from a homogeneous source, owing to the discrete nature of the MPs (Emelko et al., 2010). Random sampling error constitutes the variation in the number of particles present among replicate samples of equal size extracted from a homogeneous source. Given that discrete particles cannot be uniformly dispersed throughout the source and the particle count in a sample must be an integer, the quantity of MPs in a sample is contingent upon the specific portion of the source that is sampled and the random dispersion of particles within that region. MPs can cluster due to physical forces like currents and turbulence, as well as biological reasons, such as agglomeration after forming biofilms on their surfaces (Summers et al., 2018). Additionally, MPs may carry an electrical charge, leading to their sticking

together (Sturm et al., 2022). These factors result in clustering that deviates from the Poisson process (Schmidt et al., 2014).

Loss of MPs can occur during sample extraction and can be attributed to several factors. During density separation, some plastics may not rise to the surface of the liquid and consequently are discarded along with the sediment. Additionally, the collection of floating MPs from the surface may not be entirely efficient and a portion of MPs might be retained on the surface of floatation vessel. In addition, MPs may be retained in pipettes or glassware, or on the filtration device, and thereby become lost. Furthermore, the transfer of the filter from the filtration apparatus to the micro-FT-IR imaging system may also contribute to the loss of some MPs. MPs that do not adhere strongly to the dry filter might be lost from the filter when the filter is moved.

Non-constant analytical recovery, associated with the extraction step, is characterized by variation in recovery among replicate samples (Schmidt et al., 2010). The recovery of discrete particles may display variation among replicate samples due to either controllable and measurable factors (e.g., different lab personnel) or apparent randomness. Different categories of microplastics may also have different statistical distributions for random variation in recovery, which will be discussed in detail in Section 2.2.

The counting error refers to the discrepancy between the actual quantity of MPs present on the filter and the detected count via micro-FT-IR imaging, deep learning search, and image analysis algorithms. This discrepancy could take the form of under- or over-counting MPs due to identification challenges. The imaging and algorithm might under-count when particles cluster together or misidentify MPs as other particles. Conversely, they may over-count by misinterpreting noise or other particles as MPs. Consistent with the methodology employed by Emelko et al. (2010), this study treats counting errors as a constituent of the analytical error, implicitly incorporated within the recovery data.

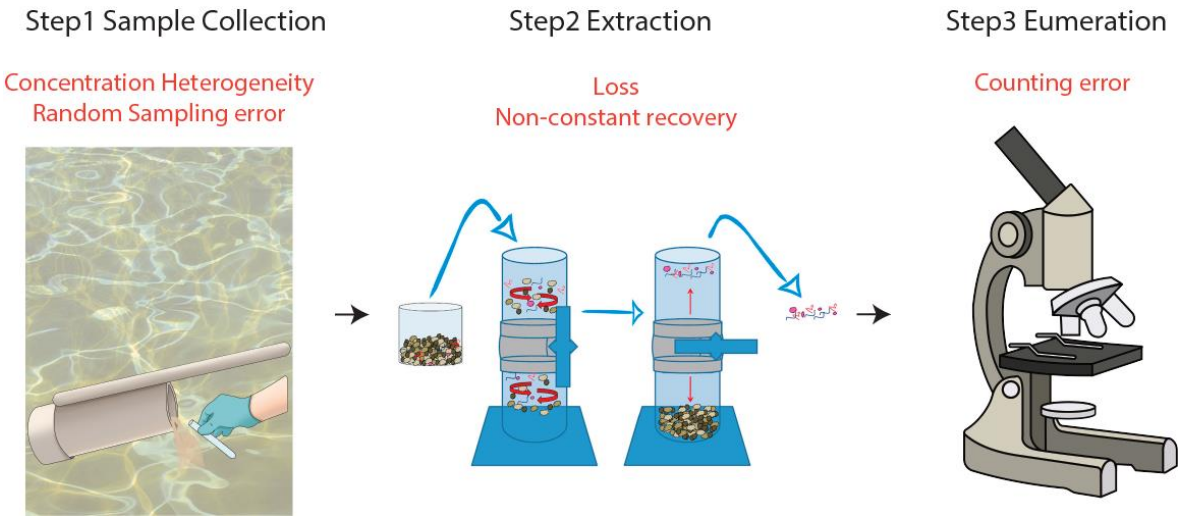

Figure 4- 1 Steps of MPs analysis and sources of error associated with each step.

Adapted from Coppock et al. (2017)

Table 4- 1 Description of errors in the analysis of discrete particles (Schmidt et al., 2010) and how they manifest in MP analysis.

Analytical steps	Error	Definition	Manifestation in MP analysis
Sample collection	Concentration heterogeneity	Spatial variability in concentration of MPs throughout a source from which samples are taken	Vertical stratification: denser MPs settle while lighter MPs remain afloat
	Random sampling error	Randomness in the number of MPs presents in a sample taken from a homogeneous source.	Inherent variability in the quantity of MPs in a homogeneous sample owing to the discrete nature of MPs Clustering of MPs within an otherwise homogeneous source
Extraction	Random analytical error	Discrepancy between true number of MPs in a sample and the number of particles eventually observed	MPs may not rise to the surface during the density separation process The collection of floating MPs from the surface of the density separation vessel may not be entirely efficient MPs may be retained in pipettes and glassware, or on the filtration device Losses may occur during transfer of the filter from the filtration apparatus to the counting system. Given the reduced adhesion between MPs and the filter when in a dried state, there is a possibility for the MPs to be lost from the filter.
	Non-constant analytical recovery	Variation in recovery among samples due to randomness. Random error due to unpredictable and non-systematic variations in measurements or observations that arise due to chance fluctuations or uncontrollable factors.	The losses described above may have varying magnitude from sample to sample.
Enumeration	Counting error	Discrepancy between the actual quantity of MPs present on the filter and the detected count	The imaging and algorithm can under-count if particles aggregate or misidentify other particles as MPs, and alternatively, over-count by interpreting noise or non-MP particles as MPs.

4.2.2 Adaptation of model to describe MP enumeration in wastewater

Having identified the sources of error in each step of MP enumeration in wastewater samples, this section focuses on developing a mathematical description of the errors with careful consideration of assumptions. The beta-Poisson model described by Emelko et al. (2010) presumes that random sampling error follows a Poisson distribution, losses follows a binomial distribution, and non-constant analytical recovery follows a beta distribution. The binomial distribution and Poisson distribution can be combined into a Poisson distribution accounting for losses, so the binomial component is not reflected in the name of the model. In this section, a thorough examination of the established model's underlying assumptions is conducted, and the agreement of these assumptions with the modeling of uncertainties pertaining to the quantification of MPs is assessed.

The established beta-Poisson model presumes that there is no concentration heterogeneity in the source and that the particles are randomly dispersed and not clustered. In another words, the heterogeneity resulting from vertical stratification, the clustering of MPs due to physical, biological, and electrical charge are not accounted for during model development. Under the first assumption, samples are independent replicates that are mutually representative of the same source concentration. The latter assumptions lead the number of particles in a sample of specified volume to follow a Poisson distribution, which is essential for making inferences about the broader source from the count of particles in the sample. The distribution of MPs in wastewater and sludge samples exhibit heterogeneity and clustering, as discussed in section 2.1, and statistically characterizing this heterogeneity presents a significant challenge. To simplify the modeling process, the absence of concentration heterogeneity is assumed, leading to the presumption that the number of MPs in a sample follows a Poisson distribution. While this approach may have certain imperfections, it serves as a starting point for obtaining a comprehensive portrayal of the sampling error.

The beta-Poisson model presumes that the observation of each particle in a sample is independent of the loss or observation of all other particles, and the particles are observed or lost according to a Bernoulli process with equal probability of observation. As a result, the number of observed particles can be modeled by a binomial distribution representing analytical error. As outlined in section 2.1, the reasons for the loss of MPs are random errors analogous to those causing the loss of discrete particles, as described in the established model. Consequently, the losses of MPs

associated with these factors adhere to a Bernoulli process that can be effectively modeled using a binomial distribution. In terms of counting error, the model assumes that these errors are restricted to losses, thereby disregarding the possibility of over-counting errors. Counts exceeding the actual quantity of MPs on the filter lie beyond the scope of this study. If we assume that these counting errors are random and do not inflate the number of MPs, then they can be considered part of the analytical recovery and modelled by a binominal distribution.

Regarding counting error, this model assumes that counting errors are limited to losses (i.e. no over-counting errors). The occurrence of counts that exceed the true number of MPs on the filter can arise from potential misclassifications, such as erroneously counting Non-MPs as MPs, or mistakenly identifying noise as MPs. Nevertheless, the addressing these specific sources of error lies outside the scope of the present study. If it is assumed, however, that these counting errors are random and cannot inflate MPs, then they can be regarded as a component of the analytical recovery and this model can still be used.

Finally, the beta-Poisson model presumes that the probability of recovery varies randomly among samples and that this variation, referred to as non-constant analytical recovery, can be described by a beta distribution due to its mathematical convenience and versatility of shape. This assumption is compatible with the modeling of uncertainties in the quantification of MPs, as non-constant analytical recovery has been reported in multiple studies (Simon et al., 2018; Konechnaya et al., 2020; Mari et al., 2021) and observed in our own research. Given that MPs are fundamentally discrete particles, non-constant analytical recovery can be characterized similarly to that of the established model.

The most problematic assumption in applying the beta-Poisson model to MP enumeration is that all particles in a sample have an equal probability of being observed, regardless of characteristics such as size, shape, and type. This assumption may not reflect errors in the quantification of MPs, as differential recovery associated with size, shape, and type of MPs has been reported in numerous studies as outlined below.

The size of MPs significantly contributes to the differential recovery of MPs. Small MPs, characterized by a larger surface-area-to-volume ratio in comparison to their larger counterparts, can exhibit enhanced adhesion to surfaces, filters, or extraction devices(Sun et al., 2021) (Sun et al., 2021). This can, in turn, result in a decreased recovery. Additionally, small MPs may possess

varying buoyancy or settling velocities, which could prompt them to settle differently during density-based separation methods (Laursen et al., 2022). Consequently, these MPs might not be separated as efficiently as larger MPs, leading to a lower recovery. Lastly, small MPs are more prone to aggregate with each other or other materials (Li et al., 2022), which could potentially obstruct their recovery. Aggregation of MPs with heavy particles can result in their loss during density separation, while aggregation with each other could lead to their misidentification as a single particle (Alimi et al., 2018) during enumeration.

In addition, the shape of MPs is a crucial contributing factor for differential recovery of MPs. Particles and fibers, due to their differing shapes, can exhibit varied buoyancy and settling velocities, which in turn can influence their flotation or sedimentation behavior during density separation (Waldschläger and Schüttrumpf, 2019). Specifically, fibers, given their elongated and thinner structure, may demonstrate unique entanglement patterns or adhesion behavior to surfaces, as compared to particulate MPs (Mendrik et al., 2023).

Furthermore, the polymer type of MPs has been observed to influence their recovery. The density of MPs can vary depending on the polymer type, which can result in diverse flotation or sedimentation behavior during density separation methods (Waldschläger and Schüttrumpf, 2019). Additionally, surface properties, such as charge and hydrophobicity, can differ between various polymer types (Burrows et al., 2020). These differences can, in turn, affect their affinity towards extraction solvents, filters, or surfaces.

To account for these variations in recovery, it is proposed to classify MPs into different categories among which it is assumed that there is differential analytical recovery (in addition to non-constant recovery within each category). In this study MPs were divided into four categories based on size and shape: Category A (20–100 µm particles), Category B (100–250 µm particles), Category C (250–500 µm particles), and Category D (fibers). This categorization assumes all particles within a given category share identical recovery and beta distribution parameters for non-constant analytical recovery, though these may vary across different categories. In addition, the recovery of MPs from a specific category is independent of the presence and concentration of particles from other categories within the sample.

This type of modeling presumes that enumeration methods are in statistical control, hence all errors are random and can be described by probabilistic distributions. Non-random errors including

analyst mistakes and predictable differences in recovery due to changes in particle characteristics, water quality attributes, sample attributes, or methodology are not addressed in this model.

Table 4- 2 Summary of assumptions in beta-Poisson model and compatibility with errors in the enumeration of MPs in wastewater

Attribute	Assumptions in Emelko et al. (2010) model	Additional Assumption
Concentration heterogeneity	No concentration heterogeneity in the source	
Random sampling error	Particles in the source are randomly dispersed and not clustered, hence number of particles in a sample is Poisson-distributed.	
Random analytical error	When assuming particles are independent of each other, the observation or lost of individual particle yields a Bernoulli process	
	All analyte particles in a sample have an equal probability of being observed so that the number observed follows a binomial distribution	MPs were classified into different categories. MPs in a category have the same recovery while particles in different categories have different recoveries.
Non-constant recovery	Recovery varies randomly among samples, which can be described by a beta distribution	Each category of MPs has a potentially unique beta distribution
Statistic Control	All errors are random errors and can be described by probabilistic distributions	

4.2.3. Probabilistic model specification

On the basis of the assumptions discussed in section 2.2, a probabilistic model for the uncertainties in enumeration of MPs was assembled and incorporates 1) Poisson-distributed random sampling error, 2) binomially-distributed random analytical error, 3) beta-distributed non-constant analytical recovery, and 4) MPs grouped into 4 categories with each category having potentially unique analytical recovery properties. The updated beta-Poisson probabilistic model describing errors leading to random variation in the count of MPs obtained is expressed as equation 1 using category A MPs as an example.

$$f(x_A) = \frac{(c_A V)^{x_A}\Gamma(a_A+b_A)}{x_A!\Gamma(a_A)\Gamma(b_A)} \int_0^1 (e^{-c_A V p_A})\,({p_A}^{x_A+a_A-1})(1-p_A)^{b_A-1} dp_A \quad (1)$$

where $f(x_A)$ is the marginal distribution of category A, x_A is the number of observed particles, c is the particle concentration in the source, V is the sample volume, p_A is the sample-specific recovery achieved in sample processing to achieve the count x, a_A,b_A are parameters of the beta distribution for non-constant analytical recovery, and $\Gamma()$ is the gamma function.

In Bayesian parameter estimation, the posterior distribution is proportional to the product of the likelihood function and a prior distribution. After assuming a proper prior, the posterior distribution for concentration maintains a direct proportionality to the likelihood function concerning certain replicate enumerations, which can be calculated using the model above.

4.3. Investigation of uncertainties: Data simulation and Bayesian analysis via MCMC

After refining the previous model based on a critical assessment of its assumptions, we now pivot to assessing the influence of operational factors on uncertainties in MP enumeration using this updated model, simulated data, and Bayesian Analysis coupled with a MCMC methodology. These methods have been reported to offer significant advantages in uncertainty quantification, including the ability to handle complex models and integrate prior knowledge with observed data, leading to more informed inference based on available information (Sorensen et al., 2002; Renard et al., 2006; Emelko et al., 2010). Simulated data was utilized as input because it can be generated with known concentration values, thereby enabling a comparison of the output with true values. In contrast, for real data, the true concentrations are typically unknown while only the sample estimates are available, rendering direct evaluation of error infeasible.

4.3.1. Data simulation

Simulated enumeration data were generated to mimic the concentrations of MPs observed in real wastewater samples, with the parameters for producing these data summarized in Table 4-3. The total amount of MPs was assumed to be 300 particles/L, consistent with concentrations reported by Conley et al. (2019). Fibers were presumed to constitute 40% (proportion in terms of count) of the total MPs, while particles accounted for the remaining 60%, in agreement with the proportion of fibers versus particles reported in recent studies (Lv et al., 2019; Magni et al., 2019). Regarding the particle size distribution, we created hypothetical proportions for each size category and the proportions was assumed to decrease with increasing size. This is consistent with findings from multiple wastewater MP studies (Murphy et al., 2016; Ziajahromi et al., 2017) that showed small MPs constitute a majority of the MPs in samples whereas large MPs represent only a small fraction. We formulated hypothetical mean recovery for MP particles, in congruence with empirical observations that recovery increases commensurately with particle size presented by (Konechnaya et al., 2020; Mari et al., 2021). Furthermore, we postulated a hypothetical mean recovery for MP fibers, in line with the observation that fibers are more readily recovered than particles by Waldschläger and Schüttrumpf (2019). A hypothetical standard deviation of recovery for each category was postulated based on a comprehensive review of figures reported from a number of

studies focused on MPs in wastewater (Magnusson and Norén, 2014; Tagg et al., 2016; Leslie et al., 2017; Loder et al., 2017), to ensure consistency between the hypothetical deviations and the empirical evidence. The corresponding beta distribution parameters were calculated from the mean and standard deviation of analytical recovery for the category. Ten replicate enumeration data (Table B1 in Appendix B) were simulated in R (code provided in supplementary content) using the model developed in Section 2.2 and parameters in Table 4-3.

Table 4- 3 Parameter values employed for creating simulated MP data

Category	Concentration (count per unit volume) and proportion (%)	Analytical recovery beta distribution parameters			
		Mean	Standard deviation	*a*	*b*
A (20-100 µm particles)	90 (30%)	0.35	0.18	2.11	3.91
B (100-250 µm particles)	60 (20%)	0.52	0.23	1.93	1.78
C (250-500 µm particles)	30 (10%)	0.81	0.14	5.55	1.30
D (fibers)	120 (40%)	0.92	0.10	5.85	0.51
Weighted average and pooled parameters		0.66	0.15	5.59	2.9

4.3.2 Bayesian uncertainty inference using MCMC methods

Bayesian analysis is a statistical approach that incorporates new evidence to update prior knowledge, resulting in posterior distributions that quantify the accuracy and uncertainty in model parameters (Berger et al., 1994; Ghosh et al., 2006). In contrast to other statistical methods, Bayesian analysis allows for the incorporation of prior information and expert knowledge into the modeling process, making it a powerful tool for addressing complex problems and uncertainty quantification. Moreover, by providing a coherent framework for uncertainty assessment, Bayesian analysis can help non-experts understand and interpret results in an intuitive manner, thereby enhancing decision-making processes.

In Bayesian uncertainty inference, the Markov chain Monte Carlo (MCMC) method is commonly used in estimating the posterior distribution of model parameters, which represents the updated

knowledge after incorporating observed data (Sorensen et al., 2002). MCMC provides an efficient numerical technique to sample from complex posterior distributions (Renard et al., 2006). It generates a Markov chain of parameter values, where each new value depends only on the current state and not on the previous history of the chain. Once the chain converges, a large number of samples are drawn to represent the posterior distribution. These samples can be used to estimate various characteristics of the posterior distribution, such as the mean, median, or credible intervals. A credible interval, stemming from Bayesian inference, reflects the uncertainty in the parameter estimate, considering both the data and prior knowledge, and denotes a range of values likely to encompass the true parameter value based on the observed data and prior beliefs. This differs from a confidence interval in frequentist statistics, which represents the range of values likely to contain the true parameter value in repeated sampling scenarios. The parameters derived from the posterior distribution offer a comprehensive understanding of the uncertainties associated with the model parameters.

In this study, Bayesian analysis coupled with MCMC was carried out in a similar procedure to that described by (Schmidt et al., 2022) using OpenBUGS. A uniform distribution wherein all outcomes are equally probable was employed as the prior for the total concentration (*Ctot*). The parameters of the uniform distribution were set with a lower bound of 0 and an upper bound of 1000 MP/L. The selection of 1000 MP/L as the upper bound is sufficiently high to ensure that it does not impose constraints on the posterior. A Dirichlet distribution with parameters (1,1,1,1) was employed as prior for the presence of each category of microplastic particles (w_1, w_2, w_3, w_4), respectively, set to confer equal prior weight to all categories. The Dirichlet distribution allows for the modeling of proportions that sum up to one across multiple categories (Wong, 1998), which is consistent with the requirement that the proportions of the MP categories sum to 1.

The analysis was carried out using the OpenBUGS software (version 3.2.3) (Lunn et al., 2009), with randomized initialization and 2,000 iterations following a 1,000-iteration burn-in period. The burn-in period refers to the number of iterations discarded before the chain converged and is required to obtain reliable inference. Rapid convergence and efficient mixing of the Markov chain was achieved so that only a small number of iterations was needed. Each iteration generated an estimate of C_{tot}, w_1, w_2, w_3, and w_4 for the MPs. The Markov chain of values produced in this manner collectively represented a sample from the posterior distribution, which characterized the

distribution of C_{tot}, w_1, w_2, w_3, and w_4 values in the sample, taking into account both the simulated data and prior information. The derived posterior values were used for evaluation of the estimates through statistical analysis techniques, including the generation of Empirical Cumulative Distribution Function (ECDF) plots. This allowed estimation of 95% credible intervals, and computation of errors based on the posterior means.

4.3.3 Investigating uncertainties caused by operating factors using varied model structures

To investigate the contribution of operating factors in the analytical procedure to the uncertainties in enumeration, the output of the full model, which integrated all assumptions, was compared with the output of models with different inputs, or the output of models with fewer features. The change of input or the omitting of features emulated operating factors that often differ between studies where MP concentrations have been reported.

The number of replicates utilized in MP studies has been found to range widely with some investigations employing single samples while others use 7 to 10 replicates. Despite this range, research efforts aimed at quantifying the uncertainties associated with varying numbers of replicates remain limited. Furthermore, there is a notable absence of guidance regarding the optimal and cost-effective number of replicates that effectively minimize uncertainty. As a result, establishing a standardized approach for determining an appropriate number of replicates in MP studies is crucial for enhancing the accuracy and reliability of MP enumeration. In an effort to address this knowledge gap, the model was applied with different numbers of simulated enumeration data as input, including scenarios with 1, 2, 3, 5, and 10 replicates. By evaluating the uncertainties associated with these varying numbers of replicates, the study aimed to provide insights into the relationship between the number of replicates and the resulting uncertainty, thereby contributing to the development of guidelines for determining an appropriate and cost-effective number of replicates in MP studies.

There are few reports of MP enumeration that categorize particles by size or morphology despite the fact that particle recovery has been found to vary with size and shape. To investigate the extent of uncertainties introduced by this approach, a simplified model was implemented using only the total count of MPs (last column in table B1) as input and pooled recovery parameters for all categories (a_{pooled}, b_{pooled}). The derivation of the pooled recovery parameter involved the computation of the weighted averages of both the mean and the variance from the various

categories. This was followed by back-calculation to ascertain the corresponding beta distribution parameters. The resultant parameters are presented in Table 4-3. The output from the simplified model was then compared with that obtained from the full model.

Though recent studies consider distinctions in terms of particle size, shape, and type, they have typically employed the same recovery for all MPs in a given sample, few studies (e.g. Xu et al. (2019)) employed a constant recovery obtained for spiking a specific category MP in a single sample to represent the recovery of MPs in all categories in all samples, effectively ignoring both non-constant recovery and differential recovery. To investigate the extent of uncertainties introduced by this approach, a simplified model was implemented using separated counts for different categories, but applying a constant recovery from category C (p_c) to categories A, B, D, which means assuming $p_A = p_B = p_C = p_D$). Category C was chosen as a representative because MPs in this size range(250-500 μm) is easier to be manipulated hence more easily used in spiking test. A random number was generated from the beta distributions corresponding category C using R simulation as recovery p_c for the simplified model considering the recovery follows a beta distribution. The output from this simplified model was then compared with that obtained from the full model.

Some other studies (e.g. (Li et al., 2018; Long et al., 2019)) acknowledged non-constant recovery by spiking replicates of samples, but only one category of MPs was spiked in these studies. The obtained non-recovery from this a specific category was used to represent the recovery from all categories, which ignores the differential recovery associated with size and morphology. To investigate the extent of uncertainties introduced by this approach, a simplified model was implemented using separated counts for different categories,but applying beta-distribution parameters from category C (a_c, b_c) to categories A, B, and D, which means assuming $a_A = a_B = a_C = a_D$, $b_A = b_B = b_C = b_D$. The output from this simplified model was then compared with that obtained from the full model.

A another possible recovery practice is to spike MPs in 4 different categories but only in one sample. The resulting data from this single run of experiment are 4 different values for each MP category This approach acknowledges differential recovery by category but ignores the non-constant recovery amongst replicates of samples. To investigate the extent of uncertainties introduced by this approach, a simplified model was implemented using separated counts, and 4

constant but different recovery ($p_A \neq p_B \neq p_C \neq p_D$) that were randomly generated based on the beta distributions corresponding category A B C D respectively. The output from this simplified model was then compared with that obtained from the full model.

4.3.4 Data analysis

ECDF curves were used to provide insights into the characteristics of each posterior distribution. Further ECDF curves were employed to compare posterior distributions obtained from the different models and datasets. The ECDF curves were created by ordering the observations in a sample from smallest to largest and calculating the cumulative proportion of observations that fell below each value. The ECDF plot shows the proportion of observations in the MCMC-generated set of concentration values that were less than or equal to each value on the x-axis.

In each case, the performance of the model was assessed in terms of both error and uncertainty of estimated parameters (i.e. C_{tot}, w_1, w_2, w_3, and w_4 in the source). The percent error of C_{tot} was calculated using equation 2 as an example:

$$\% \text{ Error } C_{tot} = (\text{Posterior mean of } C_{tot} - \text{Actual } C_{tot}) / \text{Actual } C_{tot} * 100\% \quad (2)$$

The uncertainty of estimated parameters was quantitatively described using an equal-tailed 95% credible interval provided by OpenBUGS. The credible interval is an interval within which the true concentration is believed to lie with 95% probability and is computed from the 2.5^{th} and 97.5^{th} percentiles of the posterior distribution.

4.4. Results

The impact of the number of sample replicates, the categorization of particles by size and morphology, and the consideration of losses and differential recovery on the uncertainties and accuracy of MP enumeration was assessed. Through the analysis of empirical cumulative distribution function (ECDF) curves, credible intervals, and errors, we aim to establish guidelines for MP enumeration that minimize uncertainties and optimize the use of resources, while providing accurate estimates of source concentrations and proportions of each category.

4.4.1 Number of replicates

This portion of the study sought to develop information that will inform the establishment of guidelines for the optimal number of replicates in MP studies. To study the effect of the number of replicates on the uncertainty in MP enumeration, the ECDF of the posterior distributions for models employing 1, 2, 3, 5, and 10 replicates were depicted in Figure 4-2A. The ECDF plot shows the proportion of observations in the MCMC-generated set of concentration values that were less than or equal to each value on the x-axis, which approximates the cumulative density function of the posterior distribution. Also, the errors of estimation based on posterior mean, and the uncertainty of estimation reflected by 95% credible length were calculated (see Appendix B) to evaluate the effect of replicates on uncertainty of concentration estimation.

The ECDF curves in Figure 4-2A showed distinct differences in location and shape. The ECDF curve with a steeper slope and narrower width suggests lower uncertainty, indicating concentrated data within a small range. Conversely, a gentler slope and wider width indicate higher uncertainty and a more spread-out data distribution. As shown in Figure 4- 2A, the slopes of curves generally decrease as the increase of replicates as is shown in Figure 4-2A, indicating a decreased uncertainty with the number of replicates. Moreover, the x-value at which the ECDF crosses the 0.5 mark on the y-axis corresponds to the median of the posterior. The medians from 2, 3, 5, and 10 replicates are close to the true value of 300, indicating an accurate estimation at these number of replicates.

The estimation error (calculated using equation 2) derived by comparing posterior mean with true value is an important metric to determine the optimal number of replicates. The posterior mean values derived from replicates 1, 2, 3, 5, and 10 were found to be 404 MP/L, 282 MP/L, 288 MP/L, 335 MP/L, and 316 MP/L, corresponding to errors of 51.2%, 8.7%, 6.5%, 12.7%, and 6.7%,

respectively. The model output at one enumeration reveals that the estimation exhibited a substantial error. This observation is supported by the one-enumeration ECDF curve which is noticeably shifted to the right compared to the other curves, indicating significant overestimation. The error was significantly reduced to 8.7% by increasing the number of replicates to two, and the employing of three replicates further decreased the error to 6.5%. These decreased errors indicate a notably accurate estimation, particularly when utilizing 3 replicates.

Interestingly, the error increased to 12.7% when 5 replicates were used but then decreased back to 6.7% with the inclusion of 10 replicates. This pattern can be attributed to the fact that data simulation for replicates 4 and 5 generated some larger enumeration numbers for each category (as shown in S2 Appendix B) that deviated considerably from the mean of each category. Consequently, the estimated mean was inflated (335 MP/L) when incorporating these large enumeration values. However, the simulated values in replicates 6-10 were closer to the mean. As the data is nested (e.g. ten replicates encompass all the data in the five replicates), the estimated mean at 10 replicates (316 MP/L) was pulled back closer to the actual mean (300 MP/L) hence reduced error. In summary, the analysis demonstrates a significant decrease in error when transitioning from one enumeration to two or three replicates. Additionally, the lowest error was achieved with three replicates, indicating that 3 is an optimal number for MP enumeration with reasonable resources and to maximize accuracy.

Credible intervals serve as a robust metric for quantifying uncertainty, as they provide a range in which an estimated parameter is likely to lie with a certain probability considering the observed data and Prior information. In Figure 4-2B, the 95% credible intervals obtained using varying numbers of replicates were presented. The lengths of the credible intervals were 512.7, 124.6, 105.2, 109.7, and 64.5 for replicates 1, 2, 3, 5, and 10, respectively. A significant decrease (75.6%) in uncertainty was observed when moving from 1 enumeration to 2 replicates. Furthermore, an additional 15.5% decrease in uncertainty occurred when the number of replicates increased from 2 to 3. These findings demonstrated reliable estimates were achieved at 3 replicates.

Similar to the trend observed for error, there was a slight increase in uncertainty from 105.2 to 109.7 when the number of replicates increased from 3 to 5, followed by a decrease to 64.5 with 10 replicates. This pattern can be also attributed to the fact that the data simulations in replicates 4 and 5 generated larger enumeration numbers that deviated significantly from the mean, thereby

introducing additional uncertainty in the concentration estimation. However, the simulated values in replicates 6-10 were closer to the mean, leading to a decrease in uncertainty. When observed in the context of the figure, the credible interval obtained from 5 replicates exhibited a slight expansion compared to that from 3 replicates, and it skewed towards the upper portion of the true value line. Similarly, the interval obtained from 10 replicates showed a slight shortening compared to that from 5 replicates and approached closer to the true value line. Collectively, these observations on credible interval indicate that the minimum level of uncertainty was achieved with 3 replicates, suggesting that 3 replicates represent an optimal number for MP enumeration considering resource constraints while effectively reducing uncertainty.

Viewed collectively from the ECDF curves, the errors, and the uncertainties reflected by credible intervals, these results suggest that the use of three replicates is an optimal approach to maximize accuracy and minimize uncertainties in MP enumeration. This provides a substantial reduction in error and uncertainty compared to single and two measurements, while avoiding the potential for diminishing returns associated with using more than three replicates.

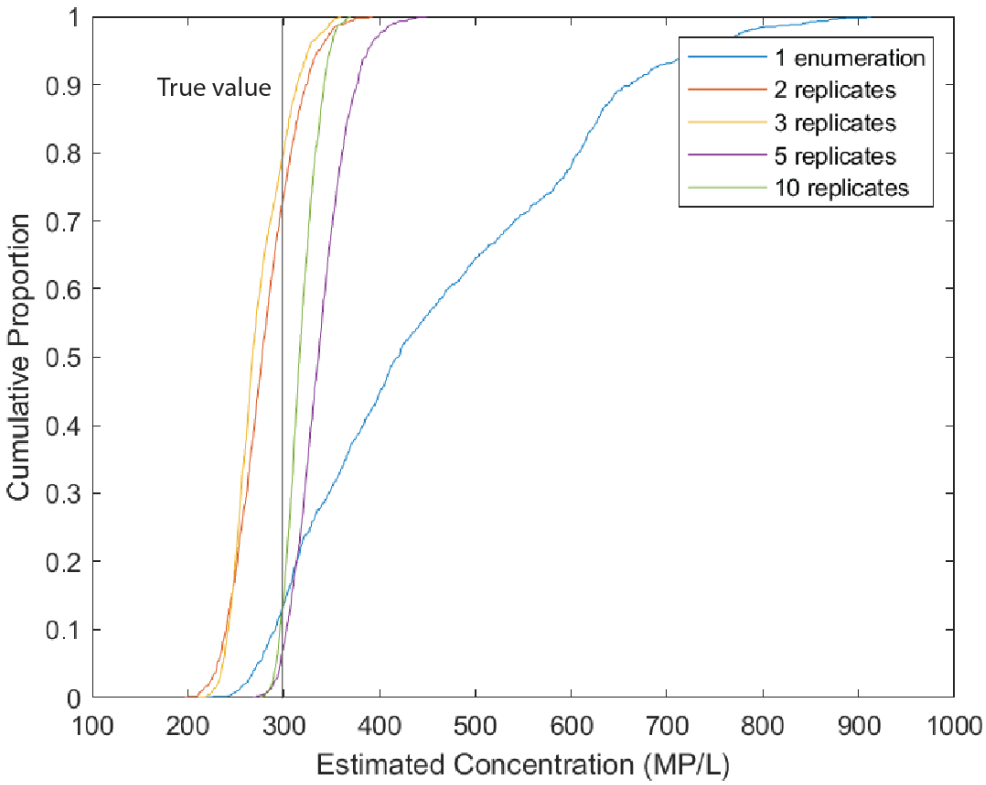

(A)

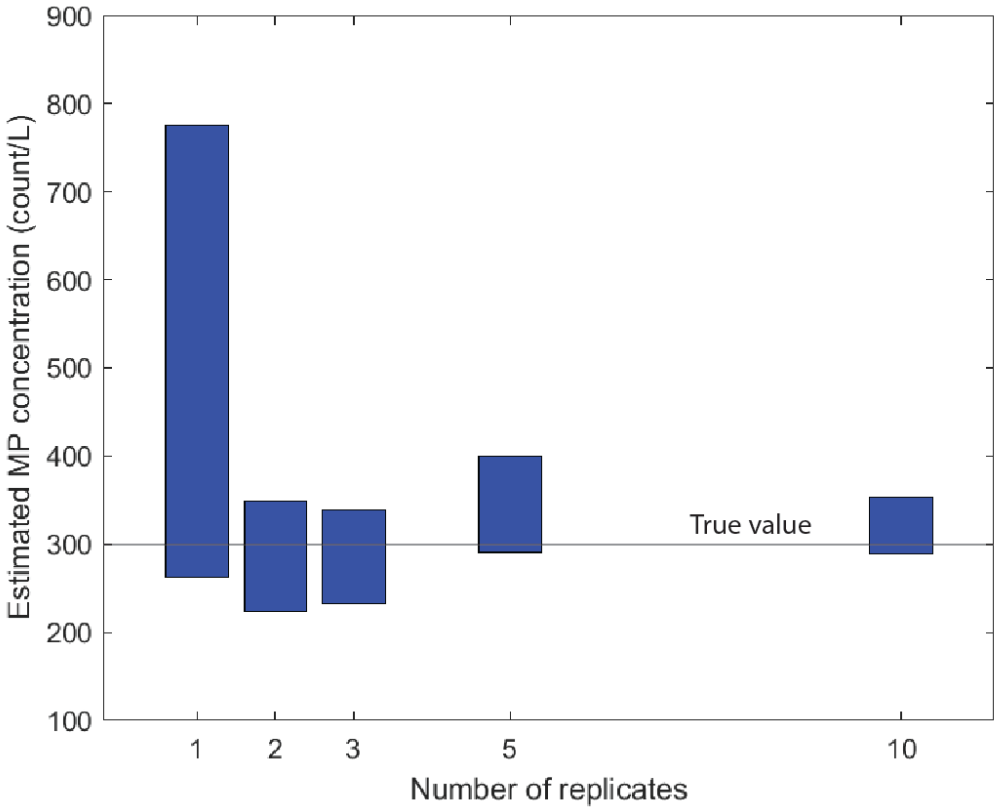

(B)

Figure 4- 2 Effect of replication on the uncertainties of MP enumeration (A) ECDF curves (B) 95% credible intervals obtained

4.4.2 Categorization of MPs

Many reports of MP enumeration do not categorize the particles by size or morphology despite the fact that particle recovery has been found to vary between size and shape categories. Hence, to investigate the impact of disregarding categories on the uncertainties of MP enumeration, ECDF curves, 95% credible interval lengths, and error of estimation from the full model and a simplified model were plotted and calculated. Based on the findings presented in Section 4.1, 3 replicates of enumeration were chosen to implement the model because it is an optimal number of replicates which optimizes the use of resources and at the same time to improve accuracy and reduce uncertainties. The simplified model was implemented using the count of all MPs together and pooled recovery parameters derived from a weighted average of each proportion as described in section 3.3.

Figure 4-3 utilizes ECDF curves to illustrate distinct characteristics between two scenarios: one that pools categories and another that considers distinctions based on the shape and size of MPs. The ECDF curve for the pooled categories scenario exhibits a gentler slope and wider width compared to the scenario that considers categories, indicating a dispersal of the posterior and a significant increase in uncertainty. This observation is further supported by the lengths of the credible intervals (see Appendix B) obtained from the two scenarios, measuring 355.5 for the scenario that neglects categories and 105.2 when the categories were considered. The considerable 237% increase in uncertainty observed when failing to categorize MPs underscores the importance of accounting for these distinctions during enumeration.

Furthermore, the posterior mean values derived from one category and four categories were found to be 429 MP/L and 288 MP/L, corresponding to errors of 46.0% and 6.5%, respectively. This demonstrates a significant decrease in error when considering the size and morphology distinctions of MPs, thus emphasizing the necessity of incorporating these categories to enhance accuracy.

In conclusion, the enumeration of MPs should encompass categories of size and morphology to improve accuracy and reduce uncertainties. The disparities of ECDF curves observed in Figure 4-3, along with the notable decrease in error and uncertainties highlight the critical role of considering size and morphology distinctions during the enumeration process.

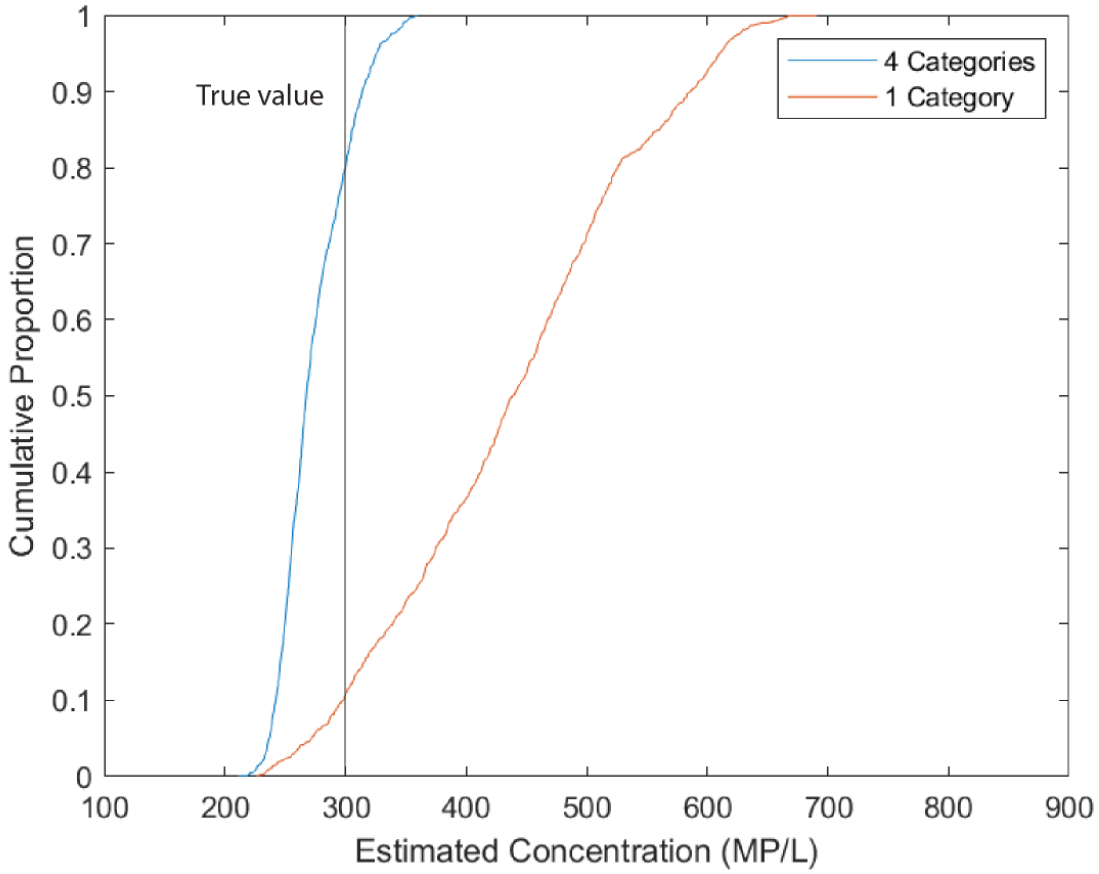

Figure 4- 3 Effect of categorization on MP enumeration as illustrated by the ECDF curves.

4.4.3 Impact of recovery practices on enumeration and practical significance

This portion of the study sought to develop information that will inform the establishment of guidelines for the optimal recovery practices in MP studies. When considering a collection of samples in a campaign, four distinct recovery practices exist to correct MP concentrations. The easiest practice is to spike one category of MPs (e.g. category C) in one sample and get one recovery(p_c), after that assuming this constant recovery value applies to MPs in all categories for all samples ($p_A = p_B = p_C = p_D$). This approach ignores both non-constant recoveries associated with replicates, as well as differential recovery associated with size and shape categories. The second possible recovery practice is to spike one category of MPs (e.g. category C) in replicate of samples, allowing for the estimation of corresponding beta distribution parameter (a_c, b_c). After that assuming beta distribution parameter from category C applies to all categories ($a_A = a_B = a_C = a_D$,

$b_A = b_B = b_C = b_D$). This recovery practice acknowledges non-constant recovery but ignored differential recovery. A third possible recovery practice is to spike 4 categories of MPs in one sample hence getting 4 different recovery constants ($p_A \neq p_B \neq p_C \neq p_D$). This practice acknowledges the differential recovery associated with categories but ignores non-constant recovery. To maintain conciseness in subsequent discussions, we refer to this practice as "Constant Recovery." The fourth recovery practice represents the most comprehensive approach, wherein replicates of samples are spiked using MPs from different categories, allowing for the estimation of beta distributions for each category ($a_A \neq a_B \neq a_C \neq a_D$, $b_A \neq b_B \neq b_C \neq b_D$). The key question remains: How much error and uncertainty are introduced by each practice, and which practice is the most optimal?

By examining the errors and uncertainties associated with each practice, it becomes possible to determine the optimal approach for MP recovery. As described in the methodology section, the recovery practices 1, 2, and 3 were modeled using three simplified models, and their outputs were compared to that of the full model. The simplified models incorporated simulated recoveries for category A B C D, which were determined to be 0.186, 0.156, 0.960, and 0.935, respectively. The estimated posterior means and credible intervals resulting from these models were presented in Table S3, available in the Appendix B. Furthermore, the results were visually depicted using bar plots in Figure 4-4.

Figure 4- 4A illustrates that the recovery practice which ignores both non-constant recovery and differential recovery leads to a significant underestimation of 40.1%. This underestimation arises from the randomly generated recovery value for category C (0.960), which was applied to all categories. As this recovery value is larger than the mean recovery value for all categories, it results in an overall underestimation of concentrations. Specifically, concentrations for categories A and B are significantly underestimated due to the utilization of an excessively high recovery value for these categories. The implications of this recovery practice are twofold. First, conducting replicates of recovery tests is crucial to obtain a more accurate estimation for category C, thereby enabling a more precise estimation of its concentration. Secondly, differential recovery should be taken into consideration to ensure more accurate estimations of concentrations for category A, B and D.

The Constant Recovery practice demonstrated a substantial overestimation of 39.3%. This overestimation arises from the significant disparity between the randomly generated recoveries for

category A (0.186) and category B (0.156) and their respective true means of A (0.35) and B (0.52). Consequently, the estimated concentrations for these two categories were significantly inflated. Although the randomly generated recoveries for categories C (0.960) and D (0.935) were slightly higher than their true means C (0.85) D (0.92), resulting in a slight underestimation of concentrations in these categories, the overall trend still indicates overestimation due to the substantial inflation estimated for categories A and B. In light of these findings, performing replicates of spiking tests is crucial to obtain a reasonable estimate of recovery and, consequently, achieve more accurate estimations of concentrations.

The recovery practice that ignores differential recovery revealed an underestimation of 21.8%. This underestimation primarily stems from the application of beta parameters of category C to categories A and B. This pair of parameters corresponds to a mean recovery value of 0.85, which is significantly higher than the mean recovery values for categories A (0.35) and B (0.52). Consequently, a significant underestimation occurs due to the utilization of this higher recovery value. Although applying a mean recovery value of 0.85 to category D leads to a slight overestimation considering its true value of 0.92, the overall trend still indicates underestimation. These findings emphasize the importance of considering differential recovery associated with size and shape in order to achieve accurate estimations for each category and, consequently, obtain a reliable estimation of the total MP concentration.

The full model, which takes into account both non-constant recovery and differential recovery, yielded an error of 6.3%, significantly smaller than the errors obtained from other recovery practices. It is important to note that only the credible interval of the full model incorporates the true value of MP concentration. This observation highlights the substantial inaccuracy introduced by other recovery practices in estimating MP concentrations.

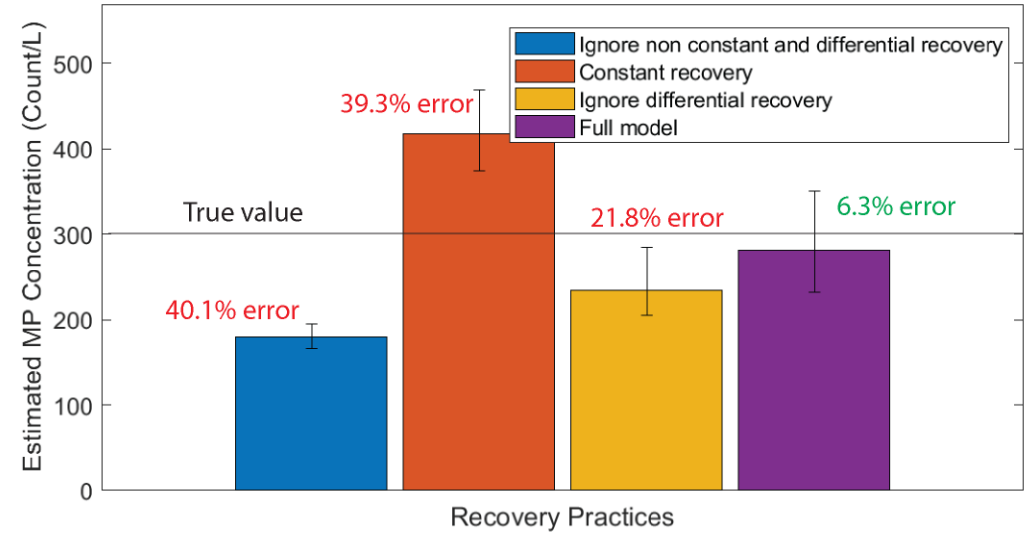

(A)

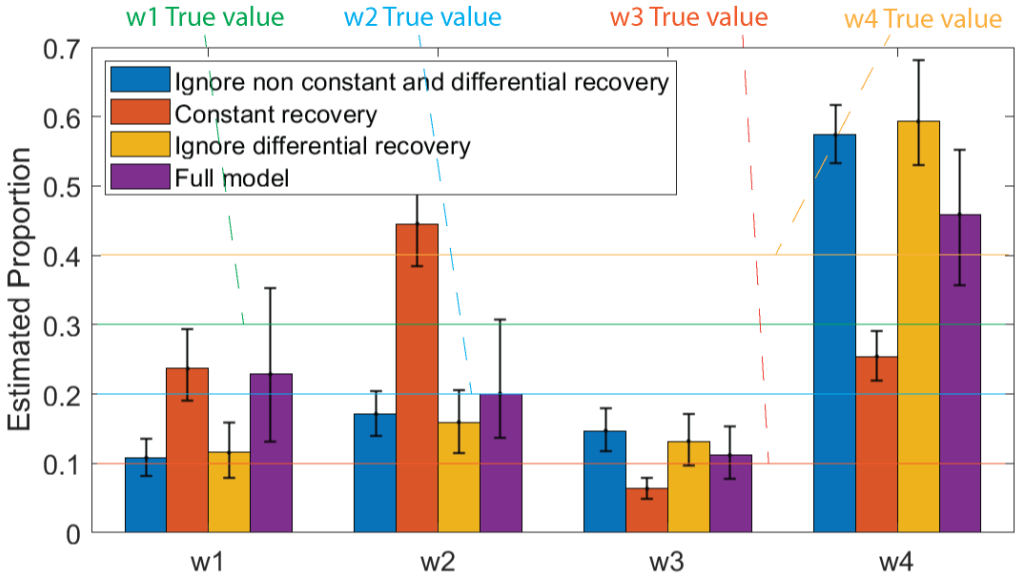

(B)

Figure 4- 4 Impacts of recovery practices on the estimated total MP concentration (A) and the proportion of each category (B)

Figure 4-4B illustrates how different recovery practices influence the estimated proportion of each category of MPs. When estimating the proportion of Category A, the errors observed were 64.0%, 21.1%, 61.5%, and 23.8% for the four models. This indicates that both the constant recovery practice and the full model may be effective approaches for estimating the proportion of this category. However, it is important to note that the credible interval derived from the constant

recovery practice does not encompass the true value of w1, while the credible interval from the full model does include the true value. This suggests that the full model performs better in this regard.

Regarding the estimation of the proportion of Category B, the errors for the four models were 14.4%, 122.7%, 20.3%, and 0.3% respectively. The notably low error obtained from the full model demonstrates the superior performance of this particular practice. A similar trend is observed when estimating the proportions of Category C and Category D, with errors of 47.1%, 36.4%, 31.9%, and 11.8% for Category C, and 43.4%, 36.5%, 48.3%, and 14.8% for Category D across the four models. Overall, the significantly low errors obtained from the full model in estimating the proportions of all four categories underscore the necessity of considering both non-constant recovery and differential recovery when calculating MP concentrations.

Taken together, considering both the non-constant recovery obtained from replicates of spiking experiments and the differential recovery associated with size and morphology categories is crucial for achieving accurate estimations of both MP concentration and the proportion of each category. From a practical standpoint, it is imperative to spike MPs from different categories into replicate samples and incorporate the resulting diverse recovery data when calculating MP concentration. Only by adopting this comprehensive approach can we obtain a deeper understanding of MPs originating from the sampled source.

4.5. Conclusion

This study investigated the uncertainties in MP enumeration using a modeling approach. Upon thoroughly examining the sources of random errors associated with each step in MP analysis, we assessed the compatibility of these errors with assumptions made in a previous uncertainty model and refined the model by modifying or adding assumptions when necessary. Specifically, we critically analyzed the causes of differential recovery of MPs related to size, shape, and type, and incorporated assumptions to account for the differential recovery in the revised model.

The newly developed model was applied using simulated data in conjunction with MCMC to generate posterior distributions that quantify the uncertainties in MP enumeration. The following conclusions were drawn after implementing the model:

- The inclusion of an increased number of replicates significantly contributes to the reduction of uncertainty. It is recommended to incorporate a minimum of three replicates within the MP enumeration process.
- When all MPs are counted collectively without discerning between distinct categories, it paves the way for inaccuracies in estimation. This approach not only compromises the accuracy of the enumeration but also precipitates an increase in uncertainty, hence undermining the reliability of the outcomes.
- To ensure accurate estimations of both MP concentration and the proportion of each category, it is essential to consider both the non-constant recovery observed across replicates of spiking experiments, and the differential recovery associated with size and morphology categories. The recovery practice ignores either one type of variability will result in significant error in estimation.
- The obtaining of recovery data cannot rely on simple spiking tests in single sample. There is a need to spike MPs from different categories into various samples, and to incorporate the resulting non-constant recovery and differential recovery in concentration estimation.

Chapter 5 Mass and Count balances of MPs in Primary Treatment Considering Differential Recoveries during MP Analysis

Abstract:

Understanding the fate and transport of Microplastics (MPs) in wastewater treatment plants (WWTPs) is essential for assessing their environmental impacts and optimizing treatment processes. Count and mass balance models are commonly used to investigate the behavior of MPs in WWTPs. While count balance models track the number of particles, mass balance models provide insights into the overall MP load. However, the impact of differential recovery on these models has not been extensively studied. This study aimed to establish count and mass balance models for MPs in primary wastewater treatment and examine the effect of differential recovery on model performance. Spiking tests using standard MPs were conducted to evaluate the influence of MP size and sample type on recovery. The derived recovery values were then used to correct MP concentrations and loads in the primary treatment at Kitchener WWTP. The results showed that MP size and sample type significantly influenced recovery, emphasizing the need for considering these variations in concentration estimations. The application of differential recovery practices led to varying changes in MP concentrations and loads across different streams. While the count balance model was not significantly improved by differential recovery, the mass balance model showed a significant improvement in closure. This discrepancy was primarily attributed to the differing proportions of the primary sludge stream load in each model. These findings highlight the importance of incorporating differential recovery into mass balance models and demonstrate the complementary nature of count and mass balance approaches in understanding the fate and transport of MPs in WWTPs.

5.1. Introduction

Understanding the fate and transport of MPs in wastewater treatment plants (WWTPs) is crucial for assessing their environmental impacts and optimizing treatment processes to minimize their release into aquatic ecosystems. WWTPs are recognized as significant pathways for MPs to enter the environment, with treated effluent (Carr et al., 2016; Estahbanati and Fahrenfeld, 2016) and land application of biosolids (Corradini et al., 2019; Yang et al., 2019) being primary routes of discharge. By examining the behavior and transformation of MPs within WWTPs, researchers can evaluate the efficiency of various treatment stages in removing MPs and identify areas for improvement (Ziajahromi et al., 2017; Conley et al., 2019). Additionally, this knowledge can inform the development of innovative treatment technologies and best management practices to reduce the MP load in effluents and biosolids (Talvitie et al., 2017a; Talvitie et al., 2017b). Furthermore, understanding the fate and transport of MPs in WWTPs can support the establishment of policies and regulations aimed at mitigating microplastic pollution from these facilities (Whitehead et al., 2021; Deme et al., 2022). Ultimately, investigating the fate and transport of MPs in WWTPs is vital for protecting water resources and preserving the health of aquatic ecosystems (Kyriakopoulos et al., 2022).

Count balances are commonly used for the investigation of the fate and transport of MPs in WWTPs. Particle count balances track the number of microplastic particles entering, exiting, and transforming within WWTPs, providing insights into the behavior and fate of different sizes and types of MPs in wastewater systems (Carr et al., 2016; Murphy et al., 2016). In addition, they can be employed to estimate the efficiency of treatment processes (Talvitie et al., 2017a; Talvitie et al., 2017b; Yang et al., 2019) in removing MPs, which can be used to optimize existing technologies or develop new strategies for improved removal. Finally, estimates of the number, sizes and types of microplastic particles discharged from WWTPs into aquatic ecosystems, can contribute to assessing potential ecological risks of microplastic pollution (Picó et al., 2021; Sönmez et al., 2023). In summary, count balance models in wastewater studies are valuable for understanding particle dynamics, evaluating treatment processes, and assessing ecological risks.

Although count balance models are crucial for understanding the fate and transport of MPs, mass balance models complement these by providing more insights into fragmentation dynamics, weight-based ecological impacts, and can provide standardization across studies and environments.

Mass, as a conserved quantity, offers a consistent measure for determining microplastic loads and comparing contributions from various sources (Simon et al., 2018; Rasmussen et al., 2021). In wastewater MP research, mass balance models offer valuable information beyond what particle count models can provide. They estimate the total mass of MPs entering, exiting, and transforming within WWTPs, revealing the overall microplastic load in the wastewater system (Chen et al., 2022). Additionally, mass balance models offer insights into fragmentation dynamics (Poulain et al., 2018) and can help assess weight-based ecological impacts (Redondo-Hasselerharm et al., 2018; Zhu et al., 2019). Moreover, these models enable better comparability and standardization across studies, environments, and treatment processes (Frehland et al., 2020), informing the development of weight-based policies and regulations focused on the mass of MPs discharged from WWTPs (Porterfield et al., 2022). In summary, mass balance models provide essential insights into MP mass, fragmentation processes, ecological consequences, and standardization, which cannot be solely addressed by count balance models.

Primary wastewater treatment serves as a good example for establishing count and mass balance models of MPs for several reasons. The simplified physical processes in primary treatment (i.e. sedimentation), are more straightforward to model in comparison to the more complex biological and chemical processes that occur in secondary and tertiary treatment stages (Henze et al., 2008; Grady Jr et al., 2011). Furthermore, primary treatment has well-defined inputs and outputs, facilitating the establishment of mass balances by quantifying the mass of MPs entering and leaving the system. Additionally, primary treatment often results in substantial removal of MPs (Murphy et al., 2016; Magni et al., 2019), providing valuable insights into the efficiency of this process. Finally, understanding the fate and transport of MPs in primary treatment lays the foundation for assessing their behavior in subsequent treatment stages, serving as an important starting point for more complex models. Overall, primary wastewater treatment's inherent characteristics make it suitable for developing mass balance models in microplastic studies. Although primary wastewater treatment is well-suited for count and mass balance models, the limited research specifically addressing MPs in this context leaves gaps in our understanding of their fate and transport during primary treatment processes, which necessitates further investigation.

While primary wastewater treatment provides an appropriate setting for count and mass balance models differential analytical recovery of MPs related to size and sample type during analysis (Simon et al., 2018; Halbach et al., 2021; Way et al., 2022), has not been considered when establishing them. Smaller MPs exhibit a larger surface-area-to-volume ratio, leading to increased adhesion to surfaces, filters, or extraction devices, different buoyancy or settling velocities, and a higher likelihood of aggregation with other materials and hence typically have low analytical recoveries (Sun et al., 2021; Laursen et al., 2022; Li et al., 2022). Further, the matrix composition varies significantly among influent, sludge, and effluent streams, with the influent containing more particulate matter and organic material, and sludge being highly concentrated with organic and inorganic matter (Li et al., 2018). Both of these factors can potentially complicate microplastic separation and recovery during analysis due to aggregation or adsorption (Konechnaya et al., 2020). Microplastic concentrations have been reported to vary across raw influent, sludge, and effluent samples, with influent and sludge typically having higher concentrations (Edo et al., 2021), potentially increasing aggregation and adhesion of MPs to surfaces or other materials, thereby affecting their recovery. It is hypothesized that count and mass balance models that take into account differential analytical recovery associated with size and sample type will provide a more accurate and reliable representation of microplastic concentrations in primary treatment systems. By acknowledging different recoveries, improved models will better account for inherent biases and limitations in the extraction process.

To address the aforementioned challenges, the present study aims to achieve two primary objectives: 1) establish count and mass balance models of MPs in primary wastewater treatment; and 2) incorporate differential recovery associated with size and sample type into these models and thereby examine the impact on model performance. To achieve the first objective, field samples from a local wastewater treatment plant were collected and analyzed. For the second objective, spike-recovery tests were conducted using standard MPs of various sizes in different matrices. MPs were identified using a focal plane array (FPA) based micro-FTIR system, and differences between recovery derived from instrument counting with that derived from visual counting were also critically evaluated. The findings from this study will significantly contribute to the improvement of strategies that can be employed to characterize the fate and transport of MPs in wastewater treatment plants.

5.2. Material and methods

5.2.1 Field sampling

Field sampling was conducted at the Kitchener WWTP which is a conventional activated sludge facility treating wastewater that is primarily from the City of Kitchener. The plant has a rated average day flow capacity of 122,745 m^3/d and a peak flow capacity of 306,862 m^3/d. The treatment processes include screening, grit removal, primary clarification, aeration, secondary clarification, and ultraviolet (UV) disinfection with the treated effluent discharged to the Grand River and the flowchart diagram can be found in Appendix C. A portion of the return activated sludge is directed to the primary clarifier influent for sludge thickening purposes. The Kitchener WWTP encompasses four different treatment trains subsequent to primary treatment which are designated as plants 1-4. The current study focused on plant 1, which employs a conventional activated sludge basin and secondary clarifier to provide secondary treatment.

To investigate the fate and transport of MPs within the primary settling process, samples were acquired from the influent, primary effluent, primary sludge, and returned activated sludge streams. The sampling points are labelled on the process flow chart. Grab sampling in triplicate was utilized at each stage, with sample volumes as follows: 3 liters from the influent, 10 liters from the primary effluent, 3 liters from the primary sludge, and 10 liters from the returned activated sludge.

For the collection of raw influent, primary sludge, and primary effluent, a stainless-steel pail was submerged approximately 0.3 meters below the open channel surface. Subsequently, these samples were transferred to HDPE pails for storage. To mitigate contamination, both the stainless-steel pails and HDPE containers were thoroughly rinsed with deionized water in advance of the sampling procedure. The return activated sludge was collected via a sampling valve located on a pumped line. To ensure sample homogeneity, the line was purged for three minutes prior to each sampling instance. Recognizing the potential for temporal heterogeneity, triplicate samples at all sampling stages were collected with a time interval of less than one minute between each replicate to enhance the likelihood of reproducible results.

The sampling campaign was conducted on November 25, 2021, with the gathered samples promptly transported to the University of Waterloo. Upon arrival, they were stored in a 4 °C cold room pending subsequent analysis.

5.2.2 Extraction of MPs

The methodology employed for extraction of MPs involved wet peroxide oxidation followed by two steps of Fenton oxidation that were separated by a density separation step, as illustrated in Figure 5-1. An enzyme treatment step was employed for primary and secondary sludge samples due to their high organic matter content, while raw influent and primary effluent underwent the second Fenton reaction directly after the density separation step. In order to effectively manage the organic load and consequently reduce filter clogging, sludge samples were initially dried at 105°C for 24 h prior to the extraction procedure. In this study, the emphasis was placed on MPs with dimensions 20-500, hence raw wastewater, primary effluent, and rehydrated sludge samples were first sequentially filtered through 500 μm and 20 μm stainless steel sieves (Youdun, China) in order to isolate the desired particle size range before proceeding with the extraction procedure.

Wet peroxide oxidation was conducted to facilitate the disaggregation of large particles and thereby enhance subsequent Fenton oxidation. To achieve this, a volume of 100 mL of hydrogen peroxide with a concentration of 30% (v/v) was introduced to the samples. The samples then underwent wet peroxide oxidation for 16 hours at room temperature.

Subsequent to wet peroxide oxidation, the initial Fenton oxidation was performed to eliminate organic matter from the samples. For this purpose, a volume of 26 mL of an acidified iron catalyst (reagent formula provided in the Appendix C) and 25 mL of 0.1M NaOH buffer were combined (Chand et al., 2021). Addition of these chemicals to the sample instigated a vigorous Fenton reaction, leading to a rapid temperature increase. As a consequence, large beakers (i.e., 2L) were employed to curtail spillage. Following the initiation of the reaction, the samples were left to rest at ambient conditions until it was visually observed that the reaction had abated (typically 4-6 hours). It has been reported that the Fenton reaction exerts minimal impact on MP spectra (Al-Azzawi et al., 2020; Yan et al., 2020). Hence, the implementation of this pretreatment method is anticipated to have a limited effect on the subsequent spectral analysis of MPs. Upon cessation of the reaction, the samples were filtered with a 20 μm sieve. The particles trapped on the sieve were subsequently rinsed with a 1.7 g/cm³ $ZnCl_2$ solution directing the particles into a 60 mL beaker in preparation for the ensuing density separation procedure.

Density separation was employed to remove heavy non-plastic particles from the samples. The density separation procedure, adapted from Konechnaya et al. (2020), was executed using a 60 mL

beaker positioned within the 2L beaker where the Fenton reaction was conducted. This approach minimizes potential microplastic loss during sample transfers, as any accidentally spilled particles would be contained within the larger exterior beaker. It also enhanced separation efficiency by concentrating particles in a limited space. A volume of 50 mL of 1.7 g/cm³ $ZnCl_2$ solution was added to fill 85% of the beaker and this was followed by gentle stirring of the suspension using a magnetic stirring bar and plate. Stirring was conducted to create a homogeneous suspension to facilitate differentiation of MPs that float due to their lower density from denser particulates that settle. The sediment was then allowed to settle for 24 h while the MPs floated, after which an overflow was created by slowly adding approximately 20 mL $ZnCl_2$ solution, causing the MPs to overflow into the 2L beaker. Subsequently, the 2L beaker was rinsed thoroughly with ultrapure water prior to filtering the contents through a 20 μm sieve.

In accordance with procedure of Lavoy and Crossman (2021), a septic cleaner treatment, was employed after the density separation step to further eliminate organic matter from sludge samples that had elevated concentrations of suspended solids (>2500 mg/L). It has been confirmed by the authors that this septic cleaning pre-treatment was have minimal impact on MP spectra hence spectra identification. A total of 100 mL of 0.04 g/mL septic tank cleaner (Bio-clean, CA) solution was added to each sample and gently stirred using a magnetic stirrer for 1 minute. The beakers were then placed in a 40°C oven for 48 hours to undergo digestion. Post-digestion, a filmy residue was observed on the samples, which could lead to the formation of foam and overflow of beakers during the second Fenton reaction. Hence, the samples were sieved through a 20-micrometer stainless steel sieve to remove the residue. The filtered sample was rinsed with ultrapure water back into the beaker in preparation for the second stage of Fenton treatment.

The second stage of Fenton treatment employed the same dosage of Fenton's reagent as in the first Fenton reaction (100 mL of hydrogen peroxide, 26 mL acidified iron catalyst, and 25 mL NaOH buffer). The samples were reacted under ambient conditions until all visible reactions ceased (approximately 4 hours). In an effort to minimize the loss of MPs during the extraction process, the same sieve, beaker, and stirrer were consistently used for each individual sample throughout the various steps of the procedure. The solution generated by the second Fenton reaction was then filtered through the same 20-micrometer stainless steel sieve, and the particles retained on the sieve were rinsed into a custom-made filtration device (see Appendix C) for subsequent FPA micro FT-

IR imaging. In order to circumvent potential losses of MPs due to adherence to vial surfaces, the storage of solutions within vials was intentionally avoided.

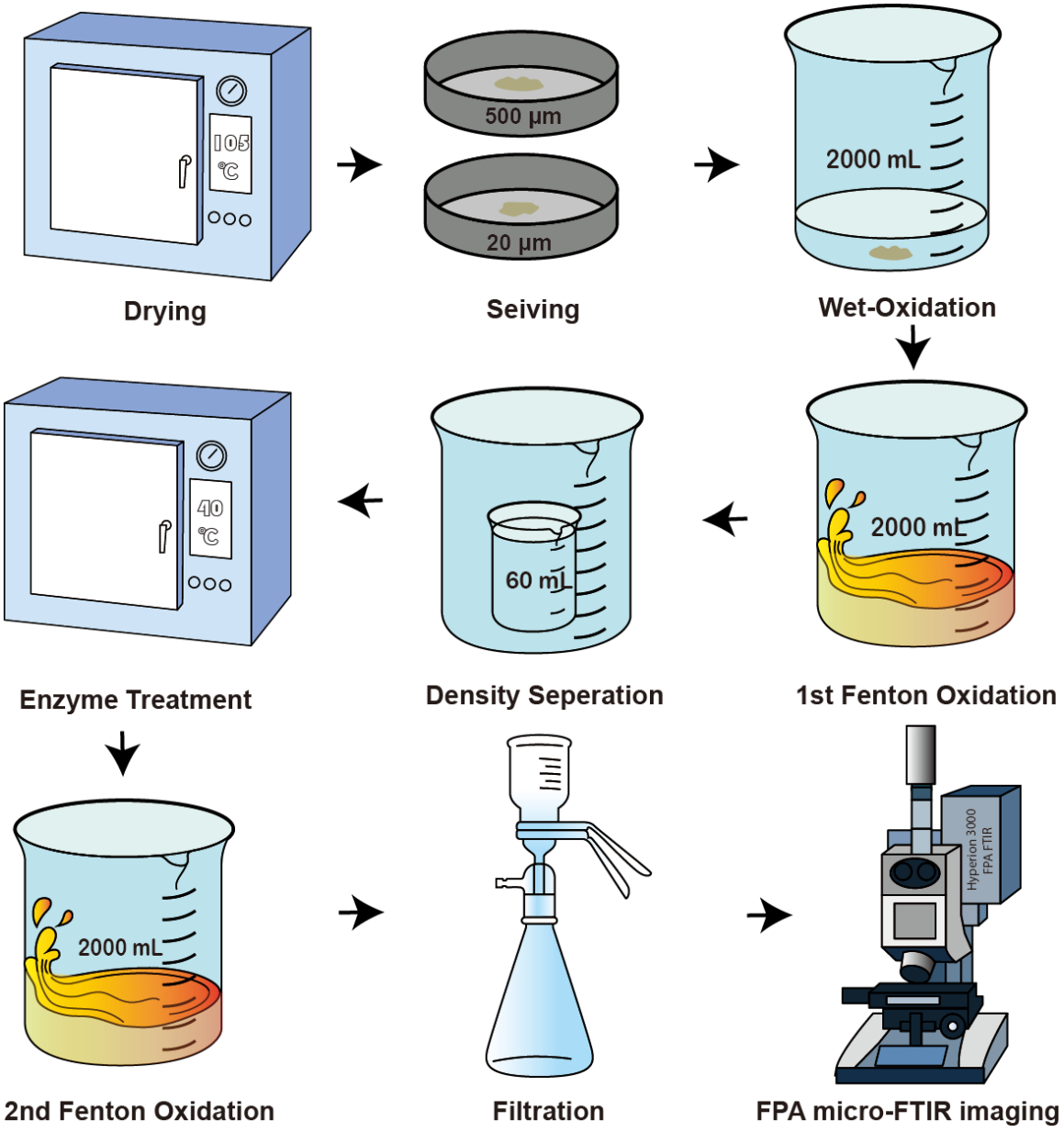

Figure 5- 1 Schematic of extraction procedure.

5.2.3 Quantification of MP count

Following the second Fenton reaction, each sample was enriched onto a 0.2 μm aluminum oxide filter (Anodisc 13 mm, GE, U.S.) using a custom-made funnel that focused the particles into a 5 mm by 5 mm region on the filter (refer to Figure C2 in the Appendix C), that maximized the scanning area of the FPA array setting. Each filter containing an enriched sample was placed on a BaF_2 window. Subsequent micro FTIR measurements were conducted with a Tensor 37 FT-IR spectrometer (Bruker Ltd, Germany) equipped with a Hyperion 3000 FT-IR microscope, a 15× Cassegrain objective, and a 64×64 FPA detector. All measurements were conducted using the optimized settings reported by Primpke et al. (2017), incorporating a binning factor of 4, a spectral resolution of 8 cm^{-1}, and 6 co-added scans in transmission mode. This approach enabled a pixel size (MP detection resolution) of 10.625 μm, employing 256 × 256 pixel to cover the 5 mm × 5 mm filtration area, with each sample requiring approximately 4.25 hours for completion.

Each pixel in the FPA micro-FTIR imaging generated a spectrum (As shown in Figure 5-2A), with the spectral information serving as input for a deep learning technique (Zhu et al., 2020) followed by an image analysis algorithm. The deep learning technique determined whether particles were plastic and identified the polymer type. The image analysis (see Appendix C) algorithm counted the number of MPs, differentiating them based on their size and shape. The significance of discriminating MPs based on their size has been extensively addressed in Chapter 4. In addition to size differentiation, the distinction of MPs based on their shape is also deemed important, because particles and fibers exhibit distinct physical properties, leading to different behaviors in the environment. For instance, fibers might pass through specific wastewater treatment processes (Ziajahromi et al., 2017), potentially contributing to their release into aquatic ecosystems. Furthermore, the varied shapes of MPs can influence their bioavailability and ingestion by organisms, with fibers being more prone to entanglement in organisms or accumulating in specific tissues(Woods et al., 2018).

For shape identification, the algorithm used the ratio of the major-axis length to the minor-axis length: particles with a ratio greater than 3:1 were classified as fibers, while other shapes were categorized as particles. For size determination of the latter, the length of the major axis was employed as the critical metric. The output from the deep learning search and image analysis algorithms reported total microplastic counts as well as counts by size, type, and shape.

5.2.4 Quantification of MP mass

The volume and mass of each identified MP in the samples was determined based on the FTIR response of individual pixels obtained from FPA micro-FT-IR imaging. This innovative quantification approach was detailed in a conference paper (Zhu et al., 2021) and is presented in Appendix D. The particle volume was calculated by summing the volumes of all pixels, that were individually estimated as the product of the pixels area and the estimated particle thickness associated with the pixel (Figure 5-2B). The area of each pixel was an instrument parameter, while the thickness was estimated using Beer's law. This law enables the estimation of a pixel's thickness based on its IR absorption relative to the absorption of a reference plastics with a known thickness (Figure 5-2C and 5-2D). The estimated volumes were rigorously validated against the true volumes of control-shaped MP spheres and fibers, demonstrating excellent performance and confirming the validity of this novel quantification method.

The MP mass was subsequently estimated using the specific gravity associated with the identified plastic type, as determined by the deep learning technique. Analogous to particle count, the combined output from the image analysis and mass quantification algorithm provided a comprehensive characterization of microplastic mass in a sample, including total mass and mass by size, type, and shape.

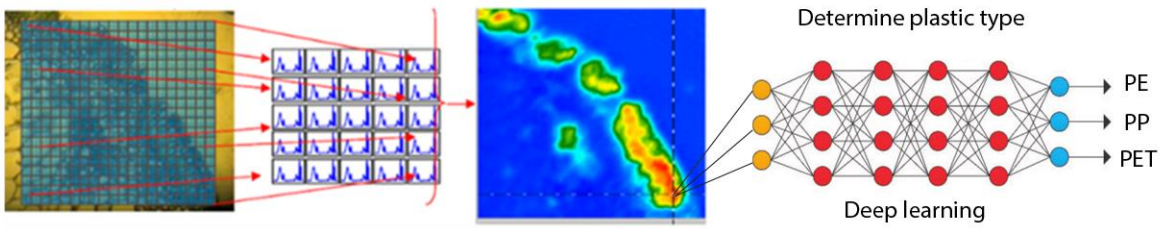

(A)

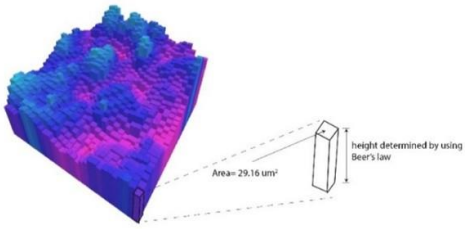

(B)

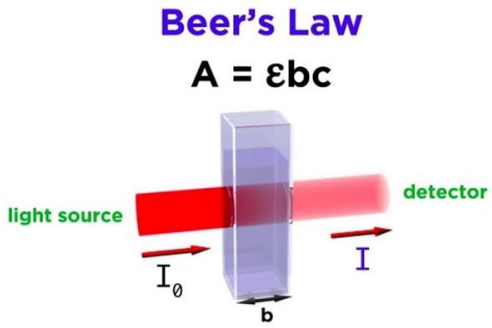

(C)

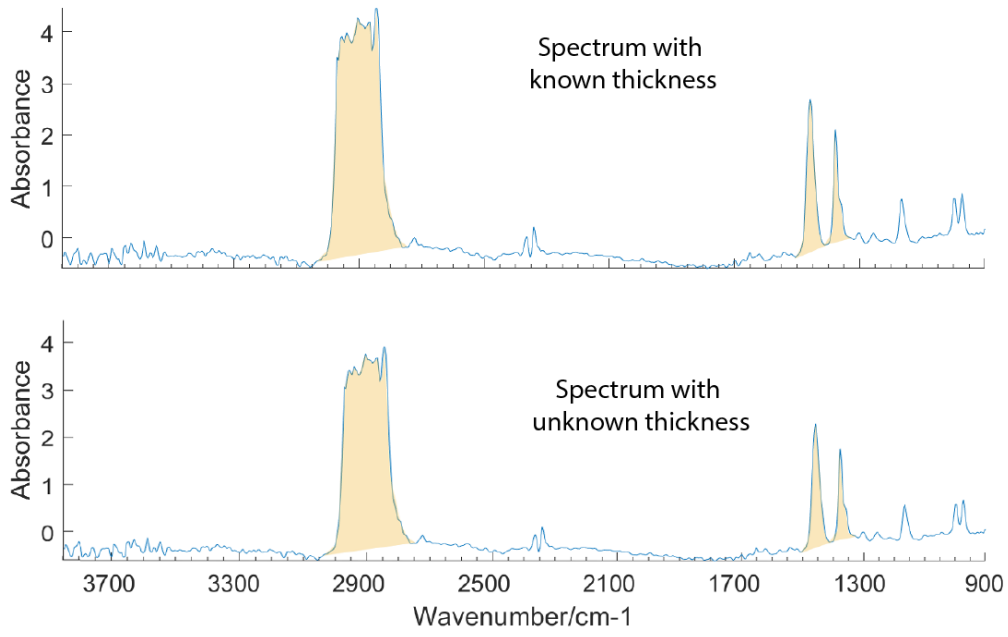

(D)

Figure 5- 2 Mass quantification of MP FPA micro-FTIR imaging.

(A) 3-D matrix representation of FPA micro-FTIR imaging output and plastic type designation using deep learning. (B) Volume calculation of a microplastic particle by summing up pixel

volumes. (C) Schematic depiction of Beer's Law. (D) Determination of PP pixel thickness through adsorption comparison. Adapted from Zhu et al. (2021)

5.2.5 Recovery tests

A focus of the present study involved integrating differential recovery of MPs associated with size and sample type into count and mass balance models and thereby assessing the effect on model performance. For this purpose, spiking tests were executed using standard MPs characterized that spanned a range of size and color. The spiked MPs included orange PE microspheres with diameters ranging from 45 to 53 µm (Cospheric, United States), as well as green PE microspheres with diameters within the 180 to 212 µm range from the same provider. Additionally, pink PP MP particles with sizes between 300 and 500 µm were utilized. The PP particles were manually produced by filing a Nestle cream bottle cap (see Appendix C) with a metal file, after which the powder was sieved through a stacked assembly of 300 µm and 500 µm meshes to achieve the desired size range.

To initiate each spiking test, standard MPs were first suspended in isopropanol to mitigate hydrophobic interactions among the MPs and thus enhance their even distribution. For each test, a 25 µL aliquot was extracted and subsequently deposited onto a clean glass slide for direct eye-counting of MPs using a stereomicroscope. The quantity of standard MPs in each aliquot varied based on the size range of the MPs, with specific details on the number of MPs spiked provided in the Appendix C. The standard MPs were then washed from the glass slides into respective samples using ultrapure water. Following this, the samples underwent the extraction procedure detailed in Section 2.4. The spiking process which included the three standard MPs, was carried out in triplicate with raw wastewater, primary effluent, and primary sludge samples.

Previous studies of microplastic enumeration have reported recoveries based on visual counting (Magnusson and Norén, 2014; Nor and Obbard, 2014) , while modern spectroscopic technology utilizes instruments and automated algorithms for counting MPs. It remains unclear whether discrepancies exist between visual and instrument-based counting methods and their respective recoveries. In this study, this knowledge gap was addressed by counting MPs on sample filters using both visual inspection and micro-FT-IR imaging. The spiked standard MPs exhibited distinct colors and circular shapes, facilitating their identification by both visual and instrumental means

respectively. Initially, white light images were taken using the built-in camera of the Hyperion 3000 system and MPs were counted visually based on the images. Subsequently, FPA micro-FT-IR imaging was performed, and a circle-detection algorithm (Mathworks, 2023) was used to count the number of circles within specific size ranges (see Appendix C for details) to represent instrument counting of the recovered MP standards.

5.2.6 Quality Assurance/Quality Control

Contamination is a critical concern when analyzing MPs, and several measures were implemented to minimize its occurrence. Glass or metal tools and vessels that were thoroughly rinsed with Ultra pure water were employed throughout the study. When a stainless-steel filter was reused for the same sample, it was stored in a closed Petri dish between uses. The use of laboratory coats and disposable nitrile gloves was employed to prevent inadvertent transfer of MP contaminants from clothing or skin to the samples. Despite these precautions, some contamination was inevitable and hence procedural blanks were employed to identify the extent of background contamination. Two procedural blanks were incorporated in the sequence of analysis: the first was run prior to the analytical cycle that handled all field samples, while the subsequent one was performed prior to analyzing of spiked samples. The blanks consisted of 200 mL of ultrapure water and were subjected to the same extraction procedure described in Section 2.4. The blank filter was imaged using FPA micro-FTIR imaging to assess potential contamination.

5.2.7 Evaluation of count and mass balances

A mass balance on Total Suspended Solids (TSS) was evaluated prior to assessing the count and mass balance of MPs. This was deemed important to ensure the reliability of subsequent MP balance analysis, because lack of mass balance closure for TSS would indicate issues in measurement or sampling that could also impact the accuracy of MP data. The mass balance of TSS was computed by comparing the TSS loads entering the clarifier, namely the influent load (L_{inf}) and the RAS load (L_{RAS}), against the loads exiting the clarifier, namely the effluent load (L_{eff}) and the sludge load (L_{sl}). The load (L) denotes the mass flow of TSS, which was calculated as the product of the volumetric flow rate (Q) and the concentration (C)(Equation (1)). The TSS

concentrations and flow rates for the 4 streams were provided through the facility's daily monitoring. To accommodate potential intraday fluctuations in flow and TSS concentration, average and standard deviations for both values were computed from a 14-day continuous period, encompassing seven days preceding and following the sampling date.

$$L = Q \cdot C \qquad \text{eq (1)}$$

Under ideal circumstances, the inflow and outflow of TSS in primary treatment should be equivalent, while a discrepancy between the two might happen due to errors in sampling and analysis. Consequently, a 'lack of balance' was defined to assess the closure of balance for TSS as per equation (2). In order to assess the contribution of each stream on the closing of balance, a 'Proportion' was defined by calculating the percentage of the load carried by each stream employing a similar methodology as that utilized in equation (2). The calculation was performed by dividing the load associated with a particular stream by the sum of all inflow loads. As an illustrative example, the proportion contributed by the WAS stream was computed using this approach as per equation (3).

$$\textit{Lack of balance} = (L_{inf} + L_{WAS} - L_{eff} - L_{sl})/(L_{inf} + L_{WAS}) \qquad \text{eq (2)}$$

$$\textit{Proportion of WAS} = L_{WAS}/(L_{inf} + L_{WAS}) \qquad \text{eq (3)}$$

When establishing count and mass balance models for MPs, the corrected concentration ($C_{corrected}$) for each sample was used, which was determined by dividing the raw concentration (C_{raw}) derived from FPA micro-FTIR analysis by a recovery factor (p)(Equation (4)). This calculation was conducted for three scenarios: (1) constant recovery across the entire balance calculation; (2) differential recovery linked to MP size; and (3) differential recovery associated with both MP size and sample type.

Building upon the balance models established for TSS, analogous count and mass balance models were developed for MPs, incorporating suitable corrections for recovery. Specifically, equation (1) was employed for these models with the substitution of MP-specific concentrations (either count-based or mass-based) for TSS concentrations. The choice of concentration was predicated on the balance type, with count-based concentrations employed for count balances and mass-based concentrations for mass balances.

The three scenarios considered for calculating the corrected concentration involved distinct approaches to the utilization of *p* values. In the first scenario, a constant value of *p* was employed across the full spectrum of the balance calculation, irrespective of MP size and type. This value was derived from spiking tests conducted on MPs within the 100-250 µm range in raw wastewater, following a commonly employed methodology in microplastic research. The second scenario, recognizing the potential for size-based variability, applied different *p* values for each size range (20-100 µm, 100-250 µm, and 250-500 µm). In this approach, *p* values from size-specific spiking tests in wastewater were employed assuming that sample type did not affect recovery. Lastly, the third scenario employed a more comprehensive strategy by considering different *p* values for each size range and sample type, thereby accommodating both of these potential factors influencing the recovery of MPs. Therefore, each scenario incrementally addresses potential recovery variations, possibly refining the accuracy of microplastic load estimations.

$$C_{corrected} = C_{raw}/p \qquad \text{eq (4)}$$

5.2.8 Removal efficiency

The removal efficiency of MPs was determined by comparing the load of MPs in the influent to that in the effluent, and then dividing it by the load in the influent. In this study, all removal efficiencies were calculated based on loads rather than based on concentrations, for two main reasons. Firstly, the primary focus of this study was on assessing the closure of count and mass balance that were based on the loads from various streams. Therefore, the loads themselves were of primary interest. Secondly, the flow rate of the influent and effluent during the calculation period were found to be relatively close (see Appendix C). As a result, the removal efficiency based on load basis closely approximates the efficiency calculated based on concentration.

$$\textit{Removal efficiency} = (L_{inf} - L_{eff,})/L_{inf,} \qquad \text{eq (5)}$$

5.2.9 Statistical Analysis

The paired Student's T-test was used to ascertain if there was statistically significant difference between instrument-based and eye-based recoveries. Additionally, a two-way ANOVA test was

employed to evaluate the influence of size and sample type on recoveries. Both types of statistical analyses were conducted using the Matlab R2022b software.

Propagation of uncertainties in count and mass balance was conducted following the method suggested by Harris (2010), considering that flow rates, concentrations, and recovery all introduced uncertainties in the mass flows. When executing addition and subtraction operations, the uncertainty in the resultant value was derived from the absolute uncertainties of each individual term. In contrast, for multiplication and division operations, all uncertainties were converted into percent relative uncertainties for calculations. Examples of error propagation calculations can be found in the Appendix C.

5.3. Results and discussion

5.3.1 Procedure blank

Two procedural blanks were integrated into the analysis sequence, with the initial blank conducted during the analytical round that processed all field samples, and the subsequent blank conducted prior to the analysis of spiked samples. The first procedural blank indicated the presence of 4 MPs, (1 PE, 1 PP, and 2 PET) with an aggregate estimated mass of 1322 ng. The second procedural blank contained three MPs, (2 PE and 1 PP) with an estimated cumulative mass of 768 ng. These MPs accounted for less than 1%, of the approximately 1,000 MPs that were found in each field sample. It was concluded that the contamination control measures that were employed were effective. Nevertheless, during the analysis of field and spiked samples, the averaged values obtained from these procedural blanks were subtracted from the measured sample values.

5.3.2 Spiking tests results

Instrument-based counting of MPs via FPA micro-FTIR coupled with image analysis (Mintenig et al., 2017; Peeken et al., 2018; Primpke et al., 2018) and eye-based counting methods (Dümichen et al., 2015; Carr et al., 2016) have been reported for wastewater characterization and it was anticipated that the method employed could impact results. The eye-based counting method is reliant on observer skills and perception, with the distinguishing factor being the unique colors of the spiked MPs. Conversely, instrument-based counting is contingent on deriving chemical information about the particles, and subsequently applying a detection algorithm. It was initially anticipatedthat the instrument-based approach may be more susceptible to bias as it could erroneously identify indigenous MPs with the same polymer type, size, and shape as the spiked MPs. Furthermore, underestimation can occur if spiked particles are in close proximity to each other, as the instrument may perceive them as a single particle (As discussed in Appendix C). While most studies that utilize spectroscopic mapping analysis of MPs rely on instrument-derived counting results, they often employ eye-based recovery to correct for concentration. As such, the recovery results derived from the two methodologies employed in the current study were compared.

Figure 5-3A graphically presents a comparison between eye and instrument-based recoveries across the different sample types and MP size ranges. It is observed that only two size ranges of MPs are presented in the figure, and there is an absence of information pertaining to the 500-250

μm MP category. This is due to the unique characteristics of 500-250 μm microspheres, which are prone to rotating away during the filter's movement after drying. To mitigate this issue, irregular-shaped 500-250 μm standards were utilized in place of circular-shaped standards, and this hindered the instrument's ability to accurately count MPs within this particular size range. Although the displayed bars subtly suggest superior performance of visual inspection-based recovery over the instrument-assisted method within the 250-100 μm category, and the converse within the 100-20 μm range, this discrepancy was not statistically significant. Paired Student's T-tests indicated no substantial difference between the visual and instrument-based recovery methods. Therefore, both methodologies were inferred to yield analogous results in determining MP recovery across various sample categories and sizes.

Figure 5-3B presents the influence of MP size range and sample type on recovery using the average results of the eye-based and instrument-based recoveries since the two methods had been determined to provide similar results. This analysis was conducted as a preliminary assessment prior to constructing count and mass balance models for MPs. If these factors did not substantially affect recovery, and subsequently the concentration correction for each sample, the model development under the three distinct conditions would be rendered inconsequential.

A two-way Analysis of Variance (ANOVA) was performed on the data represented in Figure 5-3B, using sample type and microplastic (MP) size as the independent variables. As shown in Table S1, the p-values for size range (0) and sample type (0.0467) were both less than 0.05, indicating that these two factors significantly affected the MP recovery rates. Hence, the differences in recovery across different MP sizes and sample types were deemed to be not due to random chance alone, and that both variables impacted recovery. Additionally, the large p-value for the interaction (0.6748) effect suggests that there was no significant interaction between sample type and size range on recovery. In conclusion, both MP size and sample type significantly influence the recovery of MPs, and these effects were independent of each other. These findings presented a strong statistical basis for further examination of count and mass balance models of MPs considering these two factors.

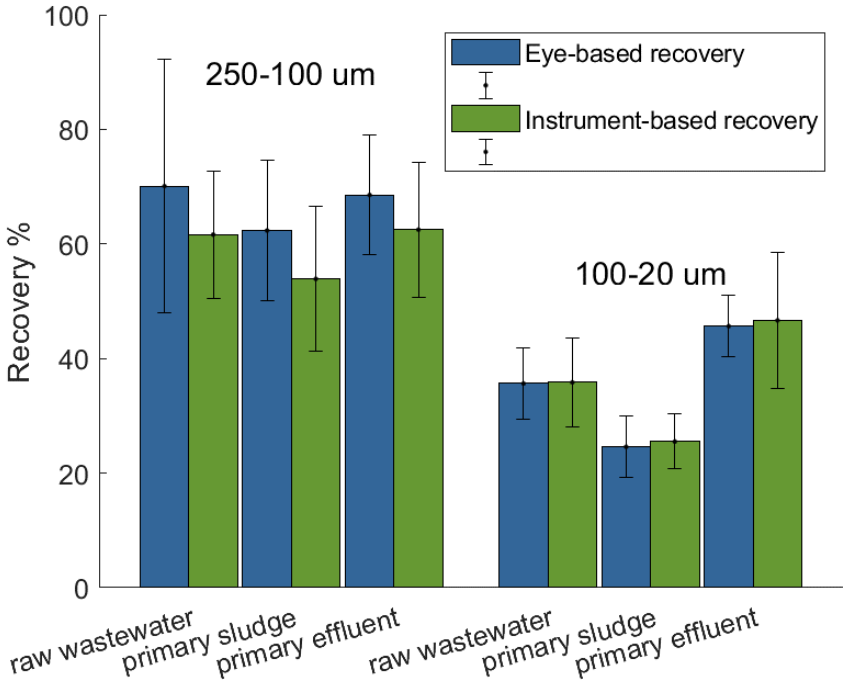

(A)

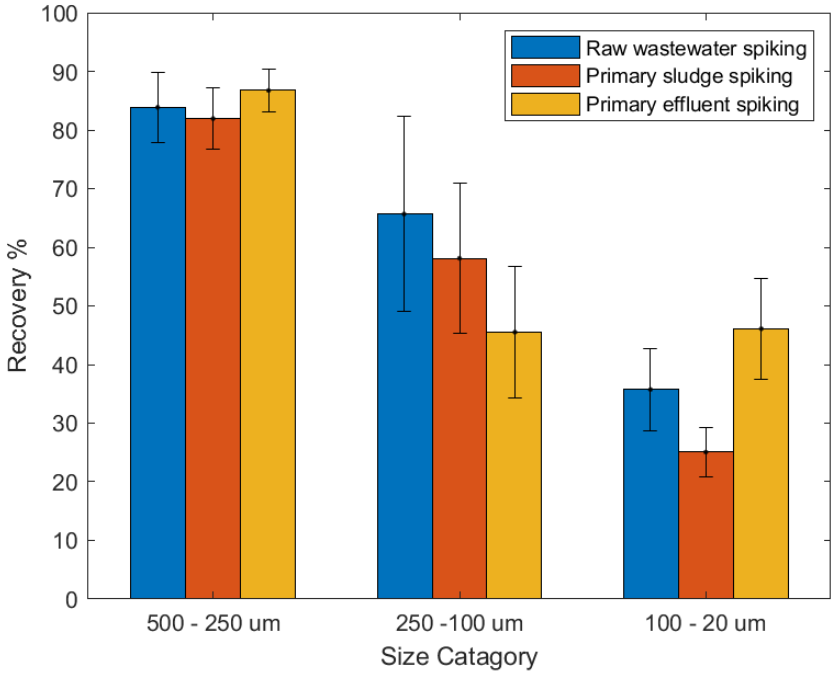

(B)

Figure 5- 3 (A) Comparative Analysis of Microplastic Recovery: Eye-Based vs. Instrument-Based Techniques. (B) Influence of Microplastic Size and Sample Type on Recovery Efficiency

5.3.3 TSS Mass balance

Figure 5-4 presents the mass balance of TSS in the primary treatment of Kitchener wastewater treatment. The analysis revealed that 41.8% of the TSS loading was transported via the influent, while a significant proportion of outlet mass flow 67.8% was transported via the primary sludge stream. A high proportion (51.2%) of TSS loading was transported via the WAS stream, reflecting the sludge thickening practice employed by the treatment plant. Approximately 8.6% of the TSS loading was unaccounted for, which was attributed to measurement uncertainties and solids losses in the bar screens. The absence of 8.6% of the TSS loads was deemed acceptable in terms of mass balance closure for this particular analyte (Lakshminarasimman et al., 2021; Chen et al., 2022). In terms of removal efficiency, the primary clarification process removed 43.8±8.4% of the TSS mass load, which aligns with common removal efficiencies observed in primary treatment (Henze et al., 2008; Grady Jr et al., 2011). The successful closure of the TSS mass balance provided a baseline for anticipating MP balance outcomes and enabled critical analysis of any deviations in this response.

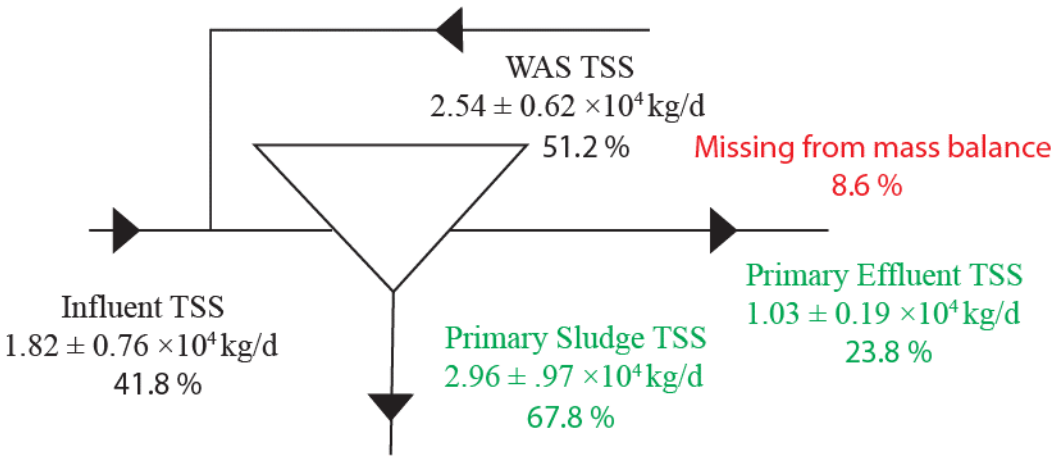

Figure 5- 4 TSS mass balance in primary treatment at Kitchener WWTP

5.3.4 Concentration of MPs

The MP concentrations in different streams of the primary treatment were depicted in Figure 5-5, considering both count and mass bases. As outlined in the methodology, the concentrations underwent correction using three different approaches: 1) constant recovery, 2) differential recovery associated with size only, and 3) differential recovery associated with both size and

sample type. The specific recovery values used for concentration correction are presented in Figure 5-3B. Figure 5-5 demonstrates that the implementation of constant recovery practice with a mean recovery of 65.7% resulted in a mean increase of 52.2% in MP concentration for all streams, both in terms of count and mass basis. This improvement underscores the necessity of correcting MP concentrations with recovery values to obtain more accurate concentration estimates.

Transitioning from practice 1) to practice 2) which considered size-based variability led to further increases in MP concentrations. However, the extent of increase varied between count and mass-based concentrations and also differed among the streams. Notably, there was a significant increase in count-based concentrations across all streams (approximately 65% higher compared to the concentrations from practice 1), contrasting with a moderate increase in mass-based concentrations of influent and primary effluent (approximately 35% higher compared to the concentrations from practice 1) and a smaller increase in mass-based concentrations of WAS and sludge (approximately 25% higher compared to the concentrations from practice 1). This discrepancy was attributed to the size distribution of MPs in the uncorrected data, as described in the Appendix C. The 20-100 μm fraction, which mainly contributed to the increase, accounted for more than 85% in count-based concentrations in uncorrected data, while this size fraction represented less than 40% in mass-based concentrations in the uncorrected data. Hence, the impact of recovery practice 2) differed between size-based and mass-based concentrations.

Transitioning from recovery practice 2) to practice 3), which incorporated both size and sample type-based variability, resulted in unchanged concentrations for influent streams on both count and mass basis. However, the concentrations in the WAS and sludge streams were elevated, while the concentrations in the primary effluent stream decreased. This was due to recovery practice 2) employing values obtained from spiking tests in raw wastewater, thus the application of recovery practice 3) did not change the applied recovery values. The applied values from recovery practice 3) were generally lower for the two sludge streams compared to that of influent, leading to elevated concentrations of MPs in the sludge streams compared to the concentrations from practice 2). Conversely, the applied values from recovery practice 3) were generally lower for primary effluent compared to that of influent, resulting in decreased concentrations of MPs in the primary effluent stream compared to concentrations from practice 2).

In summary, the application of differential recovery practices resulted in varying degrees of changes in MP concentrations across different streams, with variations observed between count and mass bases. These changes in concentrations subsequently affected the MP loads in the different streams, possibly leading to variations in the closure of the balance when different recovery practices were employed.

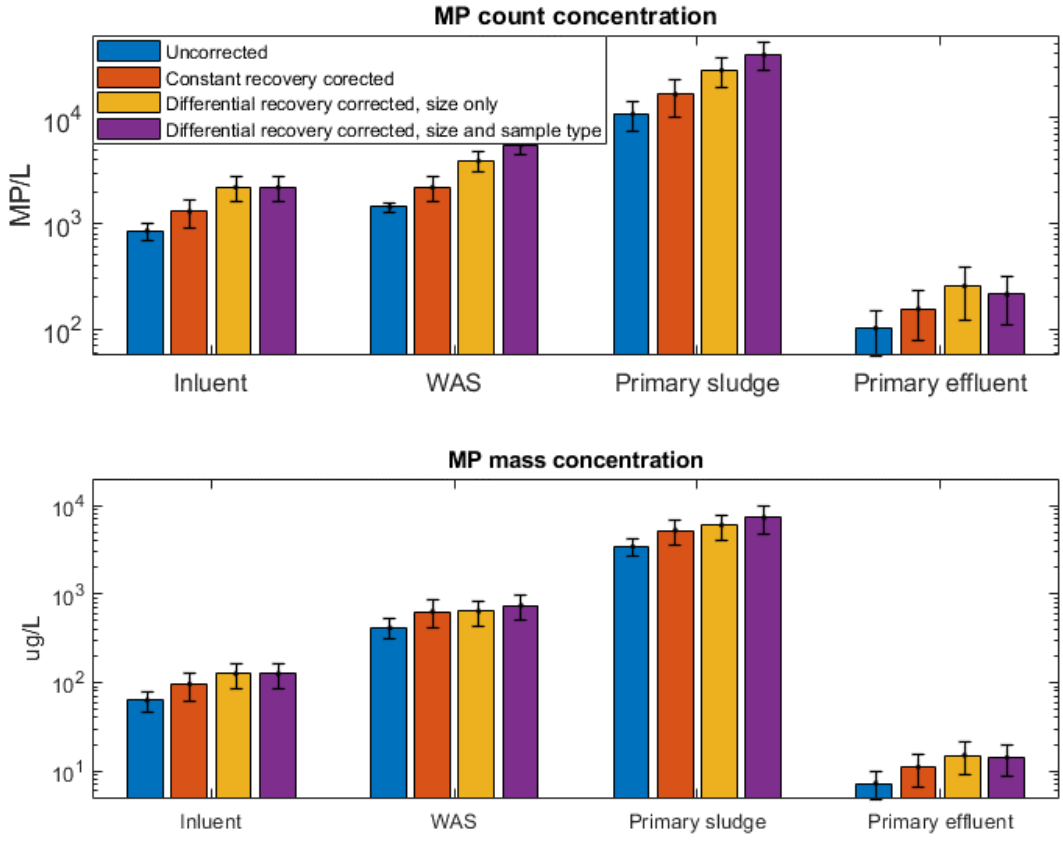

Figure 5- 5 Concentrations of MPs in different streams on both count and mass basis corrected using different recovery practices.

5.3.5 Count balance of MPs in primary treatment

The quantification of MP count loads in each stream during primary treatment, along with their corresponding contribution to the count balance expressed as proportions, as well as the 'lack of balance', are presented in Figure 5-6. The analysis started from establishing balance models for

20-100 μm, 100-250 μm, and 250-500 μm MPs respectively and then went beyond to establish count balance of total MP, which aimed to provide insights into the behavior of different size fractions of MPs within count balance models.

During the investigation of each balance, a comparative analysis was conducted between two situations: one based on the uncorrected MP concentrations, and another based on the concentrations that were corrected considering both size and sample type. By analyzing the total balance and the balance for each fraction, as well as contrasting the uncorrected and corrected balance situations, a comprehensive understanding of the fate and transport of MPs on count basis in primary wastewater treatment was obtained. The recovery used for correcting loads were presented in Figure 5-3B.

The count balance analysis of MPs within the size range of 20-100 μm depicted in Figure 5-6A shows that the count loads of all four streams increased when applying differential recovery. However, the degree of increase varied among the streams. A faster increase in loads was observed in the WAS and primary sludge streams, with the mean recovery for both two sludge streams being 25.1% corresponding to a faster mean increase of 289%. In contrast, the influent stream exhibited a mean recovery of 35.7% corresponding to a mean increase of 179.9%, while the primary effluent stream displayed a mean recovery of 46.1% corresponding to a slow mean increase of 116.9%. When a balance model lacks closure, an faster increase in the outflow loads will improve the closure of the balance, whereas an faster increase in the inflow loads reduces balance closure. By examining the contributions of the individual streams to the mass flows (in or out) the underlying reasons for the closure or lack of balance before and after data correction could be identified. As depicted in Figure 5-6A, despite the faster increase in the primary sludge load following data correction and the potential for improved balance closure, this potential improvement was offset by the corresponding increase in the WAS stream. Consequently, the application of differential recovery for 20-100 μm MPs did not lead to a significant improvement in count balance, with the lack of balance slightly decreasing from 73.8% to 70.9%.

The count balance analysis of MPs within the size range of 100-250 μm is presented in Figure 5-6B. In this size range, an mean increase of 52.3 % was observed for influent, 72.1% for primary sludge and WAS, and 119.7% for primary effluent. It is interesting to notice that the primary effluent load increased faster compared to other loads due to a lower recovery (a mean recovery

of 45.5%), which is believed to be a random error, considering that the recovery of MPs from the primary effluent is generally higher compared to other sample types. After the data correction, the faster increase observed in the two outflow loads streams contributed to an improved closure of the balance, although only a small portion of these increase was offset by the faster increase in the WAS stream. Consequently, the lack of balance decreased from 73.3% to 65.5%, which is mainly contributed by the faster increase of two outflow streams.

The count balance analysis of MPs within the size range of 250-500 μm is presented in Figure 5-6C. In this size range, the increase of loads did not vary significantly among the 4 streams, with an increase of 19.2% observed for influent, 22.0% for primary sludge and WAS, and 15.3% for primary effluent. From a balance perspective, the slightly faster increase associated with the primary sludge and the potential for improved closure of the balance was counterbalanced by the slightly faster increase in the WAS stream. These changes led to the same level of balance closure, with a lack of balance of 32.2% prior to correction and 34.7% after the adjustments.

The count balance of all MPs depicted in Figure 5-6D demonstrates that the increase of loads in each stream resulting from data correction is consistent with those observed for 20-100 μm MPs. This consistency arises due to the fact that concentrations of 20-100 μm MPs constitute approximately 90% of the MPs in all streams on a count basis in uncorrected data (see Appendix C for size distribution of MPs in uncorrected data). Consequently, in each stream, the load for 20-100 μm MPs also accounts for approximately 90%, since the flow rate for each stream remains consistent when calculating the loads in each size fraction. The dominating proportion of 20-100 μm MPs loads in total MP loads in each stream makes the trend of total MP balance behave very consistent with the 20-100 μm MP balance, with minimum change 73.0 % and 70.3 % in terms of lack of balance prior to and after adjustment.

The performance of the primary treatment in terms of MP removal was assessed using removal efficiencies based on count loads. In this study, the load calculated using corrected data was presented, as it was believed to provide a more accurate reflection of the real MP concentrations and loads. Removal efficiencies of 90.6±60.3%, 83.7±61.7%, 46.3±36.8%, and 89.6±50.5% were observed for 20-100 μm, 100-250 μm, 250-500 μm, and total MPs, respectively. Notably, the removal of MPs was more efficient for small-sized MPs (20-250 μm) compared to larger MPs (250-500 μm). The reasons for this discrepancy require further investigation. However,

considering the overall removal efficiency of approximately 90% for the total MP load, it can be concluded that the primary treatment demonstrates efficient removal of MPs.

Collectively examining the count balances discussed above, it becomes apparent that across all size ranges of MPs, the potential for improved closure of balances with recovery corrections due to the increased primary sludge loads was counteracted by the increases in the WAS stream. Consequently, the application of the differential recovery practice did not lead to a significant improvement in the closure of the balances.

(A)

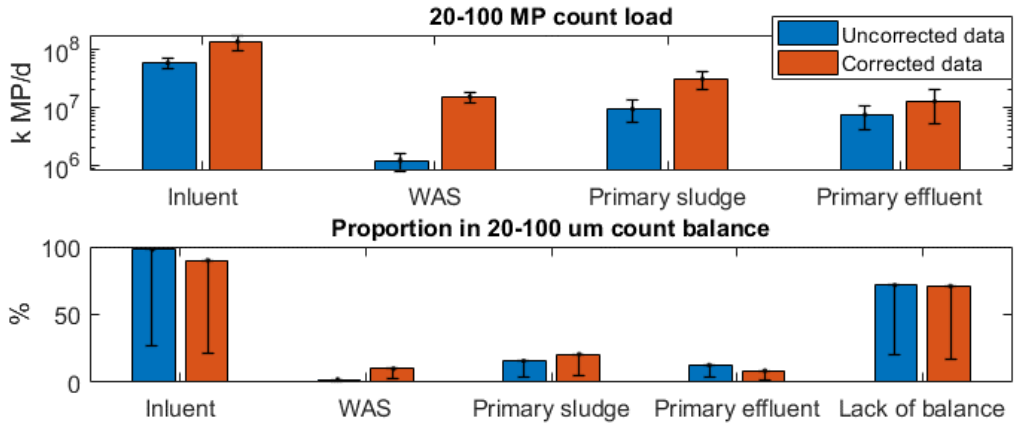
20-100 MP count load
Uncorrected data
Corrected data
k MP/d
10^8
10^7
10^6
Inluent
WAS
Primary sludge
Primary effluent
Proportion in 20-100 um count balance
%
100
50
0
Inluent
WAS
Primary sludge
Primary effluent
Lack of balance

(B)

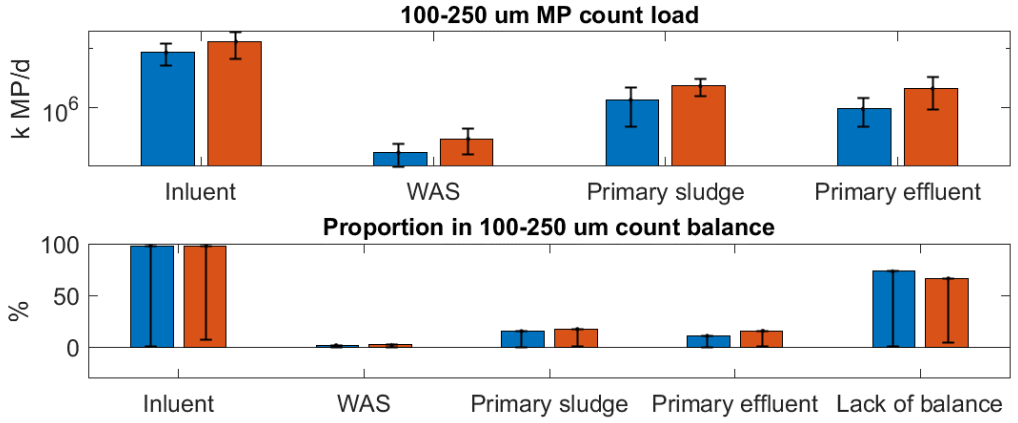
100-250 um MP count load
k MP/d
10^6
Inluent
WAS
Primary sludge
Primary effluent
Proportion in 100-250 um count balance
%
100
50
0
Inluent
WAS
Primary sludge
Primary effluent
Lack of balance

(C)

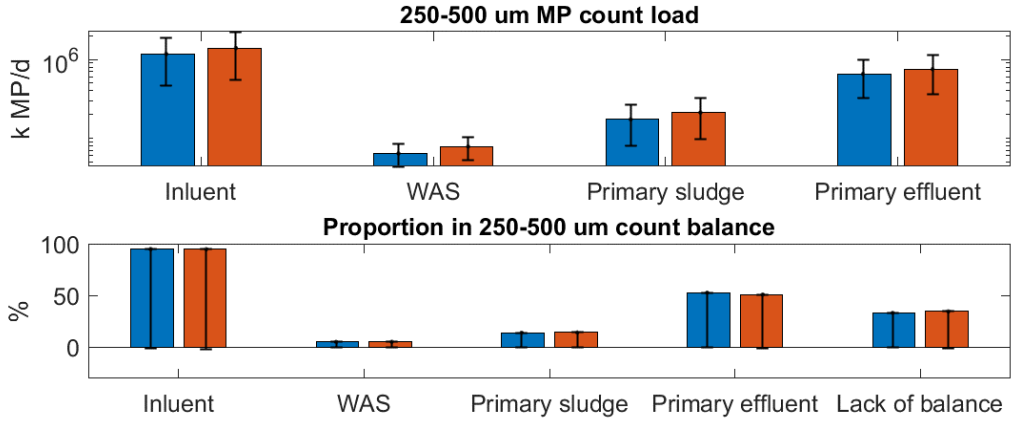
250-500 um MP count load
k MP/d
10^6
Inluent
WAS
Primary sludge
Primary effluent
Proportion in 250-500 um count balance
%
100
50
0
Inluent
WAS
Primary sludge
Primary effluent
Lack of balance

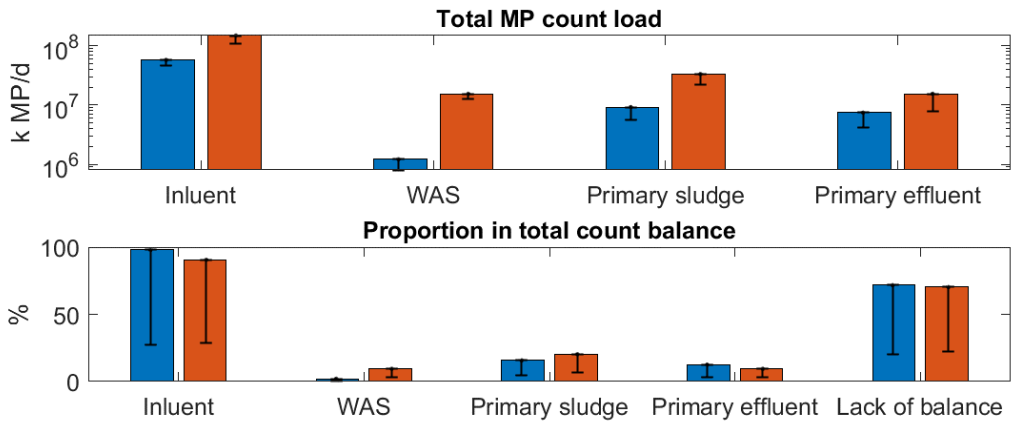

(D)

Figure 5- 6 Count Balance of MPs within Primary Wastewater Treatment in Different Size Fractions.

(A) 20-100 µm, (B); 100-250 µm, (C); and 250-500 µm, and (D) Count Balance of Total MPs. The proportion of each stream load expressed as % was calculated by dividing this load by the total inflow loads, calculated using equation (3)

5.3.6 Mass balance of MPs in primary treatment

In a similar approach to the analysis of count balance, the mass balance of MPs were examined by scrutinizing mass loads in each stream with their corresponding proportions in the mass balance, as well as the assessment of the "lack of balance". The results are presented in Figure 5-7. The analysis involved the establishment of mass balance models for 20-100 µm, 100-250 µm, 250-500 µm, and total MPs, and the balance based on uncorrected data was compared with balance based on recovery practice that considered both size and sample type.

The impact of differential recovery on the mass balance of 20-100 µm MPs is presented in Figure 5-7A. The same recovery practice used to correct the count balance in Figure 5-6A was applied to correct this mass balance, hence, same pattern of increase were observed in mass loads, with a faster increase was observed in the loads of WAS and primary sludge streams (a mean increase 289%) compared with the influent stream (a mean increase 179.9%), while a slow increase was observed for primary effluent stream (a mean increase 116.9%). In the uncorrected mass balance, the primary sludge stream contributes a significantly larger proportion (56.6%), which is in stark contrast to the low proportion (14.1%, as depicted in Figure 5-6A) of the primary sludge stream load in the uncorrected count balance. Hence, in the mass balance after data correction, the faster

increase in primary sludge load is only partially counterbalanced by the faster increase in WAS load and partially counterbalanced by the insufficient increase of primary effluent loads, leaving a portion not offset which will contribute to the closing of balance. Overall, these findings led to an improved closure of the balance, as indicated by a decrease in the lack of balance from 30.1% to 10.2%. Notably, the primary stream played a crucial role in achieving this improved closure.

The impact of differential recovery on the mass balance of 100-250 μm, 250-500 μm, and total MPs is presented in Figures 5-7B, 5-7C, and 5-7D, respectively. Similar to the large proportion of the primary sludge load in the uncorrected mass balance of 20-100 μm MPs, the mass load of the primary sludge accounted for 51.0%, 77.2%, and 58.6% in the uncorrected mass balances of 100-250 μm, 250-500 μm, and total MPs, respectively. In all three independent mass balances, the primary sludge stream exhibited faster increase compared to the increase observed in the influent, resulting in an improved closure of the balance. Though a lack of balance was caused by the faster increase of WAS streams and the slow increase of primary effluent streams (except in the 100-250 μm balance due to a random error), the high proportions of the primary sludge streams prevented the complete offsetting of the counteractive effects. This caused the lack of balance in the 100-250 μm, 250-500 μm, and total MPs models improved from 40.5% to 30.9%, from 10.5% to 9.4%, and from 30.7% to 17.2%, respectively. The 17.2% lack of balance in the total MPs model is comparable to the deficit observed in the TSS mass balance closure, indicating a good performance of the mass balance model. In summary, the application of differential recovery significantly enhanced the performance of the three mass balance models. These improvements were primarily attributed to the faster increase observed in the primary sludge loads.

In terms of removal efficiencies based on mass loads from corrected data, 88.8±60.7%, 86.5±78.3%, 86.5±58.9%, and 87.6±42.7% were observed for 20-100 μm, 100-250 μm, 250-500 μm, and total MPs, respectively. These removal efficiencies demonstrate efficient MP removal of MPs on mass basis.

When comparing the mass-based models with the count-based models, it was observed that the application of differential recovery led to an improvement in the mass balance of MPs, whereas no corresponding improvement was observed in the count balance models. The primary reason for this discrepancy lies in the differing proportions of the primary sludge stream between the count-based and mass-based models of MPs. The study serves as a noteworthy example demonstrating

that mass balance models offer crucial insights into the fate and transport of MPs in WWTPs that cannot be solely addressed by count balance models.

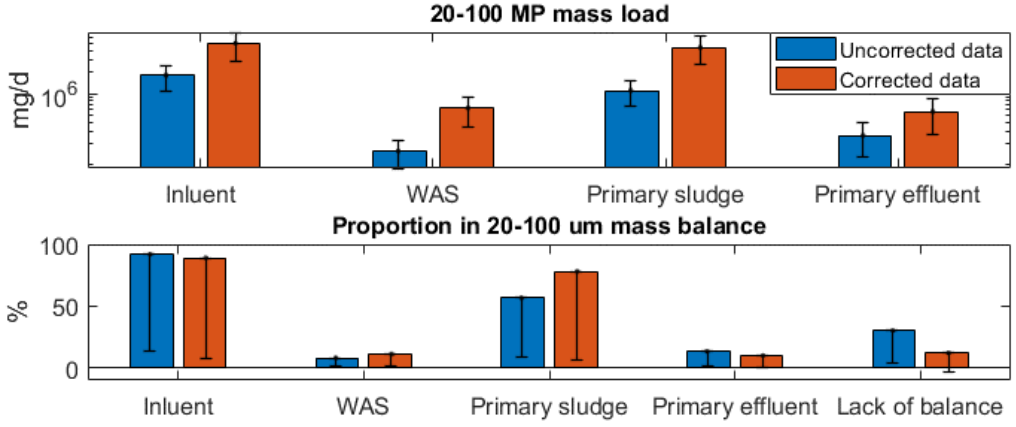

(A)

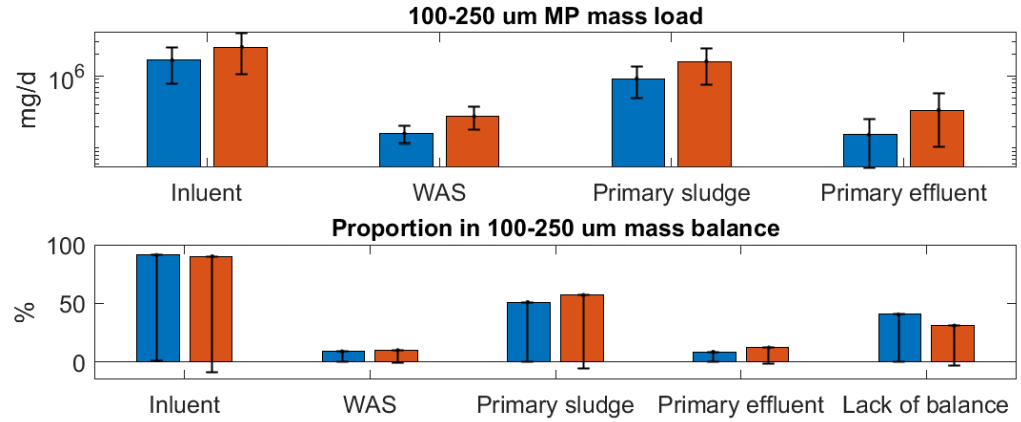

(B)

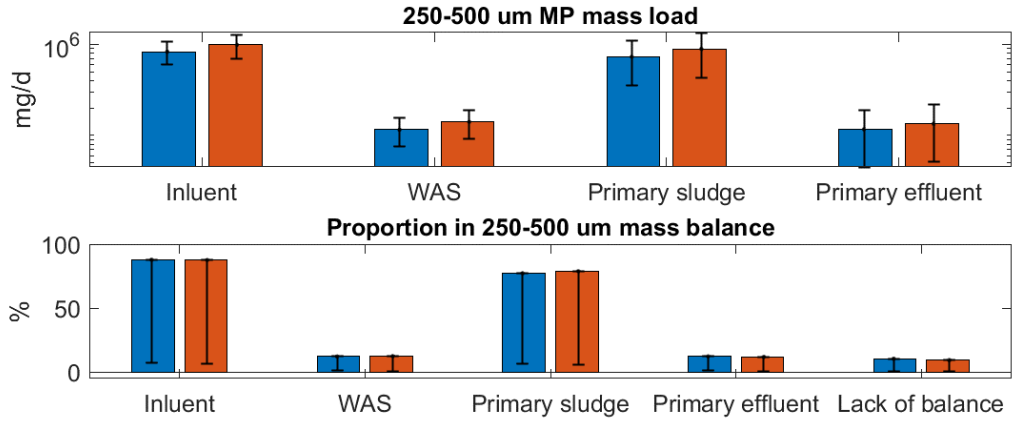

(C)

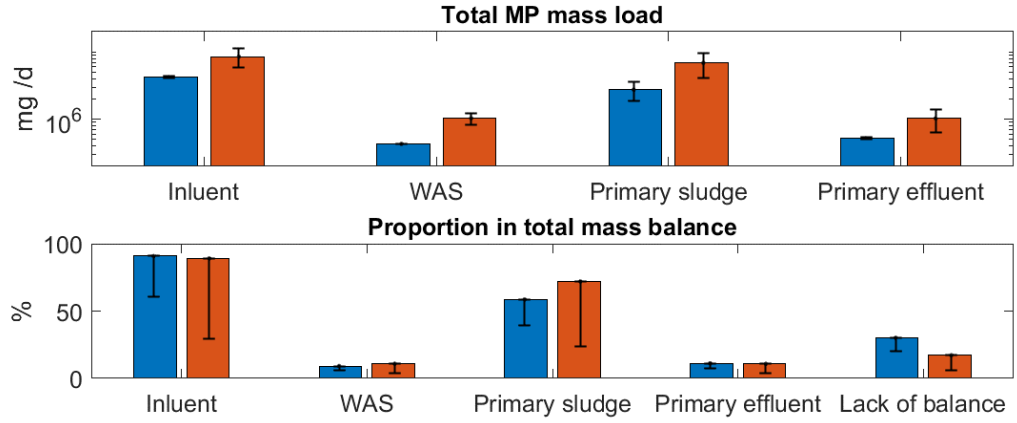

(D)

Figure 5- 7 Mass Balance of MPs within Primary Wastewater Treatment in Different Size Fractions

(A) 20-100 µm, (B); 100-250 µm, (C); and 250-500 µm, and (D) Mass Balance of Total MPs. The proportion of each stream load expressed as % was calculated by dividing this load by the total inflow loads, calculated using equation (3)

5.4. Conclusions

The study aimed to establish count and mass balance models for MPs in primary wastewater treatment and examine the impact of differential recovery on the model performance. For this purpose, spiking tests were conducted using standard MPs to critically evaluate the influence of MP size and sample type on recovery, and the derived recovery values were then utilized to correct MP concentrations and loads in the primary treatment at Kitchener WWTP. The following conclusions were drawn based on the experimental and model study:

- The recovery tests revealed that both MP size and sample type have a significant impact on MP recovery. Therefore, considering these variations is crucial for accurately estimating MP concentrations.
- The application of differential recovery practices, including constant recovery, size-based differential recovery, and differential recovery considering both size and sample type, resulted in varying changes in MP concentrations across different streams. These different recovery practices also led to variations in the increases observed in concentrations on count and mass bases. These concentration changes subsequently affected the MP loads from different streams and potentially impacted the count and mass balance models of MPs.
- While the application of differential recovery practice did not significantly improve the closure of the count balance model for MPs, it resulted in a significant improvement in the closure of the mass balance model. This highlights the importance of employing the appropriate recovery practice in model studies.

The differing proportions of the primary sludge stream load in each balance were identified as the primary reason for the differential impact of recovery practices on the two types of models. In the count balance model, the load of the primary sludge stream accounted for a small portion, which limited its influence. However, in the mass balance models, the load of the primary sludge stream had a more substantial contribution, and its increase was not offset by other. These findings underscore the significance of mass balance models in providing valuable insights into the fate and transport of MPs in WWTPs that cannot be solely addressed by count balance models.

Chapter 6 Conclusions and recommendations

6.1 Conclusions

In conclusion, this PhD thesis has made significant contributions to the field of MPs research in the context of WWTPs. The thesis consists of three studies, each focusing on a different aspect of MP analysis and modeling.

The first study of this thesis focused on leveraging deep learning techniques for automatic MP recognition in FPA-based micro-FT-IR microscopy. The development and testing of PlasticNet, a deep convolutional neural network architecture specifically designed for MP identification, yielded several significant findings. PlasticNet exhibited exceptional performance, achieving accurate classification of 11 common plastic types with an impressive accuracy rate exceeding 95%. Through a detailed analysis of identification errors using a confusion matrix, it was determined that these errors primarily stemmed from edge effects, molecular structure similarities, and contamination of MP standards. Furthermore, PlasticNet demonstrated robust performance in recognizing complex spectra associated with the presence of additives and weathering, showcasing its versatility in identifying MPs with increased complexity. Notably, the re-training of PlasticNet with more complex spectra further enhanced its capability to recognize these intricate spectra. Additionally, PlasticNet showcased its efficacy in identifying MPs despite variations in spectral signatures caused by differing MP thicknesses, outperforming traditional library search methods by achieving a 16.9% improvement in identifying polyethylene MPs within complex datasets. The successful development and application of PlasticNet provides an advanced and efficient tool for accurate MP identification, addressing the challenges associated with spectral variances and facilitating a comprehensive understanding of MP composition and distribution in environmental samples.

The second study of this thesis focused on investigating the uncertainties associated with MP enumeration through a modeling approach. By thoroughly examining the sources of random errors throughout the MP analysis process, the study aimed to refine an existing uncertainty model and incorporate appropriate assumptions. The findings revealed valuable insights into reducing data uncertainty and improving the accuracy of MP concentration estimates. Increasing the number of replicates in MP analysis was identified as a significant factor contributing to the reduction of

uncertainty, with a recommended minimum of three replicates to enhance reliability. Moreover, the study highlighted the importance of considering differential recovery associated with MP size, shape, and type for accurate estimation of MP concentrations and category proportions. The incorporation of non-constant recovery observed across replicates and the differential recovery considering size and morphology categories proved crucial in minimizing errors and uncertainty. The study emphasized the necessity of comprehensive spiking tests with MPs from different categories and the inclusion of resulting recoveries in concentration estimation. Overall, the modeling approach provided a valuable framework for quantifying uncertainties in MP enumeration, enhancing the reliability and accuracy of MP data, and enabling more informed decision-making in environmental studies.

The third study of this thesis aimed to establish count and mass balance models for MPs in primary wastewater treatment and investigate the impact of differential recovery on the performance of these models. The conducted spiking tests provided essential insights into MP recovery, specifically highlighting the significant influence of MP size and sample type on recovery rates. Considering these variations were found to be crucial for accurately estimating MP concentrations. Differential recovery practices, including constant recovery, size-based differential recovery, and differential recovery considering both size and sample type, resulted in varying changes in MP concentrations across different streams. These different recovery practices also led to variations in the observed increases in concentrations on count and mass bases, subsequently affecting the MP loads from different streams and potentially impacting the count and mass balance models of MPs. While the count balance model did not significantly improve with the application of differential recovery practices, the mass balance model demonstrated substantial improvement in closure. The differing proportions of the primary sludge stream load in each balance were identified as the primary reason for the differential impact of recovery practices on the two types of models. In the count balance model, the load of the primary sludge stream accounted for a small portion, limiting its influence. However, in the mass balance models, the load of the primary sludge stream had a more substantial contribution, and its inflation was not offset by other factors. These findings underscore the significance of mass balance models in providing valuable insights into the fate and transport of MPs in WWTPs, complementing the count balance models and offering a more

comprehensive understanding of MP dynamics. The study highlights the importance of considering differential recovery practices to enhance the accuracy and reliability of count and mass balance models, facilitating informed decision-making and improving our understanding of MP behavior in wastewater treatment processes.

In summary, each study of this PhD thesis makes contributions to the field of MP research in WWTPs. The development of PlasticNet in study 1 provides an advanced deep learning tool for accurate MP identification, addressing spectral variances and enabling a comprehensive understanding of MP composition and distribution. Study 2 focuses on reducing data uncertainty through a modeling approach, emphasizing the importance of incorporating differential recovery and the significance of spiking tests to enhance the accuracy and reliability of MP concentration estimates. Lastly, study 3 establishes count and mass balance models for MPs in primary wastewater treatment, highlighting the impact of differential recovery on model performance and emphasizing the importance of mass balance models in understanding MP dynamics. Collectively, these findings contribute to enhancing our understanding of MP behavior in WWTPs, facilitating informed decision-making, and guiding the development of effective strategies for mitigating MP pollution in aquatic environments.

6.2 Recommendations

This PhD thesis has addressed critical challenges in MPs research within the context of WWTPs. The research has contributed to the development of advanced techniques for MP identification, the reduction of data uncertainty, and the establishment of count and mass balance models for MPs in primary treatment processes. Based on the findings from the three chapters, the following recommendations are proposed:

Enhanced MP Identification:

- Consider Modern Architectures: It is recommended to explore modern deep learning architectures, such as transformers, to reduce computational complexity and potentially

improve model performance. Evaluating the suitability of transformers for microplastic identification tasks can be beneficial.

- Data Augmentation Strategy: For plastic types with a limited number of spectra, employing data augmentation strategies like artificially creating distorted baselines or generating additional peaks can augment the dataset and improve model generalization.
- Train the Model for Subtype Differentiation: To enhance environmental risk assessment, consider collecting different spectra within specific plastic types, such as polypropylene (PP) with various types of additives, and train the model to differentiate between subtypes. This would enable the model to distinguish MPs with different additives, addressing specific concerns associated with distinct additive compositions.
- Continuous Updates to MP Library: Regularly update and refine the MP library used for identification to incorporate a wider spectrum of environmentally sourced microplastics. This should include MPs with various additives, surface modifications, and weathering effects, providing the model with a more comprehensive database for accurate identification.

Uncertainty Reduction in MP Enumeration:

- Promote the use of a minimum of three replicates during MP analysis to enhance the reliability and accuracy of concentration estimates.
- Emphasize the importance of discerning and categorizing different types of MPs based on size, shape, and morphology during enumeration. This practice will improve the accuracy of concentration estimates and provide a more comprehensive understanding of MP composition in environmental samples.
- Conduct comprehensive spiking tests with MPs from various categories and different sample matrices to capture and incorporate non-constant recovery and differential recovery associated with size and sample type. This will enhance the reliability of MP concentration estimates and minimize uncertainties.

Count and Mass Balance Modeling:

- Encourage the adoption of both count and mass balance models in MP research within WWTPs. These models offer complementary insights into MP dynamics and provide a more comprehensive understanding of MP behavior during wastewater treatment.
- Promote the use of differential recovery to obtain better concentration estimates and to correct for the proportion contributed by each stream in the balance model. This approach will improve the closure of the balance models and enhance their accuracy.
- Further investigate the impact of differential recovery on count and mass balance models, including the differential recovery associated with MP size, shape, and sample type. Integrating these considerations into modeling studies will provide more accurate estimates and improve the reliability of the models.

Integration and Standardization:

- Foster collaboration and knowledge sharing among researchers, practitioners, and policymakers to enhance the integration and standardization of MP research methodologies and findings.
- Encourage the development of standardized guidelines and protocols for MP analysis, enumeration, and modeling in WWTPs. These guidelines will ensure consistency and comparability across studies, leading to more reliable and robust assessments of MP pollution and mitigation strategies.

By implementing these recommendations, future research endeavors can advance our understanding of MP pollution in WWTPs, inform effective mitigation strategies, and contribute to the development of sustainable practices for managing plastic waste. These efforts will play a crucial role in minimizing the environmental and ecological impacts of MPs and safeguarding the health and well-being of ecosystems and human populations.

References

Acquarelli, J., van Laarhoven, T., Gerretzen, J., Tran, T.N., Buydens, L.M.C. and Marchiori, E. 2017. Convolutional neural networks for vibrational spectroscopic data analysis. Anal Chim Acta 954, 22-31.

Al-Azzawi, M.S., Kefer, S., Weißer, J., Reichel, J., Schwaller, C., Glas, K., Knoop, O. and Drewes, J.E. 2020. Validation of sample preparation methods for microplastic analysis in wastewater matrices—reproducibility and standardization. Water 12(9), 2445.

Alimi, O.S., Farner Budarz, J., Hernandez, L.M. and Tufenkji, N. 2018. Microplastics and nanoplastics in aquatic environments: aggregation, deposition, and enhanced contaminant transport. Environmental science & technology 52(4), 1704-1724.

Andrade, J., Fernández-González, V., López-Mahía, P. and Muniategui, S. 2019. A low-cost system to simulate environmental microplastic weathering. Marine Pollution Bulletin 149, 110663.

Andrady, A.L. 2011. Microplastics in the marine environment. Marine pollution bulletin 62(8), 1596-1605.

Andrei, A.B., Fleschin, S. and Aboul-Enein, H.Y. 2015. Cancer diagnosis by FT-IR Spectrophotometry. Rev. Roum. Chim 60(5-6), 415-426.

Andrieu, C., De Freitas, N., Doucet, A. and Jordan, M.I. 2003. An introduction to MCMC for machine learning. Machine learning 50, 5-43.

Andrieu, C. and Thoms, J. 2008. A tutorial on adaptive MCMC. Statistics and computing 18, 343-373.

Asif, U., Bennamoun, M. and Sohel, F.A. 2017. A multi-modal, discriminative and spatially invariant CNN for RGB-D object labeling. IEEE transactions on pattern analysis and machine intelligence 40(9), 2051-2065.

Back, H.M., Vargas Junior, E.C., Alarcon, O.E. and Pottmaier, D. 2022. Training and evaluating machine learning algorithms for ocean microplastics classification through vibrational spectroscopy. Chemosphere 287(Pt 1), 131903.

Bauerlein, P.S., Erich, M.W., van Loon, W., Mintenig, S.M. and Koelmans, A.A. 2023. A monitoring and data analysis method for microplastics in marine sediments. Mar Environ Res 183, 105804.

Ben-David, E.A., Habibi, M., Haddad, E., Hasanin, M., Angel, D.L., Booth, A.M. and Sabbah, I. 2020. Microplastic distributions in a domestic wastewater treatment plant: Removal efficiency, seasonal variation and influence of sampling technique. Sci Total Environ 752, 141880.

Berger, J.O., Moreno, E., Pericchi, L.R., Bayarri, M.J., Bernardo, J.M., Cano, J.A., De la Horra, J., Martín, J., Ríos-Insúa, D. and Betrò, B. 1994. An overview of robust Bayesian analysis. Test 3(1), 5-124.

Bergmann, M., MЧMtzel, S., Primpke, S., Tekman, M.B., Trachsel, J. and Gerdts, G. 2019. White and wonderful? Microplastics prevail in snow from the Alps to the Arctic. Science Advances 5(8), eaax1157.

Bergmann, M., Wirzberger, V., Krumpen, T., Lorenz, C., Primpke, S., Tekman, M.B. and Gerdts, G. 2017. High Quantities of Microplastic in Arctic Deep-Sea Sediments from the HAUSGARTEN Observatory. Environ Sci Technol 51(19), 11000-11010.

Berisha, S., Lotfollahi, M., Jahanipour, J., Gurcan, I., Walsh, M., Bhargava, R., Van Nguyen, H. and Mayerich, D. 2019. Deep learning for FTIR histology: leveraging spatial and spectral features with convolutional neural networks. Analyst 144(5), 1642-1653.

Bianco, V., Memmolo, P., Carcagnì, P., Merola, F., Paturzo, M., Distante, C. and Ferraro, P. 2020. Microplastic identification via holographic imaging and machine learning. Advanced Intelligent Systems 2(2), 1900153.

Blair, R.M., Waldron, S. and Gauchotte-Lindsay, C. 2019. Average daily flow of microplastics through a tertiary wastewater treatment plant over a ten-month period. Water Res 163, 114909.

Blair, R.M., Waldron, S., Phoenix, V. and Gauchotte-Lindsay, C. 2017. Micro- and Nanoplastic Pollution of Freshwater and Wastewater Treatment Systems. Springer Science Reviews 5(1-2), 19-30.

Brandt, J., Fischer, F., Kanaki, E., Enders, K., Labrenz, M. and Fischer, D. 2021. Assessment of subsampling strategies in microspectroscopy of environmental microplastic samples. Frontiers in Environmental Science 8, 579676.

Bruge, A., Dhamelincourt, M., Lanceleur, L., Monperrus, M., Gasperi, J. and Tassin, B. 2020. A first estimation of uncertainties related to microplastic sampling in rivers. Sci Total Environ 718, 137319.

Burrows, S.D., Frustaci, S., Thomas, K.V. and Galloway, T. 2020. Expanding exploration of dynamic microplastic surface characteristics and interactions. TrAC Trends in Analytical Chemistry 130, 115993.

Campanale, C., Massarelli, C., Savino, I., Locaputo, V. and Uricchio, V.F. 2020. A Detailed Review Study on Potential Effects of Microplastics and Additives of Concern on Human Health. Int J Environ Res Public Health 17(4).

Carr, S.A., Liu, J. and Tesoro, A.G. 2016. Transport and fate of microplastic particles in wastewater treatment plants. Water Res 91, 174-182.

Chand, R., Rasmussen, L.A., Tumlin, S. and Vollertsen, J. 2021. The occurrence and fate of microplastics in a mesophilic anaerobic digester receiving sewage sludge, grease, and fatty slurries. Sci Total Environ 798, 149287.

Chen, H., Jia, Q., Sun, X., Zhou, X., Zhu, Y., Guo, Y. and Ye, J. 2022. Quantifying microplastic stocks and flows in the urban agglomeration based on the mass balance model and source-pathway-receptor framework: Revealing the role of pollution sources, weather patterns, and environmental management practices. Water Research 224, 119045.

Chen, X., Kroell, N., Dietl, T., Feil, A. and Greiff, K. 2021. Influence of long-term natural degradation processes on near-infrared spectra and sorting of post-consumer plastics. Waste Manag 136, 213-218.

Conley, K., Clum, A., Deepe, J., Lane, H. and Beckingham, B. 2019. Wastewater treatment plants as a source of microplastics to an urban estuary: Removal efficiencies and loading per capita over one year. Water Res X 3, 100030.

Coppock, R.L., Cole, M., Lindeque, P.K., Queirós, A.M. and Galloway, T.S. 2017. A small-scale, portable method for extracting microplastics from marine sediments. Environmental Pollution 230, 829-837.

Corradini, F., Meza, P., Eguiluz, R., Casado, F., Huerta-Lwanga, E. and Geissen, V. 2019. Evidence of microplastic accumulation in agricultural soils from sewage sludge disposal. Science of the total environment 671, 411-420.

Covernton, G.A., Davies, H.L., Cox, K.D., El-Sabaawi, R., Juanes, F., Dudas, S.E. and Dower, J.F. 2021. A Bayesian analysis of the factors determining microplastics ingestion in fishes. Journal of Hazardous Materials 413, 125405.

Cowger, W., Gray, A., Christiansen, S.H., DeFrond, H., Deshpande, A.D., Hemabessiere, L., Lee, E., Mill, L., Munno, K., Ossmann, B.E., Pittroff, M., Rochman, C., Sarau, G., Tarby, S. and Primpke, S. 2020. Critical Review of Processing and Classification Techniques for Images and Spectra in Microplastic Research. Appl Spectrosc 74(9), 989-1010.

Cowger, W., Gray, A.B., Guilinger, J.J., Fong, B. and Waldschlager, K. 2021. Concentration Depth Profiles of Microplastic Particles in River Flow and Implications for Surface Sampling. Environ Sci Technol 55(9), 6032-6041.

da Silva, V.H., Murphy, F., Amigo, J.M., Stedmon, C.A. and Strand, J. 2020. Classification and quantification of microplastic (< 100 microm) using FPA-FTIR imaging system and machine learning. Anal Chem.

De Frond, H., O'Brien, A.M. and Rochman, C.M. 2023. Representative subsampling methods for the chemical identification of microplastic particles in environmental samples. Chemosphere 310, 136772.

de Souza Machado, A.A., Lau, C.W., Kloas, W., Bergmann, J., Bachelier, J.B., Faltin, E., Becker, R., Görlich, A.S. and Rillig, M.C. 2019. Microplastics can change soil properties and affect plant performance. Environmental science & technology 53(10), 6044-6052.

Deme, G.G., Ewusi-Mensah, D., Olagbaju, O.A., Okeke, E.S., Okoye, C.O., Odii, E.C., Ejeromedoghene, O., Igun, E., Onyekwere, J.O. and Oderinde, O.K. 2022. Macro problems from microplastics:

Toward a sustainable policy framework for managing microplastic waste in Africa. Science of the Total Environment 804, 150170.
Dris, R., Gasperi, J., Rocher, V., Saad, M., Renault, N. and Tassin, B. 2015. Microplastic contamination in an urban area: a case study in Greater Paris. Environmental Chemistry 12(5), 592-599.
Dümichen, E., Barthel, A.-K., Braun, U., Bannick, C.G., Brand, K., Jekel, M. and Senz, R. 2015. Analysis of polyethylene microplastics in environmental samples, using a thermal decomposition method. Water research 85, 451-457.
Dyachenko, A., Mitchell, J. and Arsem, N. 2017. Extraction and identification of microplastic particles from secondary wastewater treatment plant (WWTP) effluent. Analytical Methods 9(9), 1412-1418.
Edo, C., Fernandez-Pinas, F. and Rosal, R. 2021. Microplastics identification and quantification in the composted Organic Fraction of Municipal Solid Waste. Sci Total Environ, 151902.
Elkhatib, D. and Oyanedel-Craver, V. 2020. A critical review of extraction and identification methods of microplastics in wastewater and drinking water. Environmental Science & Technology 54(12), 7037-7049.
Emelko, M.B., Schmidt, P.J., Reilly, P.M. and technology 2010. Particle and microorganism enumeration data: enabling quantitative rigor and judicious interpretation. Environmental Science Technology 44(5), 1720-1727.
Enfrin, M., Dumee, L.F. and Lee, J. 2019. Nano/microplastics in water and wastewater treatment processes - Origin, impact and potential solutions. Water Res 161, 621-638.
Enyoh, C.E., Wang, Q., Wang, W., Chowdhury, T., Rabin, M.H., Islam, R., Yue, G., Yichun, L. and Xiao, K. 2022. Sorption of Per-and Polyfluoroalkyl Substances (PFAS) using Polyethylene (PE) microplastics as adsorbent: Grand Canonical Monte Carlo and Molecular Dynamics (GCMC-MD) studies. International Journal of Environmental Analytical Chemistry, 1-17.
Estahbanati, S. and Fahrenfeld, N. 2016. Influence of wastewater treatment plant discharges on microplastic concentrations in surface water. Chemosphere 162, 277-284.
Frehland, S., Kaegi, R., Hufenus, R. and Mitrano, D.M. 2020. Long-term assessment of nanoplastic particle and microplastic fiber flux through a pilot wastewater treatment plant using metal-doped plastics. Water research 182, 115860.
Fries, E., Dekiff, J.H., Willmeyer, J., Nuelle, M.-T., Ebert, M. and Remy, D. 2013. Identification of polymer types and additives in marine microplastic particles using pyrolysis-GC/MS and scanning electron microscopy. Environmental Science: Processes & Impacts 15(10), 1949-1956.
Ghosh, J.K., Delampady, M. and Samanta, T. (2006) An introduction to Bayesian analysis: theory and methods, Springer.
Gies, E.A., LeNoble, J.L., Noel, M., Etemadifar, A., Bishay, F., Hall, E.R. and Ross, P.S. 2018. Retention of microplastics in a major secondary wastewater treatment plant in Vancouver, Canada. Mar Pollut Bull 133, 553-561.
Goodfellow, I., Bengio, Y. and Courville, A. (2017) Deep learning, MIT press Massachusetts, USA:.
Grady Jr, C.L., Daigger, G.T., Love, N.G. and Filipe, C.D. (2011) Biological wastewater treatment, CRC press.
Guyon, I., Gunn, S., Nikravesh, M. and Zadeh, L.A. (2008) Feature extraction: foundations and applications, Springer.
Habib, R.Z., Thiemann, T. and Al Kendi, R. 2020. Microplastics and wastewater treatment plants—a review. Journal of Water Resource and Protection 12(01), 1.
Hahladakis, J.N., Velis, C.A., Weber, R., Iacovidou, E. and Purnell, P. 2018. An overview of chemical additives present in plastics: Migration, release, fate and environmental impact during their use, disposal and recycling. Journal of hazardous materials 344, 179-199.
Halbach, M., Baensch, C., Dirksen, S. and Scholz-Bottcher, B.M. 2021. Microplastic extraction from sediments established? - A critical evaluation from a trace recovery experiment with a custom-made density separator. Anal Methods 13(44), 5299-5308.
Harris, D.C. (2010) Quantitative chemical analysis, Macmillan.

Harrison, J.P., Hoellein, T.J., Sapp, M., Tagg, A.S., Ju-Nam, Y. and Ojeda, J.J. (2018) Freshwater microplastics, pp. 181-201, Springer, Cham.
He, K., Zhang, X., Ren, S. and Sun, J. 2016 Deep residual learning for image recognition, pp. 770-778.
He, R., Wu, X., Sun, Z. and Tan, T. 2018. Wasserstein cnn: Learning invariant features for nir-vis face recognition. IEEE transactions on pattern analysis and machine intelligence 41(7), 1761-1773.
Henze, M., van Loosdrecht, M.C., Ekama, G.A. and Brdjanovic, D. (2008) Biological wastewater treatment, IWA publishing.
Hidalgo-Ruz, V., Gutow, L., Thompson, R.C. and Thiel, M. 2012. Microplastics in the marine environment: a review of the methods used for identification and quantification. Environ Sci Technol 46(6), 3060-3075.
Hu, Y., Gong, M., Wang, J. and Bassi, A. 2019. Current research trends on microplastic pollution from wastewater systems: a critical review. Reviews in Environmental Science and Bio/Technology 18(2), 207-230.
Huang, J., Chen, B., Yao, B. and He, W. 2019. ECG arrhythmia classification using STFT-based spectrogram and convolutional neural network. IEEE access 7, 92871-92880.
Hufnagl, B., Stibi, M., Martirosyan, H., Wilczek, U., Möller, J.N., Löder, M.G., Laforsch, C. and Lohninger, H. 2021. Computer-assisted analysis of microplastics in environmental samples based on μFTIR imaging in combination with machine learning. Environmental science & technology letters 9(1), 90-95.
Hurley, R.R., Lusher, A.L., Olsen, M. and Nizzetto, L. 2018. Validation of a Method for Extracting Microplastics from Complex, Organic-Rich, Environmental Matrices. Environ Sci Technol 52(13), 7409-7417.
Johansen, M.P., Cresswell, T., Davis, J., Howard, D.L., Howell, N.R. and Prentice, E. 2019. Biofilm-enhanced adsorption of strong and weak cations onto different microplastic sample types: Use of spectroscopy, microscopy and radiotracer methods. Water research 158, 392-400.
Kahane-Rapport, S., Czapanskiy, M., Fahlbusch, J., Friedlaender, A., Calambokidis, J., Hazen, E., Goldbogen, J. and Savoca, M. 2022. Field measurements reveal exposure risk to microplastic ingestion by filter-feeding megafauna. Nature Communications 13(1), 6327.
Kedzierski, M., Falcou-Prefol, M., Kerros, M.E., Henry, M., Pedrotti, M.L. and Bruzaud, S. 2019. A machine learning algorithm for high throughput identification of FTIR spectra: Application on microplastics collected in the Mediterranean Sea. Chemosphere 234, 242-251.
Kingsbury, B.E., Morgan, N. and Greenberg, S. 1998. Robust speech recognition using the modulation spectrogram. Speech communication 25(1-3), 117-132.
Kinigopoulou, V., Pashalidis, I., Kalderis, D. and Anastopoulos, I. 2022. Microplastics as carriers of inorganic and organic contaminants in the environment: A review of recent progress. Journal of Molecular Liquids, 118580.
Kirstein, I.V., Hensel, F., Gomiero, A., Iordachescu, L., Vianello, A., Wittgren, H.B. and Vollertsen, J. 2021. Drinking plastics? - Quantification and qualification of microplastics in drinking water distribution systems by microFTIR and Py-GCMS. Water Res 188, 116519.
Kirstein, I.V., Kirmizi, S., Wichels, A., Garin-Fernandez, A., Erler, R., Löder, M. and Gerdts, G. 2016. Dangerous hitchhikers? Evidence for potentially pathogenic Vibrio spp. on microplastic particles. Marine environmental research 120, 1-8.
Koelmans, A.A., Mohamed Nor, N.H., Hermsen, E., Kooi, M., Mintenig, S.M. and De France, J. 2019. Microplastics in freshwaters and drinking water: Critical review and assessment of data quality. Water Res 155, 410-422.
Koelmans, A.A., Redondo-Hasselerharm, P.E., Nor, N.H.M., de Ruijter, V.N., Mintenig, S.M. and Kooi, M. 2022. Risk assessment of microplastic particles. Nature Reviews Materials 7(2), 138-152.
Konechnaya, O., Luchtrath, S., Dsikowitzky, L. and Schwarzbauer, J. 2020. Optimized microplastic analysis based on size fractionation, density separation and mu-FTIR. Water Sci Technol 81(4), 834-844.

Kyriakopoulos, G.L., Zamparas, M.G. and Kapsalis, V.C. 2022. Investigating the human impacts and the environmental consequences of microplastics disposal into water resources. Sustainability 14(2), 828.
Lakshminarasimman, N., Gewurtz, S.B., Parker, W.J. and Smyth, S.A. 2021. Removal and formation of perfluoroalkyl substances in Canadian sludge treatment systems - A mass balance approach. Sci Total Environ 754, 142431.
Lam, T.W.L., Fok, L., Lin, L., Xie, Q., Li, H.X., Xu, X.R. and Yeung, L.C. 2020. Spatial variation of floatable plastic debris and microplastics in the Pearl River Estuary, South China. Mar Pollut Bull 158, 111383.
Lares, M., Ncibi, M.C., Sillanpää, M. and Sillanpää, M. 2018. Occurrence, identification and removal of microplastic particles and fibers in conventional activated sludge process and advanced MBR technology. Water research 133, 236-246.
Laursen, S., Fruergaard, M. and Andersen, T. 2022. Rapid flocculation and settling of positively buoyant microplastic and fine-grained sediment in natural seawater. Marine Pollution Bulletin 178, 113619.
Lavoy, M. and Crossman, J. 2021. A novel method for organic matter removal from samples containing microplastics. Environ Pollut 286, 117357.
LeCun, Y., Bengio, Y. and Hinton, G. 2015a. Deep learning. Nature 521(7553), 436-444.
LeCun, Y., Bengio, Y. and Hinton, G. 2015b. Deep learning. nature 521(7553), 436-444.
Lee, W., Lenferink, A.T.M., Otto, C. and Offerhaus, H.L. 2019. Classifying Raman spectra of extracellular vesicles based on convolutional neural networks for prostate cancer detection. Journal of Raman Spectroscopy.
Leslie, H.A., Brandsma, S.H., van Velzen, M.J. and Vethaak, A.D. 2017. Microplastics en route: Field measurements in the Dutch river delta and Amsterdam canals, wastewater treatment plants, North Sea sediments and biota. Environ Int 101, 133-142.
Li, W., Zu, B., Hu, L., Lan, L., Zhang, Y. and Li, J. 2022. Migration behaviors of microplastics in sediment-bearing turbulence: Aggregation, settlement, and resuspension. Marine Pollution Bulletin 180, 113775.
Li, X., Chen, L., Mei, Q., Dong, B., Dai, X., Ding, G. and Zeng, E.Y. 2018. Microplastics in sewage sludge from the wastewater treatment plants in China. Water research 142, 75-85.
Liu, P., Zhan, X., Wu, X., Li, J., Wang, H. and Gao, S. 2020. Effect of weathering on environmental behavior of microplastics: Properties, sorption and potential risks. Chemosphere 242, 125193.
Liu, X., Sun, P., Qu, G., Jing, J., Zhang, T., Shi, H. and Zhao, Y. 2021. Insight into the characteristics and sorption behaviors of aged polystyrene microplastics through three type of accelerated oxidation processes. Journal of Hazardous Materials 407, 124836.
Loder, M.G.J., Imhof, H.K., Ladehoff, M., Loschel, L.A., Lorenz, C., Mintenig, S., Piehl, S., Primpke, S., Schrank, I., Laforsch, C. and Gerdts, G. 2017. Enzymatic Purification of Microplastics in Environmental Samples. Environ Sci Technol 51(24), 14283-14292.
Löder, M.G.J., Kuczera, M., Mintenig, S., Lorenz, C. and Gerdts, G. 2015. Focal plane array detector-based micro-Fourier-transform infrared imaging for the analysis of microplastics in environmental samples. Environmental Chemistry 12(5), 563.
Long, Z., Pan, Z., Wang, W., Ren, J., Yu, X., Lin, L., Lin, H., Chen, H. and Jin, X. 2019. Microplastic abundance, characteristics, and removal in wastewater treatment plants in a coastal city of China. Water Res 155, 255-265.
Lunn, D., Spiegelhalter, D., Thomas, A. and Best, N. 2009. The BUGS project: Evolution, critique and future directions. Statistics in medicine 28(25), 3049-3067.
Lv, X., Dong, Q., Zuo, Z., Liu, Y., Huang, X. and Wu, W.-M. 2019. Microplastics in a municipal wastewater treatment plant: Fate, dynamic distribution, removal efficiencies, and control strategies. Journal of Cleaner Production 225, 579-586.
Magni, S., Binelli, A., Pittura, L., Avio, C.G., Della Torre, C., Parenti, C.C., Gorbi, S. and Regoli, F. 2019. The fate of microplastics in an Italian Wastewater Treatment Plant. Science of the Total Environment 652, 602-610.

Magnusson, K. and Norén, F. 2014 Screening of microplastic particles in and down-stream a wastewater treatment plant.
Makantasis, K., Karantzalos, K., Doulamis, A. and Doulamis, N. 2015 Deep supervised learning for hyperspectral data classification through convolutional neural networks, pp. 4959-4962, IEEE.
Mari, A., Bordos, G., Gergely, S., Buki, M., Hahn, J., Palotai, Z., Besenyo, G., Szabo, E., Salgo, A., Kriszt, B. and Szoboszlay, S. 2021. Validation of microplastic sample preparation method for freshwater samples. Water Res 202, 117409.
Mason, S.A., Garneau, D., Sutton, R., Chu, Y., Ehmann, K., Barnes, J., Fink, P., Papazissimos, D. and Rogers, D.L. 2016. Microplastic pollution is widely detected in US municipal wastewater treatment plant effluent. Environ Pollut 218, 1045-1054.
Massarelli, C., Campanale, C. and Uricchio, V.F. 2021. A handy open-source application based on computer vision and machine learning algorithms to count and classify microplastics. Water 13(15), 2104.
Mathworks 2022a Detrend.
Mathworks 2022b Nomarlize.
Mathworks 2023 imfindcircles.
Mendrik, F., Fernández, R., Hackney, C.R., Waller, C. and Parsons, D.R. 2023. Non-buoyant microplastic settling velocity varies with biofilm growth and ambient water salinity. Communications Earth & Environment 4(1), 30.
Michel, A.P.M., Morrison, A.E., Preston, V.L., Marx, C.T., Colson, B.C. and White, H.K. 2020. Rapid Identification of Marine Plastic Debris via Spectroscopic Techniques and Machine Learning Classifiers. Environ Sci Technol 54(17), 10630-10637.
Michielssen, M.R., Michielssen, E.R., Ni, J. and Duhaime, M.B. 2016. Fate of microplastics and other small anthropogenic litter (SAL) in wastewater treatment plants depends on unit processes employed. Environmental Science: Water Research & Technology 2(6), 1064-1073.
Mintenig, S., Kooi, M., Erich, M., Primpke, S., Redondo-Hasselerharm, P., Dekker, S., Koelmans, A. and van Wezel, A. 2020. A systems approach to understand microplastic occurrence and variability in Dutch riverine surface waters. Water Research, 115723.
Mintenig, S.M., Int-Veen, I., Loder, M.G.J., Primpke, S. and Gerdts, G. 2017. Identification of microplastic in effluents of waste water treatment plants using focal plane array-based micro-Fourier-transform infrared imaging. Water Res 108, 365-372.
Miranda, M.N., Sampaio, M.J., Tavares, P.B., Silva, A.M.T. and Pereira, M.F.R. 2021. Aging assessment of microplastics (LDPE, PET and uPVC) under urban environment stressors. Sci Total Environ 796, 148914.
Mohamed Nor, N.H., Kooi, M., Diepens, N.J. and Koelmans, A.A. 2021. Lifetime accumulation of microplastic in children and adults. Environmental science & technology 55(8), 5084-5096.
Morgado, V., Palma, C. and Bettencourt da Silva, R.J.N. 2022. Bottom-Up Evaluation of the Uncertainty of the Quantification of Microplastics Contamination in Sediment Samples. Environ Sci Technol 56(15), 11080-11090.
Murphy, F., Ewins, C., Carbonnier, F. and Quinn, B. 2016. Wastewater Treatment Works (WwTW) as a Source of Microplastics in the Aquatic Environment. Environ Sci Technol 50(11), 5800-5808.
Ng, W., Minasny, B. and McBratney, A. 2020. Convolutional neural network for soil microplastic contamination screening using infrared spectroscopy. Sci Total Environ 702, 134723.
Ng, W., Minasny, B., Montazerolghaem, M., Padarian, J., Ferguson, R., Bailey, S. and McBratney, A.B. 2019. Convolutional neural network for simultaneous prediction of several soil properties using visible/near-infrared, mid-infrared, and their combined spectra. Geoderma 352, 251-267.
Nor, N.H. and Obbard, J.P. 2014. Microplastics in Singapore's coastal mangrove ecosystems. Mar Pollut Bull 79(1-2), 278-283.
Nunes, L.S., Silva, A.G., Espínola, L.A., Blettler, M.C. and Simões, N.R. 2021. Intake of microplastics by commercial fish: a Bayesian approach. Environmental Monitoring and Assessment 193(7), 402.

Oehlmann, J., Schulte-Oehlmann, U., Kloas, W., Jagnytsch, O., Lutz, I., Kusk, K.O., Wollenberger, L., Santos, E.M., Paull, G.C. and Van Look, K.J. 2009. A critical analysis of the biological impacts of plasticizers on wildlife. Philosophical Transactions of the Royal Society B: Biological Sciences 364(1526), 2047-2062.

Ovide, B.G., Cirino, E., Basran, C.J., Geertz, T. and Syberg, K. 2022. Assessment of Prevalence and Heterogeneity of Meso-and Microplastic Pollution in Icelandic Waters. Environments 9(12), 150.

Padarian, J., Minasny, B. and McBratney, A. 2019a. Using deep learning to predict soil properties from regional spectral data. Geoderma Regional 16, e00198.

Padarian, J., Minasny, B. and McBratney, A.B. 2019b. Using deep learning for digital soil mapping. Soil 5(1), 79-89.

Peeken, I., Primpke, S., Beyer, B., Gutermann, J., Katlein, C., Krumpen, T., Bergmann, M., Hehemann, L. and Gerdts, G. 2018. Arctic sea ice is an important temporal sink and means of transport for microplastic. Nat Commun 9(1), 1505.

Picó, Y., Soursou, V., Alfarhan, A.H., El-Sheikh, M.A. and Barceló, D. 2021. First evidence of microplastics occurrence in mixed surface and treated wastewater from two major Saudi Arabian cities and assessment of their ecological risk. Journal of Hazardous Materials 416, 125747.

Poria, S., Cambria, E. and Gelbukh, A. 2015 Deep convolutional neural network textual features and multiple kernel learning for utterance-level multimodal sentiment analysis, pp. 2539-2544.

Porterfield, K.K., Hobson, S.A., Neher, D.A., Niles, M.T. and Roy, E.D. 2022. Microplastics in composts, digestates and food wastes: A review. Journal of Environmental Quality.

Poulain, M., Mercier, M.J., Brach, L., Martignac, M., Routaboul, C., Perez, E., Desjean, M.C. and Ter Halle, A. 2018. Small microplastics as a main contributor to plastic mass balance in the North Atlantic subtropical gyre. Environmental science & technology 53(3), 1157-1164.

Prajapati, A., Narayan Vaidya, A. and Kumar, A.R. 2022. Microplastic properties and their interaction with hydrophobic organic contaminants: a review. Environmental Science and Pollution Research 29(33), 49490-49512.

Prata, J.C. 2018. Microplastics in wastewater: state of the knowledge on sources, fate and solutions. Marine pollution bulletin 129(1), 262-265.

Primpke, S., Cross, R.K., Mintenig, S.M., Simon, M., Vianello, A., Gerdts, G. and Vollertsen, J. 2020. Toward the Systematic Identification of Microplastics in the Environment: Evaluation of a New Independent Software Tool (siMPle) for Spectroscopic Analysis. Applied Spectroscopy, 1127-1138.

Primpke, S., Lorenz, C., Rascher-Friesenhausen, R. and Gerdts, G. 2017. An automated approach for microplastics analysis using focal plane array (FPA) FTIR microscopy and image analysis. Analytical Methods 9(9), 1499-1511.

Primpke, S., Wirth, M., Lorenz, C. and Gerdts, G. 2018. Reference database design for the automated analysis of microplastic samples based on Fourier transform infrared (FTIR) spectroscopy. Anal Bioanal Chem 410(21), 5131-5141.

Qiu, Y., Zhou, S., Zhang, C., Qin, W., Lv, C. and Zou, M. 2023. Identification of potentially contaminated areas of soil microplastic based on machine learning: A case study in Taihu Lake region, China. Sci Total Environ 877, 162891.

Randolph, T.W. 2006. Scale-based normalization of spectral data. Cancer Biomarkers 2(3-4), 135-144.

Rasmussen, L.A., Iordachescu, L., Tumlin, S. and Vollertsen, J. 2021. A complete mass balance for plastics in a wastewater treatment plant - Macroplastics contributes more than microplastics. Water Res 201, 117307.

Redondo-Hasselerharm, P.E., Falahudin, D., Peeters, E.T. and Koelmans, A.A. 2018. Microplastic effect thresholds for freshwater benthic macroinvertebrates. Environmental science & technology 52(4), 2278-2286.

Renard, B., Garreta, V. and Lang, M. 2006. An application of Bayesian analysis and Markov chain Monte Carlo methods to the estimation of a regional trend in annual maxima. Water resources research 42(12).

Satt, A., Rozenberg, S. and Hoory, R. 2017 Efficient Emotion Recognition from Speech Using Deep Learning on Spectrograms, pp. 1089-1093.
Schmidt, P.J., Cameron, E.S., Müller, K.M. and Emelko, M.B. 2022. Ensuring that fundamentals of quantitative microbiology are reflected in microbial diversity analyses based on next-generation sequencing. Frontiers in microbiology 13, 258.
Schmidt, P.J., Emelko, M.B. and Reilly, P.M. 2010. Quantification of analytical recovery in particle and microorganism enumeration methods. Environmental science technology 44(5), 1705-1712.
Schmidt, P.J., Emelko, M.B. and Thompson, M.E. 2014. Variance decomposition: A tool enabling strategic improvement of the precision of analytical recovery and concentration estimates associated with microorganism enumeration methods. Water research 55, 203-214.
Scott, J.W., Gunderson, K.G., Green, L.A., Rediske, R.R. and Steinman, A.D. 2021. Perfluoroalkylated substances (Pfas) associated with microplastics in a lake environment. Toxics 9(5), 106.
Selvam, S., Jesuraja, K., Venkatramanan, S., Roy, P.D. and Kumari, V.J. 2021. Hazardous microplastic characteristics and its role as a vector of heavy metal in groundwater and surface water of coastal south India. Journal of Hazardous Materials 402, 123786.
Shabbir, S., Faheem, M., Ali, N., Kerr, P.G., Wang, L.-F., Kuppusamy, S. and Li, Y. 2020. Periphytic biofilm: An innovative approach for biodegradation of microplastics. Science of The Total Environment 717, 137064.
Shi, H., Yang, Y., Zhu, X., Liao, S., Lei, Z., Zheng, W. and Li, S.Z. 2016 Embedding deep metric for person re-identification: A study against large variations, pp. 732-748, Springer.
Shim, W.J., Hong, S.H. and Eo, S.E. 2017. Identification methods in microplastic analysis: a review. Analytical Methods 9(9), 1384-1391.
Simon, M., van Alst, N. and Vollertsen, J. 2018. Quantification of microplastic mass and removal rates at wastewater treatment plants applying Focal Plane Array (FPA)-based Fourier Transform Infrared (FT-IR) imaging. Water Res 142, 1-9.
Simonyan, K. and Zisserman, A. 2014. Very deep convolutional networks for large-scale image recognition. arXiv preprint arXiv:1409.1556.
Smith, B.C. (2011) Fundamentals of Fourier transform infrared spectroscopy, CRC press.
Sönmez, V.Z., Akarsu, C. and Sivri, N. 2023. Impact of coastal wastewater treatment plants on microplastic pollution in surface seawater and ecological risk assessment. Environmental Pollution 318, 120922.
Sorensen, D., Gianola, D. and Gianola, D. 2002. Likelihood, Bayesian and MCMC methods in quantitative genetics.
Sturm, M.T., Schuhen, K. and Horn, H. 2022. Method for rapid biofilm cultivation on microplastics and investigation of its effect on the agglomeration and removal of microplastics using organosilanes. Science of The Total Environment 806, 151388.
Summers, S., Henry, T. and Gutierrez, T. 2018. Agglomeration of nano-and microplastic particles in seawater by autochthonous and de novo-produced sources of exopolymeric substances. Marine pollution bulletin 130, 258-267.
Sun, J., Dai, X., Wang, Q., van Loosdrecht, M.C. and Ni, B.-J. 2019. Microplastics in wastewater treatment plants: Detection, occurrence and removal. Water Research.
Sun, Y., Wang, X., Xia, S. and Zhao, J. 2021. New insights into oxytetracycline (OTC) adsorption behavior on polylactic acid microplastics undergoing microbial adhesion and degradation. Chemical Engineering Journal 416, 129085.
Sun, Y., Yuan, J., Zhou, T., Zhao, Y., Yu, F. and Ma, J. 2020. Laboratory simulation of microplastics weathering and its adsorption behaviors in an aqueous environment: A systematic review. Environ Pollut 265(Pt B), 114864.
Sutton, R., Mason, S.A., Stanek, S.K., Willis-Norton, E., Wren, I.F. and Box, C. 2016. Microplastic contamination in the San Francisco Bay, California, USA. Marine pollution bulletin 109(1), 230-235.

Tagg, A.S., Harrison, J.P., Ju-Nam, Y., Sapp, M., Bradley, E.L., Sinclair, C.J. and Ojeda, J.J. 2016. Fenton's reagent for the rapid and efficient isolation of microplastics from wastewater. Chem Commun (Camb) 53(2), 372-375.

Takeshita, K.M., Iwasaki, Y., Sinclair, T.M., Hayashi, T.I. and Naito, W. 2022. Illustrating a Species Sensitivity Distribution for Nano - and Microplastic Particles Using Bayesian Hierarchical Modeling. Environmental Toxicology and Chemistry 41(4), 954-960.

Talsness, C.E., Andrade, A.J., Kuriyama, S.N., Taylor, J.A. and Vom Saal, F.S. 2009. Components of plastic: experimental studies in animals and relevance for human health. Philosophical Transactions of the Royal Society B: Biological Sciences 364(1526), 2079-2096.

Talvitie, J., Mikola, A., Koistinen, A. and Setala, O. 2017a. Solutions to microplastic pollution - Removal of microplastics from wastewater effluent with advanced wastewater treatment technologies. Water Res 123, 401-407.

Talvitie, J., Mikola, A., Setala, O., Heinonen, M. and Koistinen, A. 2017b. How well is microlitter purified from wastewater? - A detailed study on the stepwise removal of microlitter in a tertiary level wastewater treatment plant. Water Res 109, 164-172.

Tanoiri, H., Nakano, H., Arakawa, H., Hattori, R.S. and Yokota, M. 2021. Inclusion of shape parameters increases the accuracy of 3D models for microplastics mass quantification. Mar Pollut Bull 171, 112749.

Ter Halle, A., Ladirat, L., Martignac, M., Mingotaud, A.F., Boyron, O. and Perez, E. 2017. To what extent are microplastics from the open ocean weathered? Environmental Pollution 227, 167-174.

Thiros, N.E., Siirila-Woodburn, E.R., Dennedy-Frank, P.J., Williams, K.H. and Gardner, W.P. 2023. Constraining Bedrock Groundwater Residence Times in a Mountain System with Environmental Tracer Observations and Bayesian Uncertainty Quantification. Water Resources Research, e2022WR033282.

Tunali, M., Uzoefuna, E.N., Tunali, M.M. and Yenigun, O. 2020. Effect of microplastics and microplastic-metal combinations on growth and chlorophyll a concentration of Chlorella vulgaris. Science of the Total Environment 743, 140479.

Unice, K.M., Kreider, M.L. and Panko, J.M. 2013. Comparison of tire and road wear particle concentrations in sediment for watersheds in France, Japan, and the United States by quantitative pyrolysis GC/MS analysis. Environ Sci Technol 47(15), 8138-8147.

Vermeiren, P., Lercari, D., Munoz, C.C., Ikejima, K., Celentano, E., Jorge-Romero, G. and Defeo, O. 2021. Sediment grain size determines microplastic exposure landscapes for sandy beach macroinfauna. Environmental Pollution 286, 117308.

Waldman, W.R. and Rillig, M.C. 2020 Microplastic research should embrace the complexity of secondary particles, ACS Publications.

Waldschläger, K. and Schüttrumpf, H. 2019. Effects of particle properties on the settling and rise velocities of microplastics in freshwater under laboratory conditions. Environmental science & technology 53(4), 1958-1966.

Wang, Z., Lin, T. and Chen, W. 2020. Occurrence and removal of microplastics in an advanced drinking water treatment plant (ADWTP). Sci Total Environ 700, 134520.

Waterloo, R.o. 2018 Waste Water Treatment Mater Plan.

Way, C., Hudson, M.D., Williams, I.D. and Langley, G.J. 2022. Evidence of underestimation in microplastic research: A meta-analysis of recovery rate studies. Sci Total Environ 805, 150227.

Wei, D., Zhou, B., Torrabla, A. and Freeman, W. 2015. Understanding intra-class knowledge inside cnn. arXiv preprint arXiv:1507.02379.

Whitehead, P.G., Bussi, G., Hughes, J.M., Castro-Castellon, A.T., Norling, M.D., Jeffers, E.S., Rampley, C.P., Read, D.S. and Horton, A.A. 2021. Modelling microplastics in the River Thames: Sources, sinks and policy implications. Water 13(6), 861.

Wong, T.-T. 1998. Generalized Dirichlet distribution in Bayesian analysis. Applied Mathematics and Computation 97(2-3), 165-181.

Woods, M.N., Stack, M.E., Fields, D.M., Shaw, S.D. and Matrai, P.A. 2018. Microplastic fiber uptake, ingestion, and egestion rates in the blue mussel (Mytilus edulis). Marine pollution bulletin 137, 638-645.

Wu, P., Tang, Y., Cao, G., Li, J., Wang, S., Chang, X., Dang, M., Jin, H., Zheng, C. and Cai, Z. 2020. Determination of Environmental Micro(Nano)Plastics by Matrix-Assisted Laser Desorption/Ionization-Time-of-Flight Mass Spectrometry. Anal Chem 92(21), 14346-14356.

Wu, X., Pan, J., Li, M., Li, Y., Bartlam, M. and Wang, Y. 2019. Selective enrichment of bacterial pathogens by microplastic biofilm. Water research 165, 114979.

Xu, X., Jian, Y., Xue, Y., Hou, Q. and Wang, L. 2019. Microplastics in the wastewater treatment plants (WWTPs): Occurrence and removal. Chemosphere 235, 1089-1096.

Xu, Z., Sui, Q., Li, A., Sun, M., Zhang, L., Lyu, S. and Zhao, W. 2020. How to detect small microplastics (20-100 mum) in freshwater, municipal wastewaters and landfill leachates? A trial from sampling to identification. Sci Total Environ 733, 139218.

Yan, Z., Zhao, H., Zhao, Y., Zhu, Q., Qiao, R., Ren, H. and Zhang, Y. 2020. An efficient method for extracting microplastics from feces of different species. Journal of hazardous materials 384, 121489.

Yang, L., Li, K., Cui, S., Kang, Y., An, L. and Lei, K. 2019. Removal of microplastics in municipal sewage from China's largest water reclamation plant. Water Res 155, 175-181.

Zhang, H., Zhou, Q., Xie, Z., Zhou, Y., Tu, C., Fu, C., Mi, W., Ebinghaus, R., Christie, P. and Luo, Y. 2018. Occurrences of organophosphorus esters and phthalates in the microplastics from the coastal beaches in north China. Science of the total environment 616, 1505-1512.

Zhang, X., Chen, J. and Li, J. 2020. The removal of microplastics in the wastewater treatment process and their potential impact on anaerobic digestion due to pollutants association. Chemosphere 251, 126360.

Zhao, J., Liu, L., Zhang, Y., Wang, X. and Wu, F. 2018. A novel way to rapidly monitor microplastics in soil by hyperspectral imaging technology and chemometrics. Environmental Pollution 238, 121-129.

Zhao, W. and Du, S. 2016. Spectral–spatial feature extraction for hyperspectral image classification: A dimension reduction and deep learning approach. IEEE Transactions on Geoscience and Remote Sensing 54(8), 4544-4554.

Zhu, F., Zhu, C., Wang, C. and Gu, C. 2019. Occurrence and ecological impacts of microplastics in soil systems: a review. Bulletin of environmental contamination and toxicology 102, 741-749.

Zhu, Z., Parker, W. and Wong, A. 2020. PlasticNet: Deep learning for automatic microplastic recognition via FT-IR spectroscopy. Journal of Computational Vision and Imaging Systems 6(1), 1-3.

Zhu, Z., Parker, W. and Wong, A. 2021 Quantification of the mass of microplastics using FPA-based FT-IR Imaging, London, Ontario.

Ziajahromi, S., Neale, P.A., Rintoul, L. and Leusch, F.D. 2017. Wastewater treatment plants as a pathway for microplastics: Development of a new approach to sample wastewater-based microplastics. Water Res 112, 93-99.

Ziccardi, L.M., Edgington, A., Hentz, K., Kulacki, K.J. and Driscoll, S.K. 2016. Microplastics as vectors for bioaccumulation of hydrophobic organic chemicals in the marine environment: A state-of-the-science review. Environmental toxicology and chemistry 35(7), 1667-1676.

Zimmermann, L., Göttlich, S., Oehlmann, J., Wagner, M. and Völker, C. 2020. What are the drivers of microplastic toxicity? Comparing the toxicity of plastic chemicals and particles to Daphnia magna. Environmental Pollution 267, 115392.

Appendices

Appendix A Supplementary information related to leverage deep learning for MP identification

Table A1 Comparison of molecular structure for PET and PMMA, Nylon and PMMA

Confusion pairs	Comparison of molecular structure	
PET and PMMA	PET 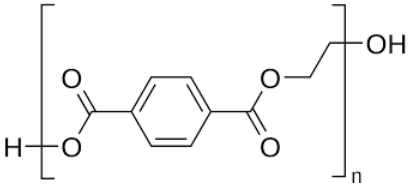	PMMA 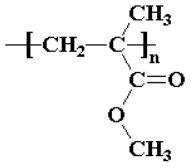
Nylon and PMMA	Nylon 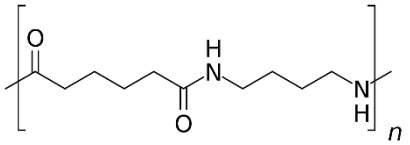	PMMA 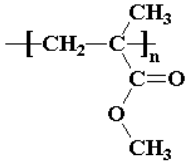

PET and PMMA confusion

The comparison of molecular structure from Table S1 showed that there is a lot of similarity between the molecular structure of PET and PU. The C-H(3100-2695 cm^{-1}), O-H (1440-1310 cm^{-1}), C=O (1780-1650 cm^{-1}), C-O (1250-1050 cm^{-1}) exists in both two types of molecular.

The plotting of an erroneously classified PET (Fig.S1)spectrum showed that the spectra of PET and PMMA are similar in both range 3200-2800 cm^{-1} and 1800-1250 cm^{-1}. A comparison of the molecular structure and the examination on the spectra showed that the molecular similarity is the main source of error for the confusion between PET and PMMA.

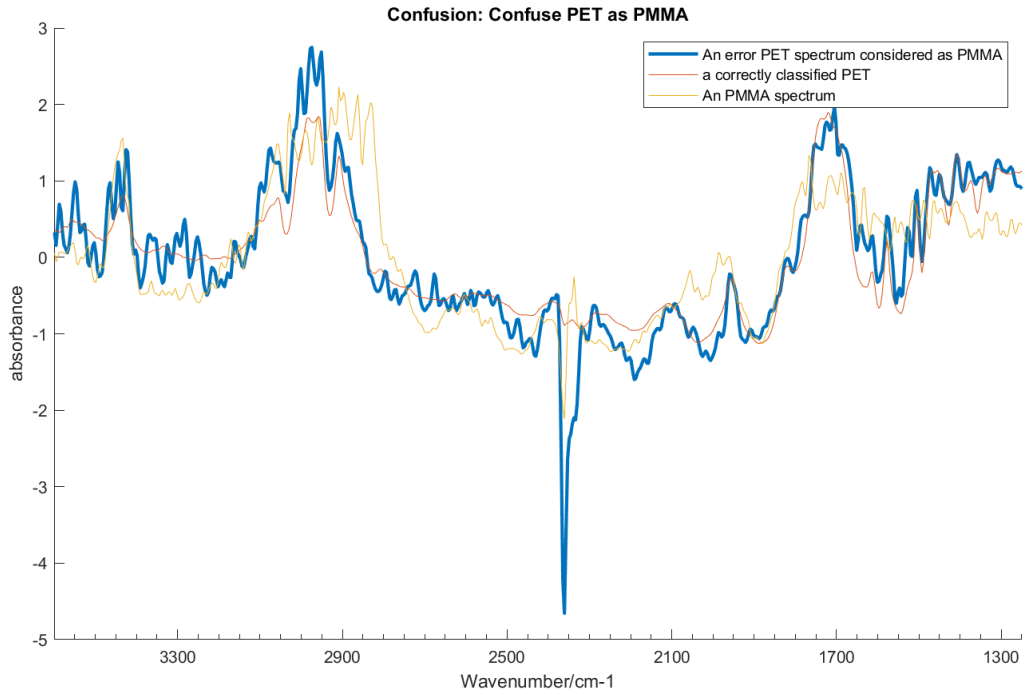

Fig A1 Plotting of confusion between PET and PMMA

Nylon and PMMA confusion

The comparison of molecular structure from Table S1 showed that there is some similarity between the molecular structure of Nylon and PMMs because C-H (3100-2695 cm^{-1}), C=O (1780-1650 cm^{-1}), C-O (1250-1050 cm^{-1}) exists in both two types of molecular. However, the N-H bonding (3500-3300 cm^{-1}) on Nylon spectra does not exist on PMMA. Further examination on the spectra is needed to see what contribute to the confusion between Nylon and PMMA.

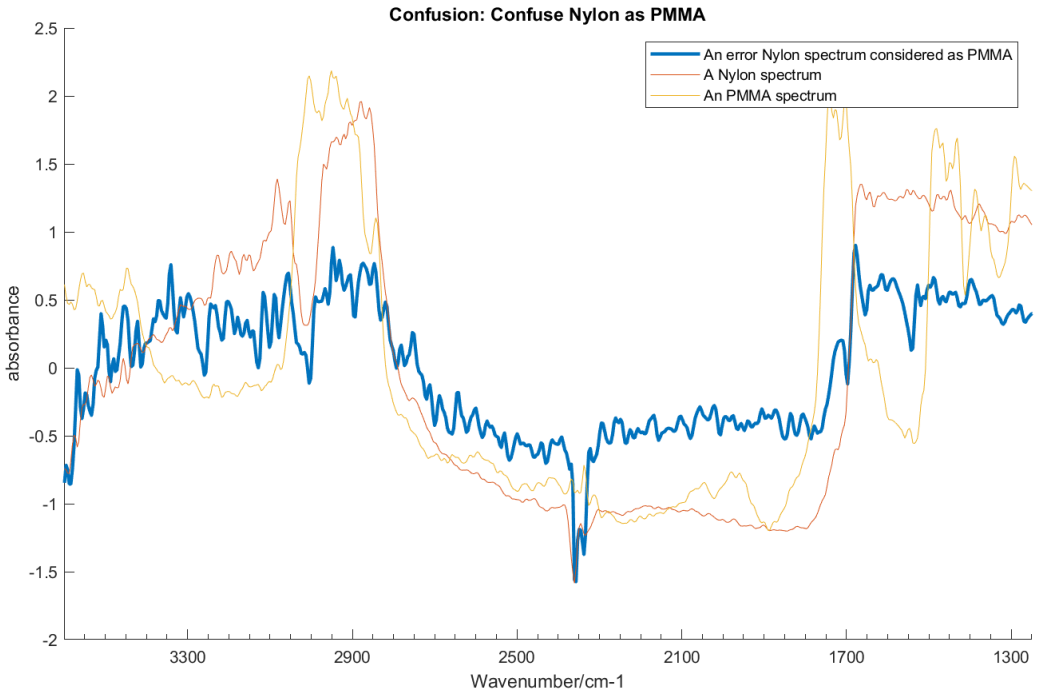

Fig A2 Plotting of confusion between Nylon and PMMA

As shown in the figure A2, the Nylon spectrum that is erroneously classified as PMMA must be collected from the edge of a Nylon particle and the signature peaks are weak. Examination on the spectra of mis-classified Nylon showed that edge effect is the source contribute to the error. It is concluded that edge effect might be the source between Nylon and PMMA

(A) 

(B) 

(C) 

Fig A3 PP with (A)glass fiber, (B)flame retardant and (C)$CaCO_3$

(A) 

(B) 

(C) 

Fig A4 Colored PP with (A)white, (B)light blue and (C)red

(A)

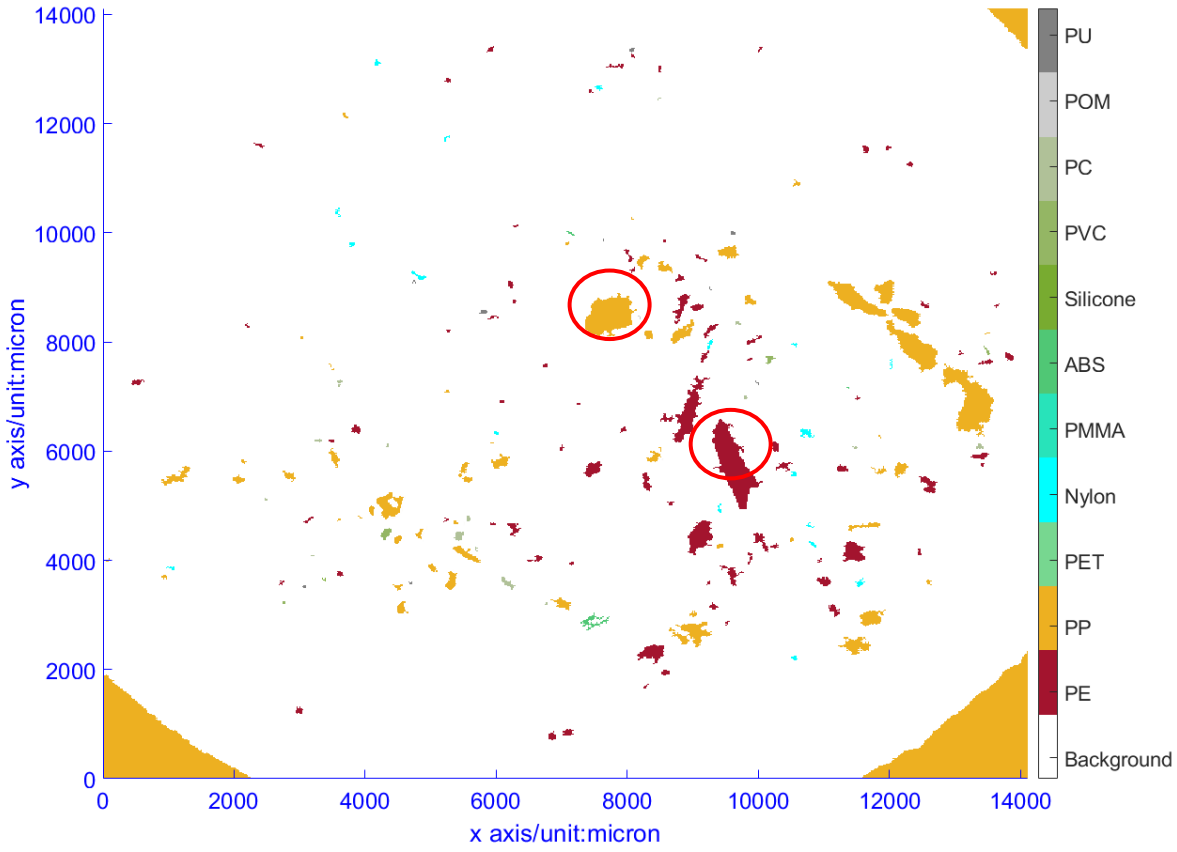
14000
12000
10000
8000
6000
4000
2000
0
y axis/unit:micron
0
2000
4000
6000
8000
10000
12000
14000
x axis/unit:micron
PU
POM
PC
PVC
Silicone
ABS
PMMA
Nylon
PET
PP
PE
Background

(B)

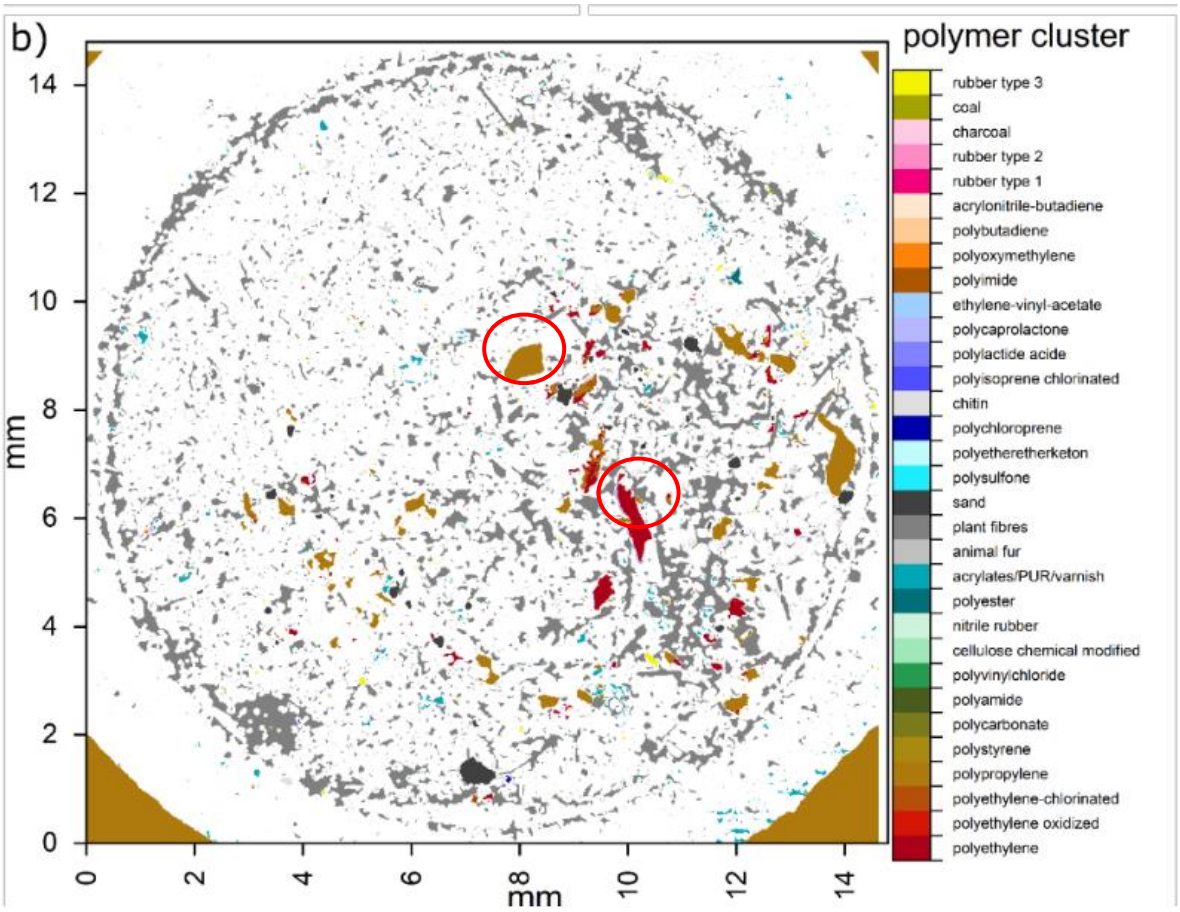

Fig.A5. Comparison of the recognition results of Dataset 3B by PlasticNet approaches and library search. (A) Recognition results by PlasticNet. (B) Recognition results by the library search by Primpke et al. (2020). The spectra from the two circled large PE , PP MPs were used as referecnce for manual assessment

Appendix B Supplementary information related to modelling uncertainties in MP enumeration

R code for simulating 10 replicates of enumeration data based on parameters in Table 3

```
## 10 replicates

mu<-300

weight<-c(0.3,0.2,0.1,0.4)

betaA<-c(2.11,1.93,5.55,5.85)

betaB<-c(3.91,1.78,1.30,0.51)

set.seed(5)

#simulate Y values Y~Poisson(mu*weight)

Y<-rpois(40, mu*weight)

#simulate recovery values

recovery<-rbeta(40, betaA, betaB)

#simulate X values X~binomial(Y, recovery)

X<-rbinom(40, Y, recovery)

Dataframe<-data.frame(Y,recovery,X)

X.mat<-matrix(X,nrow=10,ncol=4,byrow=TRUE)
```

Table B1 Simulated MP count in different categories based on parameters in Table 3. Each row corresponds to one replicate (e.g. in replicate #1, enumeration yields 30, 30, 27, 129 MPs for category A, B, C,D respectively.

Replicate #	Category A	Category B	Category C	Category D
1	30	30	27	129
2	4	21	25	47
3	21	37	24	121
4	71	61	27	126
5	22	6	24	114
6	45	17	25	108
7	36	16	28	125
8	14	6	32	14
9	64	44	22	100
10	11	49	27	126

Table S2: Assessment of Errors and Credible Interval Lengths in Posterior Distributions, as Derived from Varying Numbers of Replicates and MP Categorizations

		Mean	Error	Credible interval length
Number of replicates	1 enumeration	403.6	51.2	512.7
	2 replicates	281.6	8.7	124.6
	3 replicates	287.6	6.5	105.2
	5 replicates	335.1	12.7	109.7
	10 replicates	316.2	6.2	64.5
Categorization	1 category	438.1	46.0	355.5
	4 category	287.6	6.5	105.2

R code for simulating pA, pB, pC, pD

```
## Generate random recovery data

set.seed(5)

# Generate a random number from the beta distributions for example
(5.55,1.30), the first argument means generate one replicate

random_recovery_1 <- rbeta(1, 2.11, 3.91)

random_recovery_2 <- rbeta(1, 1.93, 1.78)

random_recovery_3 <- rbeta(1, 5.55, 1.30)

random_recovery_4 <- rbeta(1, 5.85, 0.51)

# Print the generated random number

print(random_recovery_1)

print(random_recovery_2)

print(random_recovery_3)

print(random_recovery_4)
```

Table S-3 Mean and Credible Interval of Total MP concentrations and MP proportions estimated by different models

	Model comparison	True value	mean	error	credible interval 2.5pc	credible interval 97.5pc
	Ignore non-constant and differential recovery	300	180	40.1	165.2	194.8
	Ignoring non-constant recovery	300	418	39.3	373.6	469.1
	ignore differential	300	235	21.8	205.7	285.8
Ctot	Full model	300	281	6.3	232	350.5
	Ignore non-constant and differential recovery	0.3	0.108	64.0	0.08213	0.1353
	Ignoring non-constant recovery	0.3	0.237	21.1	0.1902	0.294
	ignore differential	0.3	0.116	61.5	0.07941	0.1584
w1	Full model	0.3	0.229	23.8	0.1311	0.3524
	Ignore non-constant and differential recovery	0.2	0.171	14.4	0.1396	0.2041
	Ignoring non-constant recovery	0.2	0.445	122.7	0.3841	0.5026
	ignore differential	0.2	0.159	20.3	0.115	0.206
w2	Full model	0.2	0.201	0.3	0.1363	0.3074
	Ignore non-constant and differential recovery	0.1	0.147	47.1	0.1176	0.1793
	Ignoring non-constant recovery	0.1	0.064	36.4	0.04843	0.0796
	ignore differential	0.1	0.132	31.9	0.09743	0.171
w3	Full model	0.1	0.112	11.8	0.07729	0.1528
	Ignore non-constant and differential recovery	0.4	0.574	43.4	0.5328	0.617
	Ignoring non-constant recovery	0.4	0.254	36.5	0.2187	0.2904
	ignore differential	0.4	0.593	48.3	0.5306	0.6814
w4	Full model	0.4	0.459	14.8	0.3573	0.5523

Appendix C Supplementary information related to count and mass balance models of MPs in Primary treatment plant

T test values for instrument vs eye-based recovery

Paired Student's T-tests were conducted for each pair in Fig.3A to ascertain statistical differences, yielding p-values of 0.4912, 0.9496, 0.6306, 0.8082, 0.5955, and 0.8949 respectively. These results imply no significant difference between the eye and instrument-based recoveries, and that both methods provide comparable results for determining MP recovery across the various sample types and sizes.

Two way anova for MP size and sample types

Source	SS	df	MS	F	Prob>F
Columns	1214.5	2	607.25	3.65	0.0467
Rows	10499.5	2	5249.76	31.55	0
Interaction	392.1	4	98.01	0.59	0.6748
Error	2995.3	18	166.41		
Total	15101.4	26			

Fenton reaction Formula :

- 100 mL 30% v/v H2O2
- 26 mL 0.1 M NaOH
- 25 mL 0.1M acidified FeSO4

Preparation of 0.1M acidified FeSO4

Using 1L glass container, dissolve 13.9g FeSO4 7H2O in 500 mL DI water. After that add 6 mL concentrated H2SO4

Propagation of uncertainties

When executing addition and subtraction operations on hypothetical numbers as per equation (4), where uncertainties are designated as e1, e2, and e3 (as specified in subscript), the uncertainty in the resultant value is derived from the absolute uncertainties of each individual term, in accordance with equation (5). For multiplication and division operations, all uncertainties should first be converted into percent relative uncertainties as designated in equation (6), after which the uncertainties of the product or quotient can be computed with relative uncertainties using equation (7).

$$(1.75 \pm (0.89)_{e1})\text{-}(2.73 \pm (0.77)_{e2})\text{+}(4.33 \pm (0.32)_{e3})$$

$$=(1.75 - 2.73 + 4.33) \pm\sqrt{(0.89)^2 + (0.77)^2 + (0.32)^2} \qquad \text{eq(4)}$$

$$e4 = \sqrt{(e1)^2 + (e2)^2 + (e3)^2} \qquad \text{eq(5)}$$

$$\frac{(1.75\pm(0.89)_{e1})-(2.73\pm(0.77)_{e2})}{(4.33\pm(0.32)_{e3})} = \frac{(1.75\pm(50.9\%)_{\%e1})-(2.73\pm(28.2\%)_{\%e2})}{(4.33\pm(7.4\%)_{\%e3})}$$

$$=\frac{(1.75)-(2.73)}{(4.33)} \pm \sqrt{(50.9\%)^2 + (28.2\%)^2 + (7.4\%)^2} \qquad \text{eq(6)}$$

$$\%e4 = \sqrt{(\%e1)^2 + (\%e2)^2 + (\%e3)^2} \qquad \text{eq(7)}$$

Nestle cream bottle cap with PP recycling label

Number of spiked standard MPs in each type of sample

Raw wastewater

		spiked
spiking1	PP（300-500 um）	29
	PE （180-212 um）	29
	PE （45-53 um）	637
spiking2	PP（300-500 um）	20
	PE （180-212 um）	49
	PE （45-53 um）	642
spiking3	PP（300-500 um）	14
	PE （180-212 um）	34
	PE （45-53 um）	553

Primary sludge spiking

		spiked
	PP（300-500 um）	24
	PE （180-212 um）	65
spiking1	PE （45-53 um）	589
	PP（300-500 um）	18
	PE （180-212 um）	65
spiking2	PE （45-53 um）	493
	PP（300-500 um）	16
	PE （180-212 um）	27
spiking3	PE （45-53 um）	480

Primary effluent spiking

		spiked
	PP（300-500 um）	24
	PE （180-212 um）	37
spiking1	PE （45-53 um）	289
	PP（300-500 um）	24
	PE （180-212 um）	48
spiking2	PE （45-53 um）	433
	PP（300-500 um）	13
	PE （180-212 um）	22
spiking2	PE （45-53 um）	154

Size distribution of MPs in different streams on count and mass basis

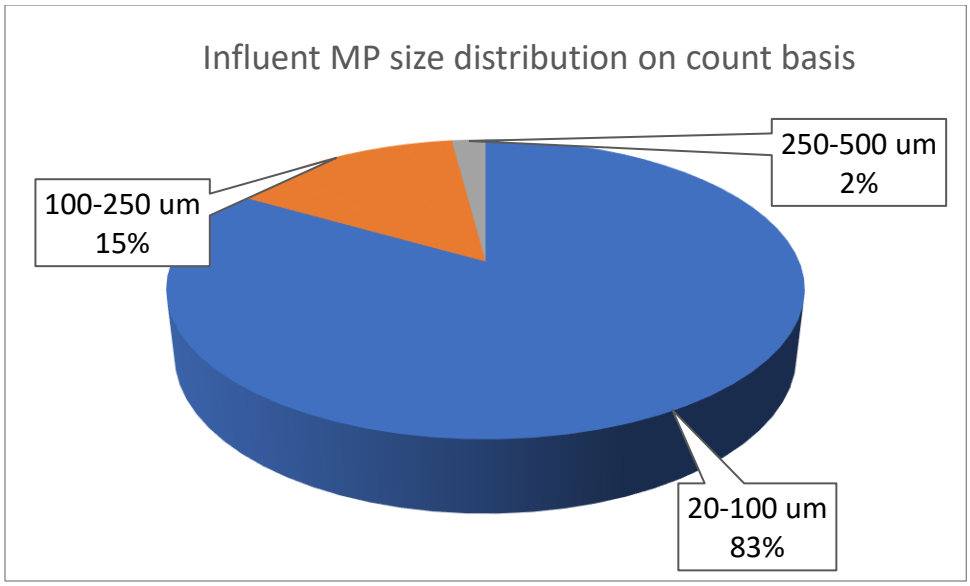
Influent MP size distribution on count basis
250-500 um
2%
100-250 um
15%
20-100 um
83%

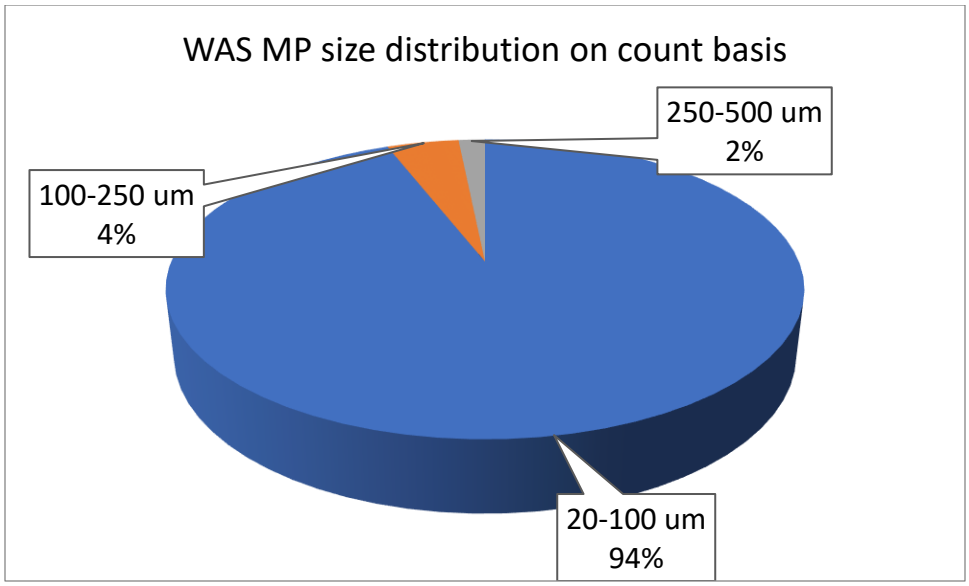
WAS MP size distribution on count basis
250-500 um
2%
100-250 um
4%
20-100 um
94%

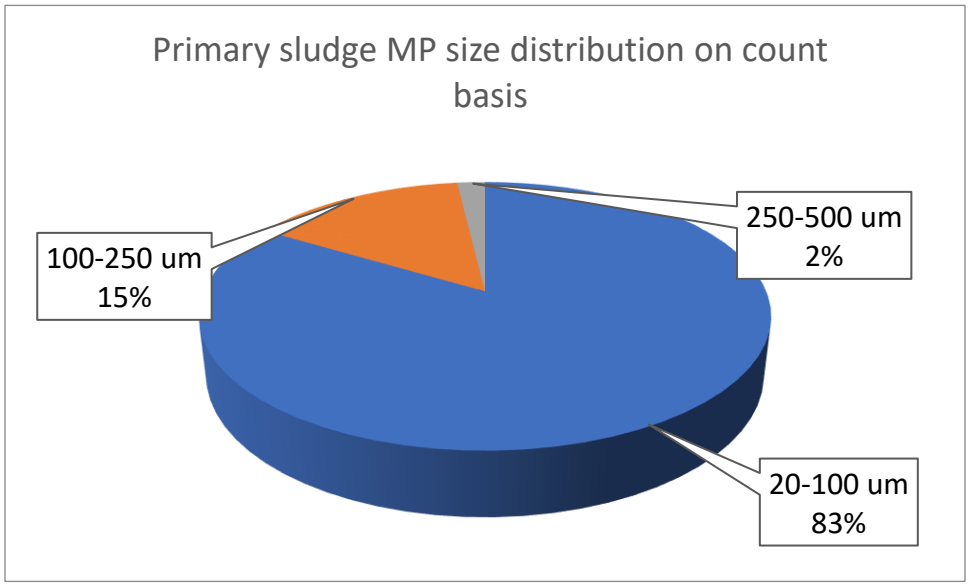
Primary sludge MP size distribution on count basis
250-500 um
2%
100-250 um
15%
20-100 um
83%

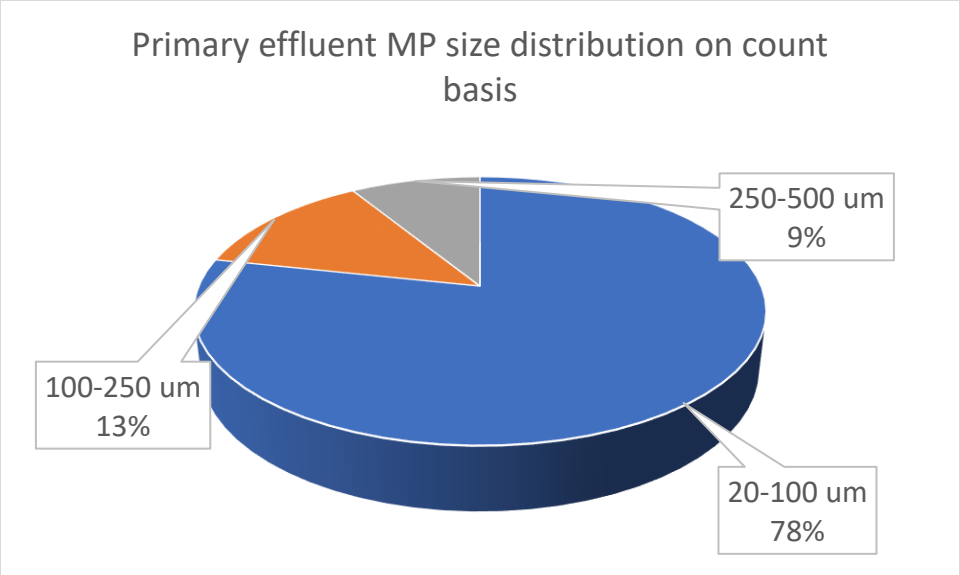
Primary effluent MP size distribution on count basis
250-500 um
9%
100-250 um
13%
20-100 um
78%

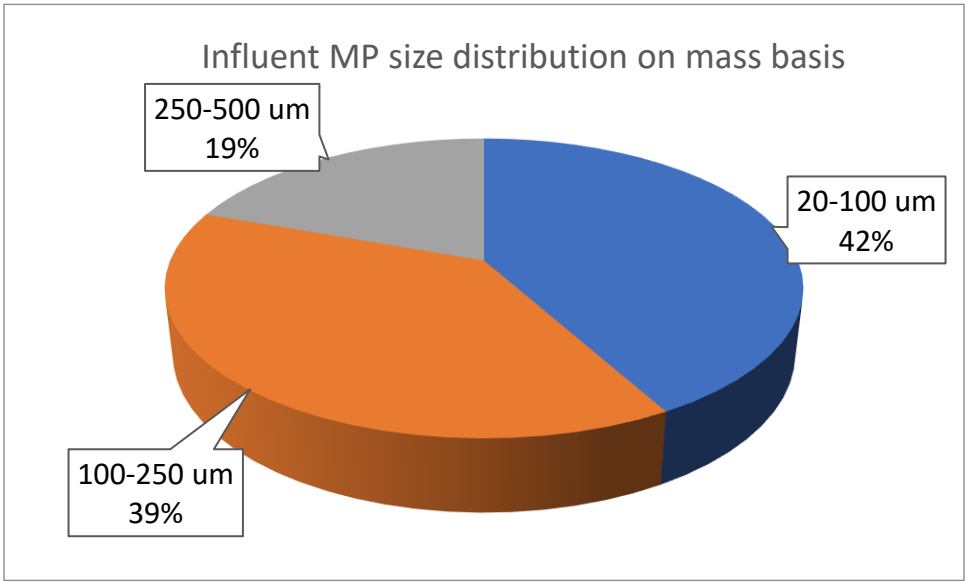
Influent MP size distribution on mass basis
250-500 um
19%
20-100 um
42%
100-250 um
39%

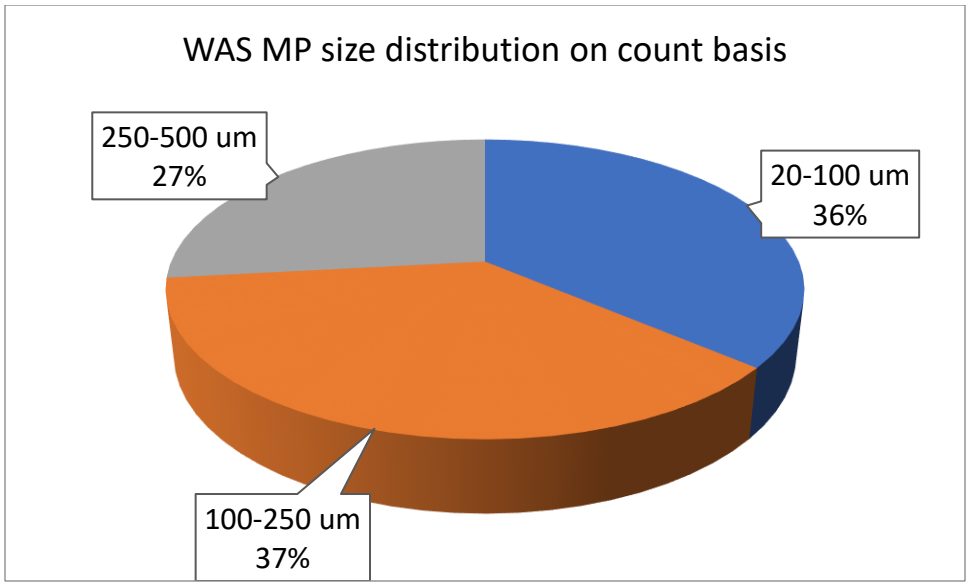
WAS MP size distribution on count basis
250-500 um
27%
20-100 um
36%
100-250 um
37%

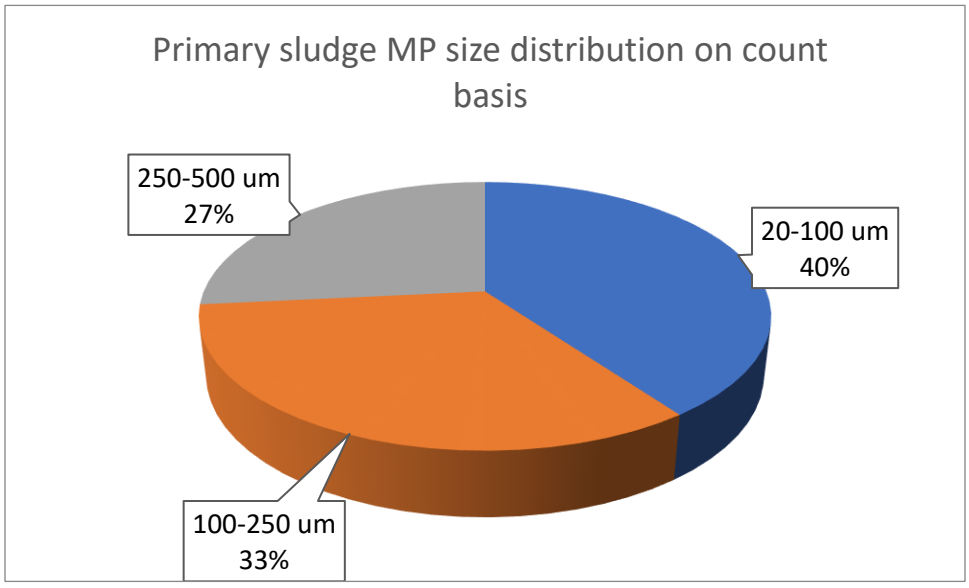
Primary sludge MP size distribution on count basis
250-500 um
27%
20-100 um
40%
100-250 um
33%

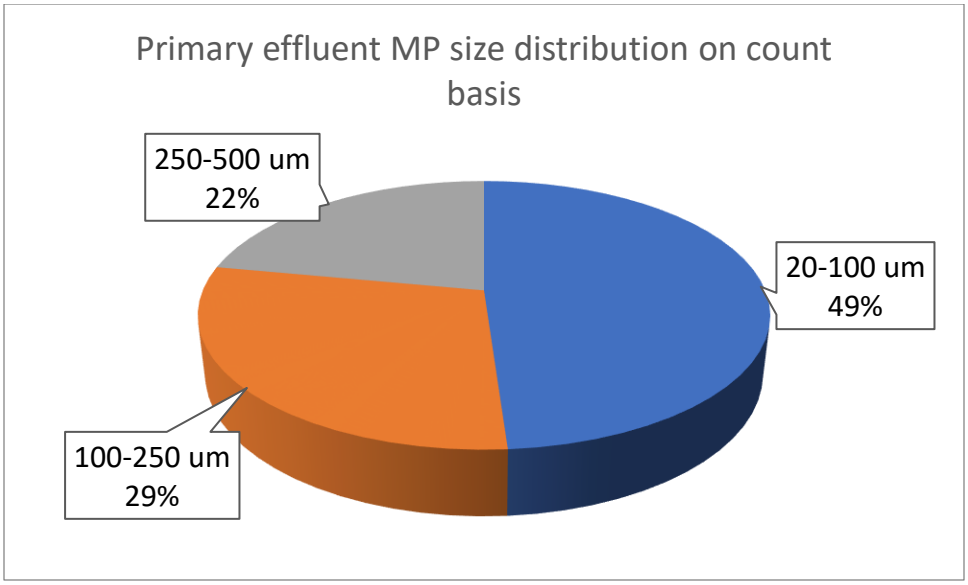

Custom-made Filtration device

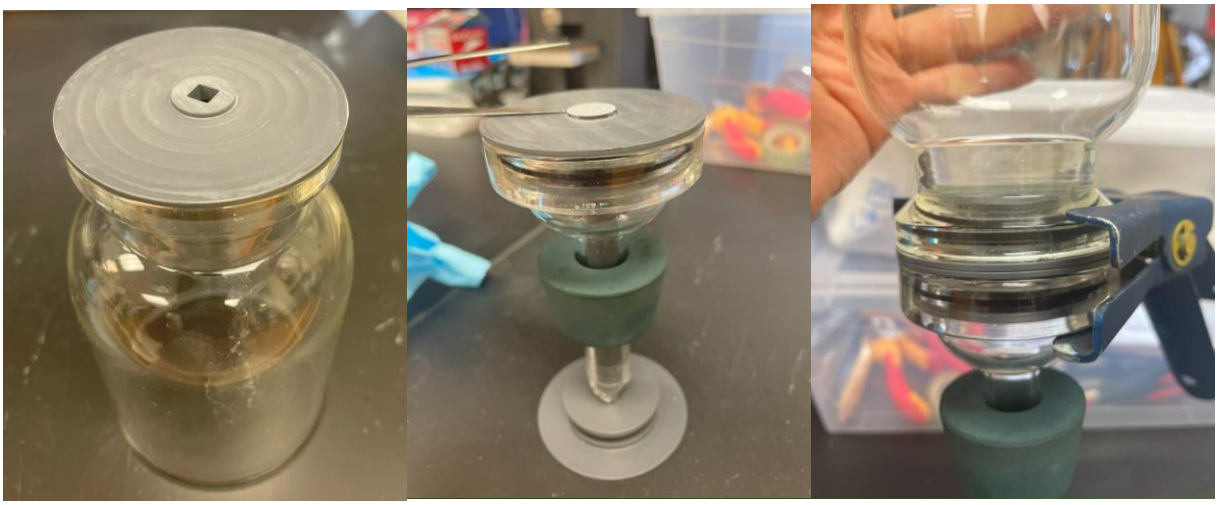

Circle detection function

The **imfindcircles** function automatically detect and measure circular objects in an image using various techniques in image processing. The initial steps involve loading the image, which contains round plastic chips of diverse colors. Next, the radius range for searching circles is determined using the drawline function on a chip's approximate diameter. The imfindcircles function is then used to detect circles within a specific range of radii.

See details

https://www.mathworks.com/help/images/detect-and-measure-circular-objects-in-an-image.html

Classify fiber and particles

The quantification of the dimensions of microplastics, specifically the major-axis and the minor-axis, was achieved utilizing the '**regionprops**' function within the MATLAB computational programming environment. This specific function computes a set of properties for each connected component in the binary image, thus returning the lengths in pixels of both the maximum (major) and minimum (minor) axis of the identified object. Through the implementation of this method, we were able to classify the objects based on their dimensional properties. If the ratio of the major length to the minor length was observed to be 3:1, the object was classified as a fiber. Conversely, objects which did not fit this specific criterion, irrespective of their shape, were designated as particles. This classification protocol enabled a more accurate and nuanced differentiation of microplastic types within the sample set.

See details

https://www.mathworks.com/help/images/ref/regionprops.html

Flow rate(m3/d) of different streams in primary treatment of Kitchener WWTP, based on data from 2021-Nov-18 to 2021-Nov-25

	mean	std	%std
Influent	68067.8	1892.9	2.8
WAS	2806.0	6.1	0.2
Primary sludge	852.7	277.7	32.6
Primary effluent	72712.2	2550.2	3.5

Appendix D WEAO Conference Paper: Quantification of the mass of Microplastics using FPA-based FT-IR Imaging

Ziang Zhu* , Wayne Parker*, Department of Civil and Environmental Engineering, University of Waterloo

Alexander Wong, Department of Systems Design Engineering, University of Waterloo

***200 University Avenue West., Waterloo, ON, N2L 3G1**
z259zhu@uwaterloo.ca, wjparker@uwaterloo.ca

ABSTRACT

Wastewater treatment plants (WWTPs) have been found to be a significant source of microplastics into the environment. The use of mass as a conserved base quantity would be preferable when addressing MP behaviour in WWTPs and when quantifying MP discharges to receiving waters, because the mass of MPs will not be affected by the physical and chemical processes to which the MP are typically exposed. In this study, an accurate method for the quantification of volumes and hence masses of MPs based on Beer's law and FPA micro-FT-IR imaging was developed. Linear regression was used to fit the absorbance vs. thickness data collected from the imaging of plastic membranes with controlled thickness, and the fitted models were used to estimate volumes of controlled shaped particles. The linear responses between absorbance and plastic thickness showed that Beer's law can be used for the accurate quantification of the thickness of pixels and hence the volume and mass of MPs. The errors between known and estimated volumes of MPs with well defined geometries are less than 5%, showing that the proposed method is valid and accurate. The method developed in this study has the potential to become the standard approach for accurate quantification of the mass of MPs in water systems.

KEYWORDS

Microplastic; Quantitative analysis; Mass; Beer's law; FPA micro-FT-IR imaging;

1. INTRODUCTION

Pollution of waterbodies by microplastics (MPs) has become a growing environmental concern. An increasing number of studies have shown that wastewater treatment plant (WWTP) effluents represent a significant point of entry for MPs into the aquatic environment. Prior studies have typically reported particle counts when addressing MP behaviour in WWTPs and when quantifying MP discharges to receiving waters. It has been suggested that this type of quantitative analysis is flawed because particle numbers are not a conserved base unit (Simon et al., 2018; Wu et al., 2020; Tanoiri et al., 2021). Due to the brittle nature of MPs, they can fragment in the environment and during analysis. The use of mass as a conserved base quantity would be preferable as it will not be affected by the physical and chemical processes to which the MPs are typically exposed (Simon et al., 2018). Consequently, the mass of MPs should be included when quantifying MP discharge to the environment and calculating mass balances around WWTPs, to supplement the conventional approach of reporting particle numbers.

Focal plane array (FPA) micro-FT-IR imaging is a promising technique for the quantification of the mass of MPs in the size range 20-500 um. Simon et al. (2018) proposed that the volume of each MP particle can be estimated based on the x-y dimension of particles obtained from 2-D imaging with the assumption that all MPs have an ellipsoid shape. The ellipsoid assumption is subject to error because many particles are in the shape of fragments, films, foams, spheres, pellets (Sun et al., 2019). The current study aims to develop accurate methods for the quantification of volumes and hence masses of MPs based on enhanced FPA micro-FT-IR imaging.

2. MATERIAL AND METHODS

2.1 Volume Quantification Method

In the proposed method the volume of each MP particle is based on the response of each pixel obtained from FPA micro-FT-IR imaging. The output of FPA micro-FT-IR measurement is a 3-D matrix, where each pixel has a pair of (x,y) coordinates and at the same time corresponds to a FT-IR spectrum (As shown in Fig.1A). The spectral information is employed as the input to a deep learning technique (Zhu et al., 2020) that identifies the type of plastic making up the MP. The type of plastic then determines which regression model is subsequently employed to estimate the MP

thickness. The volume of particles is calculated by summing up the volume of all pixels which are estimated from the product of the area of each pixel and it's thickness (As shown in Fig.1B). The area of each pixel is an instrument parameter, and the thickness of each pixel is estimated using Beer's law. Beer's law allows the thickness of a pixel to be estimated on the basis of its IR absorption relative to the absorption of a reference plastic of known thickness. (As shown in Fig.1C and Fig.1D). The mass of the MP is then estimated from the specific gravity associated with the type of plastic.

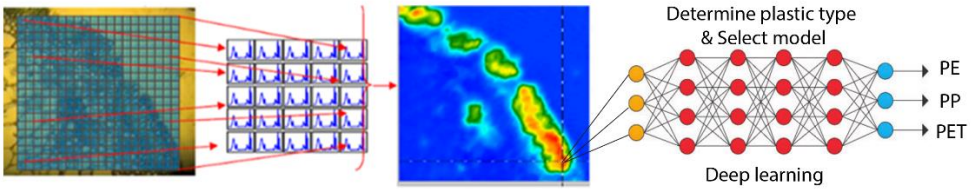

(A)

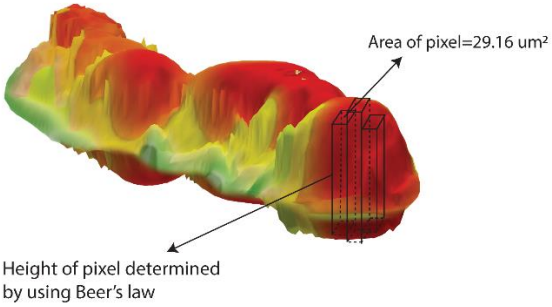

(B)

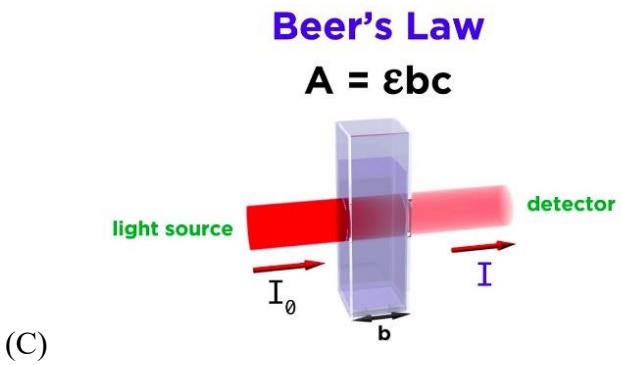

(C)

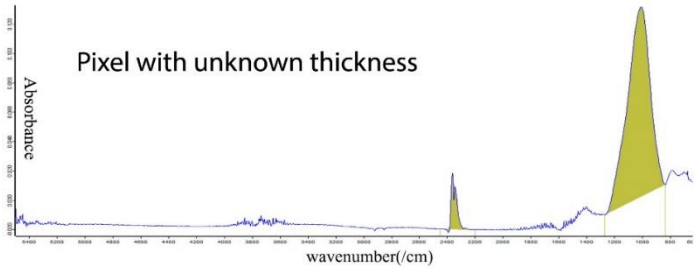

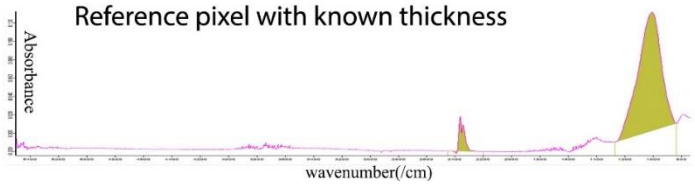

(D)

Figure 1. Volume estimation of an MP particle from FPA micro-FT-IR imaging. (A) 3-D matrix of the output of FPA micro-FT-IR imaging and model selection using deep learning. (B) Calculate the volume of a MP particle by summing up volume of pixels. (C) Schematic illustration of Beer's law (D) Calculate the thickness of the sample pixel by comparing the adsorption.

2.2 Materials

The materials that were imaged included plastic films, spheres and fibers. Plastic films with controlled thickness were made using a heat-pressing process. A plastic particle was heated to its melting point and then pressed within a spacing ring in a film-making kit (GS03970, SPECAC, UK). After each plastic film was made, a digital micrometer (Mitutoyo, Japan) was used to evaluate its thickness. The types and thickness of plastic films are summarized in Table S1. Clear HDPE spheres were purchased from Cospheric (Cospheric, US). Clear PET and Nylon fibers were purchased form Xingdeyuan Plastic (Xingdeyuan, China)

2.3 FPA Imaging and Data Analysis

FPA FT-IR imaging was performed on a Bruker Hyperion 3000 FT-IR microscope equipped with a 64 ×64 focal plane array (FPA) detector (Bruker, USA). A set of two 15× Cassegrain objectives allowing confocal measurements were used. IR radiation was provided by a Bruker TENSOR 37 FTIR spectrometer (Bruker, USA) which was connected to the microscope. Data collection was performed with OPUS© (version 7.5). All data were measured in transmission mode with no binning of pixels, at a resolution of 8 cm^{-1} with 32 co-added scans in accordance with reported settings (Löder et al., 2015; Primpke et al., 2017). A BaF_2 high-transmission window was used to support films, spheres and fibers in imaging.

Plastic films were imaged to gather spectra for the development of quantitative models between absorbance and thickness. When imaging each film, the detector was moved to 3 different positions to collect data for the evaluation of the evenness of films. A background tile, with no plastic material present, was used as a zero-calibration point. Spheres and fibers in well-defined geometries were imaged for validation purposes. Each sphere and fiber was imaged in triplicate to check the reproducibility of imaging.

The raw OPUS data was saved in MATLAB® format and all data analysis was performed using MATLAB® R2018a. One-way ANOVA tests were used to assess the statistical difference between datasets.

3. RESULTS

A series of steps were employed to assess the data obtained from FPA-FTIR microscopy to arrive at a model that could be employed to estimate the thickness of plastic particles. Figure 2 shows the procedure for the development and validation of linear regression models for the quantification of the volume of MPs. Firstly, the evenness of films was evaluated using one-way ANOVA tests, and after that the outliers of spectral response at each thickness were removed. In step 3, the peaks for integration were selected for different thickness ranges and for different types of plastics. After each spectrum was converted to an absorption value based on the selected integration peaks, linear regression was used to fit the data in step 4. The last step was to use the fitted models to check control-shaped particles for validation purposes.

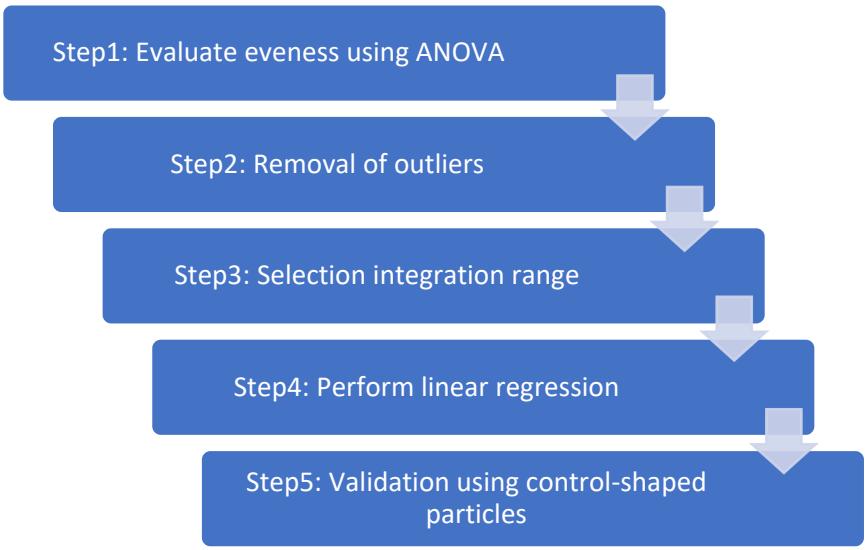

Figure 2 Procedure of the development and validation of linear regression models

3.1 ANOVA Tests

One-way ANOVA tests were used to determine whether there were any statistically significant differences between the means of thickness of each plastic membrane for the 3 positions where signals were collected. For each spectrum, the absorption at 3200-2650 cm^{-1}, corresponding to the stretching of C-H bonds which is a skeleton of plastic, was integrated. A one-way ANOVA that

considered 3 positions as the levels with 4096 values was performed. As is shown in Table S1 in the Appendix, most p values were larger than 0.05, showing that there was no statistical difference in the means of thickness at 3 positions. Hence, the results from the ANOVA tests showed that the plastic films had a consistent thickness and the responses from the films could be used for the calibration of linear models for the quantification of the volume of MPs.

3.2 Removal of Outliers

Outliers were removed from the datasets prior to fitting the regression models as they could disproportionately affect the results and thereby cause misleading interpretations. The presence of outliers at each thickness was examined by plotting the absorbance of all 3*4096 pixels at each thickness as a histogram. The histogram of adsorption values for PE films with thicknesses of 12 um and 80 um PE films is shown in Fig. S1 as an example. As is shown in Fig.S1, the distribution of absorbance at each thickness was approximately normally distributed, but there were several positive outliers which may have been due to erroneous responses of a few pixels on the detector or due to protruding dots on the plastic films. Consequently, outliers outside of the 2.5th and 97.5th percentiles were removed.

3.3 Selection of Integration Range

Integration ranges were selected to convert each spectrum into a single absorption value. Integration ranges were selected to avoid portions of the spectra that may have resulted from the presence of additives that were not representative of the base plastic polymer. In addition, ranges had to be selected such that saturation of absorption in the plastic did not occur and thereby linear responses of absorption with thickness were obtained. For the purposes of describing the method for selecting the appropriate integration range the method employed for PET is presented. The spectra obtained from films of PET for different thickness are plotted in Fig. 3 and the absorption vs thickness were examined.

The peaks at 3300-2600 cm^{-1} were selected as target zone for integration because the spectra response at this peak range corresponds to the stretching of C-H bonds which is a primary

component of all types of plastics. Though the absorption of other peaks might increase linearly with the increase of thickness (e.g. peaks at 2200 cm^{-1}), those peaks were not selected because they may have originated from additives.

As is shown in Fig.3, the adsorption at 3167 cm^{-1}-2823 cm^{-1} (zone 1) increased linearly as the thickness of the plastic increased from 12 to 80 microns, which indicated that Beer's law is valid this portion of the spectrum 3167 cm^{-1}-2823 cm^{-1} and for this range of thicknesses. However, the linear increase of absorption at 3167 cm^{-1}-2823 cm^{-1} changed as the thickness increased from 120 to 500 micron, indicating that the adsorption at 3167 cm^{-1}-2823 cm^{-1} might be saturated at 120 - 500 micron, and that Beer's law did not apply for the high thickness range. In contrast, the adsorption at 2824 cm^{-1}-2762 cm^{-1} (zone 2) increased linearly as the thickness increased from 120 to 500 micron, showing that the 2824 cm^{-1}-2762 cm^{-1} zone is a good candidate for predicting thickness of unknown pixels in the 120-500 micron thickness range. However, the adsorption in the 2824 cm^{-1}-2762 cm^{-1} zone was weak for films with a thickness of 12 - 80 microns. It is anticipated that this might cause errors when using 2824 cm^{-1}-2762 cm^{-1} zone in predicting thickness of unknown pixel in 12 - 80 micron thickness range. Hence, two integration zones for the two different thickness ranges were employed: integrating 3167 cm^{-1}-2823 cm^{-1} for the thickness range 0-100 micron while integrating 2824 cm^{-1}-2762 cm^{-1} for the thickness range 100-500 micron.

Similar to the selection of peak ranges for PET, spectra of other types of plastic films were plotted, and two integration zones for two different thickness ranges (0-100 um, 100-500 um) were selected. The selected integration ranges are listed in Table 1. Each spectrum was converted to an absorption value by integrating the selected integration ranges.

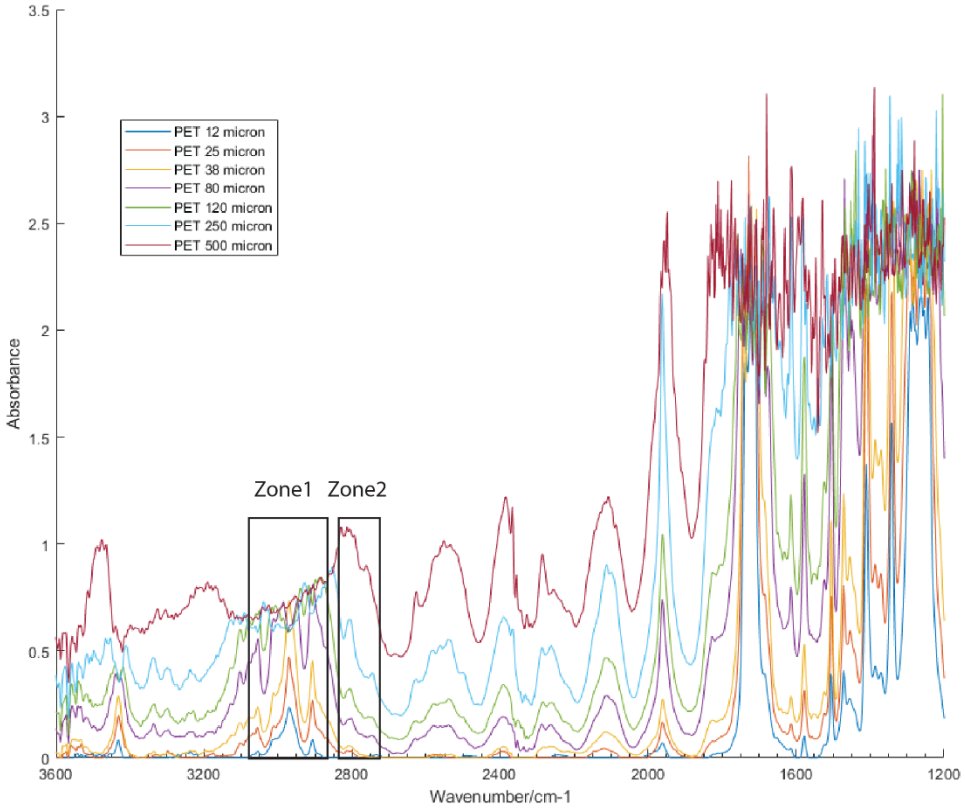

Figure 3 Spectra of PET films of different thickness. Zone 1: peaks at 3167 cm^{-1}-2823 cm^{-1}; Zone 2: peaks at 2824 cm^{-1}-2762 cm^{-1}.

3.4 Linear Regression Models

The low and high thickness range linear regression models (Equation 1) for PET are shown in Fig. 4. The r^2 values for the two models were larger than 0.99, indicating a linear relationship between absorbance and plastic thickness for both ranges.

$$Y = \text{intercept} + \text{slope} \times X \qquad (1)$$

Where: X = Absorbance (cm^{-1}) within target range; Y = thickness of pixel (µm)

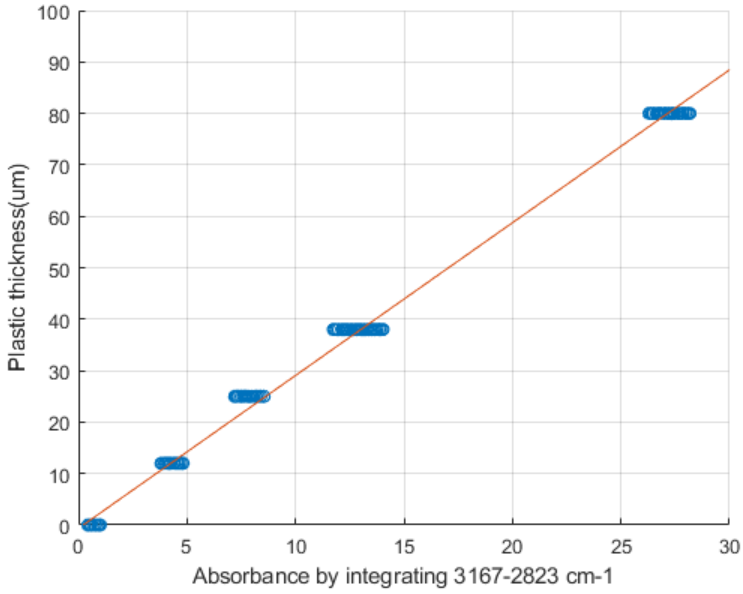

(A)

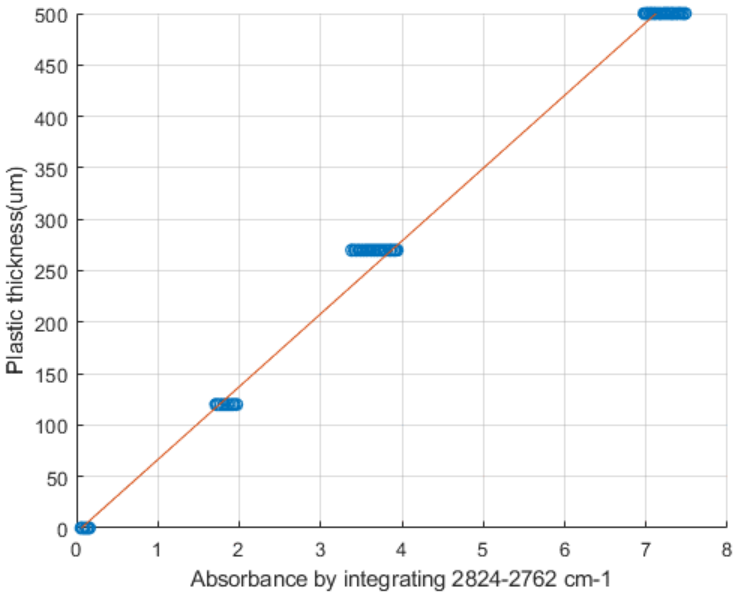

(B)

Figure 4 Linear regression models for PET. (A) Low thickness ranges (0-100 micron) (B) High thickness range (100-500 micron)

Linear regression models were employed to fit the absorption versus thickness values for the low (0-100 um) and high range (100-500 um) thicknesses for all the types of plastic that were tested. Table 1 presents the estimates and standard errors of the parameters for the linear regression models

for the various plastics that were tested. For all models, the standard errors of the intercept were around 1%, the standard errors of slopes were around 0.2% of the estimated values, and the r^2 values were larger than 0.99. Hence, it was concluded that Beer's law can be used as a foundation for the quantification of the thickness of pixels and subsequently the volume and mass of MPs.

Table1 Linear regression models for different types of plastics

Plastic Type	Thickness range (um)	Intercept (um)		Slope (um/abs)		r^2	Integration range(cm^{-1})
		Estimate	Standard error	Estimate	Standard error		
ABS	0-100	-1.39	2.95×10^{-1}	1.77	1.29×10^{-2}	0.997	2727-3148
	100-500	-5.5	2.37×10^{-1}	34.3	4.19×10^{-2}	0.992	2858-2746
Nylon	0-100	-2.65	2.37×10^{-1}	1.18	2.56×10^{-3}	0.998	3167-2677
	100-500	-2.24	1.74×10^{-1}	19.5	2.20×10^{-2}	0.993	2769-2519
PC	0-100	-1.83	6.16×10^{-2}	2.19	2.40×10^{-3}	0.994	3167-2823
	100-500	-1.15	1.50×10^{-1}	31.7	2.35×10^{-2}	0.997	2820-2746
PE	0-100	-1.05	2.80×10^{-2}	1.75	7.59×10^{-4}	0.998	3117-2577
	100-500	-2.26	8.73×10^{-2}	16.5	5.02×10^{-3}	0.999	2692-2500
PET	0-100	-0.642	1.24×10^{-2}	2.97	7.35×10^{-4}	0.998	3167-2823
	100-500	-4.32	1.37×10^{-1}	70.8	3.07×10^{-2}	0.998	2824-2762
PMMA	0-100	-1.94	1.59×10^{-2}	3.01	1.18×10^{-3}	0.999	3121-2793
	100-500	-7.41	2.10×10^{-1}	109	1.01×10^{-1}	0.995	2789-2700
POM	0-100	-2.13	4.80×10^{-1}	2.16	1.67×10^{-3}	0.995	3063-2743
	100-500	0.0769	1.71×10^{-2}	41.5	3.20×10^{-2}	0.995	2773-2654
PP	0-100	-1.39	2.22×10^{-2}	2.21	1.04×10^{-3}	0.999	3132-2754
	100-500	-2.65	2.13×10^{-1}	66.9	7.80×10^{-2}	0.993	2596-2515
PS	0-100	-10.3	1.53×10^{-2}	1.64	6.08×10^{-4}	0.999	3136-2762
	100-500	-8.24	2.28×10^{-1}	129	1.02×10^{-1}	0.994	2816-2746
PVC	0-100	-2.53	4.32×10^{-2}	3.64	3.39×10^{-3}	0.996	3097-2769
	100-500	-7.47	1.68×10^{-1}	85.9	7.01×10^{-1}	0.996	2820-2746
Silicone	0-100	-0.763	8.68×10^{-3}	1.19	5.44×10^{-4}	0.999	3155-2754
	100-500	-1.35	1.89×10^{-1}	34.5	4.18×10^{-2}	0.992	2689-2619

3.5 Validation

Model validation is an important step to check the accuracy and performance of models. The true volumes and estimated volumes of control-shaped particles were compared, and the results were presented in Table 2. The procedures for calculating true volume, estimated volume, error, and confidential levels are summarized as follows:

- The true volumes were calculated based on the dimensions and geometry of the spheres and fibers.

- The volume of a particle in a single image was calculated by summing up the volume of all pixels, and the thickness and volume of an individual pixel was estimated based on Beer's law as is shown in Fig.1B-1D. The estimated volumes in Table 2 were calculated by averaging the triplicate of 3 images ± standard deviations of the triplicates.
- The errors were calculated based on the difference between the known volume and estimated volume for the same particle.
- The 95% confidence level (Cl) was calculated as

$$Cl = V_{estimate} \pm \mathrm{t} \times u_{particle} \quad (2)$$

where $V_{estimate}$ was the estimated volume of particle, t is the t statistic, and $u_{particle}$ was the uncertainty in estimating the volume of this particle, which was calculated as

$$u_{particle} = \sum u_{pixel} \quad (3)$$

where u_{pixel} was the uncertainty in estimating volume of individual pixel, which was calculated as

$$u_{pixel} = A_{pixel} \times u_{thickness} \quad (4)$$

where A_{pixel} was the cross-section of a pixel, and $u_{thickness}$ was the uncertainty in estimating the thickness of the pixel, which was associated with the linear regression model and was calculated as

$$u_{thickness} = \sqrt{S_{Y \cdot X}^2 \left[1 + \frac{1}{n} + \frac{(X - \bar{X})^2}{\sum x^2}\right]} \quad (5)$$

where $S_{Y \cdot X}^2$ was residual mean square, n was the number of observations in the linear regression model, X was the absorbance that was used to estimate the thickness, $\bar{X}$ was the average of absorbance in the linear regression model, $\sum x^2$ was sum of squares from the linear regression model.

Table 2 Known volumes and imaging-estimated volumes of selected particles

Type	shape	Dimension	Known volume (um^3)	Estimated volume ± std dev (um^3)	Error (%)	95% confidence level of estimate (um^3)
PE	Sphere	44 um diameter	3.61×10^4	$3.42\times 10^4\pm 1.62\times 10^2$	-5.08	$4.62\times 10^4 \pm 1.22\times 10^4$
PE	Sphere	110 um diameter	6.97×10^5	$6.88\times 10^5\pm 1.39\times 10^3$	-1.14	$6.86\times 10^5 \pm 7.67\times 10^4$
PE	Sphere	242 um diameter	7.42×10^6	$7.41\times 10^6\pm 2.59\times 10^4$	-0.14	$5.86\times 10^6 \pm 3.15\times 10^5$
PE	Sphere	460 um diameter	5.09×10^7	$5.26\times 10^7\pm 3.43\times 10^5$	3.25	$4.53\times 10^7 \pm 1.23\times 10^6$
Nylon	Fiber	50 um diameter, 170 um length	3.34×10^5	$3.45\times 10^5\pm 6.75\times 10^2$	3.38	$3.35\times 10^5 \pm 6.24\times 10^4$
PET	Fiber	78 um diameter, 170 um length	8.12×10^5	$8.02\times 10^5\pm 6.35\times 10^3$	-1.19	$7.33\times 10^5 \pm 1.18\times 10^5$

From Table 2 it can be seen that, the standard errors of the triplicates from imaging were relatively small (less than 0.7%), indicating a good repetition of imaging. The estimated volumes for spheres and fibers had low error (less than 5%), indicating the volume estimation based on Beer's law gave accurate volumes. It is worthwhile to note that the errors were randomly distributed, indicating that there was no consistent over or under estimation. The known volume of each particle was within the corresponding 95% confidence interval of the estimate for the same particle that was obtained from the imaging approach.

The accurate estimation of the volumes of 3 different types of plastics showed that the method has the potential for the accurate quantification of the volume of MPs. Hence, when combined with

a deep learning algorithm for the recognition of the type of plastic (and thereby the specific gravity) in an FPA FT-IR dataset the mass of a range of plastics could be estimated.

4. CONCLUSION

Linear responses were observed between absorbance and plastic thickness showing that Beer's law can be used for accurate quantification of the thickness of plastics and hence the volume and mass of MPs. The comparison between known and estimated volumes of MPs with well defined geometries showed that the proposed method is valid and accurate. This method has the potential to become the standard approach for accurate quantification of the mass of MPs in water systems. It is anticipated that this methodology will be a valuable tool for understanding the fate and transport of MPs in WWTPs by allowing the assembly of mass balances and for investigating removal mechanisms.